Extension of the ring polymer molecular dynamics approach to state-selective molecular reactive scattering simulations

Dissertation
zur Erlangung des Doktorgrades
an der Fakultät für Mathematik, Informatik und Naturwissenschaften
Fachbereich Physik
der Universität Hamburg

vorgelegt von

Adrien Marjollet

Hamburg
2022

Gutachter der Dissertation:	Prof. Dr. Robin Santra Dr. Mariana Rossi
Zusammensetzung der Prüfungskommission:	Prof. Dr. Robin Santra Dr. Mariana Rossi Prof. Dr. Jochen Küpper Dr. Ludger Inhester
Vorsitzende der Prüfungskommission:	Prof. Dr. Daniela Pfannkuche
Datum der Disputation:	30.05.2022
Vorsitzender Fach-Promotionsausschusses PHYSIK:	Prof. Dr. Wolfgang J. Parak
Leiter des Fachbereichs PHYSIK:	Prof. Dr. Günter H. W. Sigl
Dekan der Fakultät MIN:	Prof. Dr. Heinrich Graener

Eidesstattliche Versicherung / Declaration on oath

Hiermit versichere ich an Eides statt, die vorliegende Dissertationsschrift selbst verfasstund keine anderen als die angegebenen Hilfsmittel und Quellen benutzt zu haben.

Hamburg, den 20.03.2022

Unterschrift der Doktorandin

Abstract

The state-resolved knowledge of molecular scattering dynamics is paramount to the understanding and control of chemical reactions. The ideal approach to rigorously simulate such systems is a full-dimensional treatment with quantum mechanical calculations. Current generation of computers allows such calculations to be carried out up to six atoms for zero total angular momentum. It is not likely that the computational power will allow significant progress in the near future, as the computational time grows exponentially with the number of degrees of freedom. Thus, there is a demand for alternative methods that would allow the inclusion of quantum effects while remaining computationally efficient.

This thesis consists of the development of such an approach. Inspired by the success of the efficient ring polymer molecular dynamics (RPMD) approach applied to quantum systems at thermal equilibrium, I extend the scope of RPMD to state-selective chemistry.

I start by presenting the method development groundwork toward microcanonical simulations of triatomic reactions using RPMD. I expose the steps to prepare a specific initial vibrational state for a diatomic molecule. The assessment of the method revolves around the computation of integral cross sections (ICS) in the ring polymer phase space. I report an ansatz for the reciprocal temperature depending on the characteristics of the reactions. The benchmark reactions Mu/H/D + H_2 with H_2 either in its ground $(v = 0)$ or first excited vibrational state $(v = 1)$ are chosen to test the method. Good agreement for the Mu/H/D + $H_2(v = 0, 1)$ reactions with exact quantum scattering calculations is found. It is shown that RPMD can describe to a good approximation zero-point energy (ZPE) effects and tunneling effects for these reactions while remaining computationally efficient.

Following these encouraging preliminary results, the robustness and applicability of the method is further tested. I present a detailed review of the approach. The reactions Mu/H/D/Cl/F+$H_2(v = 0, 1)$ are considered over a wide range of collision energies. The accuracy and stability of the vibrational excitation scheme are tested. It is found that the ICS results are strongly sensitive to the spring constant of the ring polymers. A refined ansatz for the reciprocal temperature is suggested. I observe a convergence of the ICS above a number of beads that depends on the characteristics of the diatomic reactant. I show that the tunneling contributions to the reactivity stem from the spatial extension of both ring polymer reactants. However,

it is found that RPMD is unable to describe dynamical resonance effects. Shortcomings in the vibrational excitation scheme at low collision energies are reported.

Finally, I further test the approach with larger and more intricate systems. In particular, the reactions F,H+CH_4 and its isotopic variants for the case of the ground state CH_4 and CHD_3 and, in the presence of the C-H excited stretch in CHD_3. Accurate RPMD ICS results for most of the aforementioned reactions are reported. It is found that the ZPE leakage problem usually present in classical dynamics is prevented. It is found that the vibrational excitation scheme is accurate for most purposes except for reactions involving a very low energy barrier.

Zusammenfassung:

Die Berechnung möglicher Zustände von einem Molekül in einem Streuexperiment ist von größter Bedeutung für das Verständnis und die Kontrolle von chemischen Reaktionen. Ein umfassender Ansatz solche Systeme zu berechnen ist durch eine vollständige dreidimensionale Behandlung des quantenmechanischen Problems gegeben. Aktuelle Computer erlauben die Simulation von bis zu sechs Atomen mit der Einschränkung dass der Gesamtdrehimpuls des Systems Null beträgt. Eine Erweiterung der Simulation auf größere Systeme ist seitens der Rechenleistung von konventionellen Computern in naher Zukunft nicht zu erwarten, insbesondere da die Rechenzeit exponentiell mit den Freiheitsgraden des Systems ansteigt. Folgend wird nach Alternativen gesucht, die eine effiziente quantenmechanische Behandlung des Problems erlauben.

Die vorliegende Arbeit beschreibt die Entwicklung eines solchen Ansatzes. Angelehnt an die erfolgreiche Methode der Ring-Polymer Molekulardynamik Simulationen (ring polymer molecular dynamics (RPMD)) aber begrenzt auf Quantensysteme im thermischen Gleichgewicht wurde die RPMD Methode über die kanonische Gesamtheit hinaus für die zustandsselektive Chemie erweitert.

Ich beginne mit der Entwicklung einer Methode für die mikrokanonische Simulation eines dreiatomigen Systems unter RPMD. Ausgeführt werden die einzelnen Schritte zur Erzeugung eines spezifischen Anfangsschwingungszustands in einem zweiatomigen Molekül. Die Bewertung der Methode erfolgt durch die Berechnung von integralen Querschnitten (integral cross sections (ICS)) im Ring polymer-Phasenraum. Unter den Bedingungen der Reaktionen verfolge ich einen alternativen Ansatz der reziproken Temperatur. Ich wähle die Vergleichsreaktion Mu/H/D

+ H_2 mit H_2 entweder in seinem Grundzustand $(v = 0)$ oder im ersten angeregten Schwingungszustand $(v = 1)$, um die Methode zu testen. Für die Reaktionen Mu/H/D + $H_2(v = 0, 1)$ wird eine gute Übereinstimmung mit exakten Berechnungen für den quantenmechanischen Streuquerschnitt gefunden. Es wird gezeigt, dass RPMD in guter Näherung Nullpunktsenergie (zero-point-energy (ZPE))- und Tunneleffekte für diese Reaktionen beschreiben kann und dabei rechnerisch effizient bleibt.

Nach den vielversprechenden vorläufigen Ergebnissen wird die Robustheit und Anwendbarkeit der Methode tiefergehend analysiert. Der Ansatz wird im Detail erläutert. Die Reaktionen Mu/H/D/Cl/F+$H_2(v = 0, 1)$ werden über einen breiten Bereich von Kollisionsenergien betrachtet. Die Genauigkeit und Stabilität der Schwingungsanregung wird überprüft. Es zeigt sich, dass die ICS-Ergebnisse stark auf die Federkonstante der Ringpolymere reagieren. Es wird ein verfeinerter Ansatz für die reziproke Temperatur vorgeschlagen. Ich beobachte die Konvergenz der ICS oberhalb einer bestimmten Anzahl von Koordinaten abhängig von der Wirkung zwischen den zwei Atomen. Ich zeige, dass die Beiträge zur Reaktivität durch Tunnelprozesse aus der räumlichen Ausdehnung der beiden Ringpolymer-Reaktanten stammen. Es zeigt sich jedoch, dass die RPMD nicht in der Lage ist, dynamische Resonanzeffekte zu beschreiben. Die Unzulänglichkeiten der Schwingungsanregung bei niedrigen Kollisionsenergien werden besprochen.

Schlussendlich wird die Anwendung des RPMD Ansatzes über dreiatomige Systeme hinaus auf größere und kompliziertere Systeme erweitert. Insbesondere die F,H+CH_4-Reaktionen und ihre isotopischen Varianten für den Fall des Grundzustands CH_4 und CHD_3 sowie angeregten C-H-Dehnung in CHD_3. Es werden genaue RPMD ICS-Ergebnisse für die meisten der oben genannten Reaktionen präsentiert. Es wird gezeigt, dass Verluste der Nullpunktsenergie wie sie üblicherweise in der klassischen Mechanik auftreten vermieden werden können. Außerdem ist die Methode zur Schwingungsanregung für die meisten Zwecke genau, außer für Reaktionen mit einer sehr niedrigen Anregungsenergie.

Contents

List of Publications

1. **"*Nuclear quantum effects in state-selective scattering from ring polymer molecular dynamics*"**,
   Marjollet, A., Welsch, R., *J. Chem. Phys.* **152**, 194113 (2020).

2. **"*State-selective cross sections from ring polymer molecular dynamics*"**,
   Marjollet, A., Welsch, R., *Int J Quantum Chem.* **121**:e26447 (2021).

3. **"*Initial state-selected scattering for the reactions H+CH_4/CHD_3 and F+CHD_3 employing ring polymer molecular dynamics*"**,
   Marjollet, A., Inhester, L., Welsch, R., *J. Chem. Phys.* **156**, 044101 (2022).

List of Abbreviations

BO	**B**orn-**O**ppenheimer
ICS	**I**ntegral **C**ross **S**ection
MD	**M**olecular **D**ynamics
NE-RPMD	**N**on-**E**quilibrium **R**ing **P**olymer **M**olecular **D**ynamics
NM	**N**ormal **M**ode
NQE	**N**uclear **Q**uantum **E**ffect
PES	**P**otential **E**nergy **S**urface
PIMD	**P**ath **I**ntegral **M**olecular **D**ynamics
QCT	**Q**uasi**C**lassical **T**rajectory method
QD	**Q**uantum **D**ynanics
QM	**Q**uantum **M**echanics
RP	**R**ing **P**olymer
RPMD	**R**ing **P**olymer **M**olecular **D**ynamics
TCF	**T**ime **C**orrelation **F**unction
ZPE	**Z**ero-**P**oint **E**nergy

Chapter 1

Introduction

The long-standing goals of physical chemistry include the detailed understanding and control of chemical reactions. The detailed knowledge of the dynamics of reactive collisions between atoms and molecules plays a key role in many research areas such as condensed-phase molecular systems [1], combustion [2], atmospheric [3–5] and interstellar chemistry [6–8], catalysis [9] and fundamental biological mechanisms [10].

Theoretical computer simulations and scientific experiments play central roles in the study of chemical processes. On the one hand, experiments provide tests of theoretical models leading to evidences of their predictive power or otherwise their inaccuracies. Also, manifestations of unexpected new phenomena not yet explained can also be found via simulations [11].

On the other hand, simulation tools can provide detailed information on how specific forms of energy (e.g., translational, vibrational, rotational and thermal) flow as molecules and atoms collide in condensed and gas phase conditions. They are capable of theoretically probing and monitoring on an atomistic degree of precision the motion of reacting species and can provide detailed knowledge which otherwise cannot be observed in experiments. Also, they can complement the experiments whose design and interpretation require simulations [12].

Among the different phases in which chemical reactions occur, the gas phase is of primary importance as the fruits of its study impact the theoretical concepts and methods of investigation of reactions dynamics in the condensed phases and interfaces (gas-liquid, gas-surface, surface-liquid). Indeed, molecular dynamics in the gas phase lies at the core of chemistry as they encompass the most elementary molecular steps and mechanisms which can occur during the course of chemical reactions. Also, chemical processes can be observed independently in the gas phase and compared to high level theoretical models. In addition, gas phase chemistry

is important in many fields such as combusion, astrochemistry and atmospheric chemistry [13–15]. The study of chemical reactions under equilibrium conditions leads to information that is averaged over several initial states, hiding the reaction details. Thus, being able to predict the dynamics and outcomes of state-resolved bimolecular gas phase reactions is paramount to the understanding of the dynamics which drive chemistry at the most fundamental level [16]. Through experiments such information can be obtained via measuring the differential and integral cross sections. These are the most detailed observables that can be measured experimentally for chemical reactions [17]. They provide detailed information about the dynamics, how and which specific initial states influence the reactivity and distribution of products states and which form of energy is the most effective at promoting the reactivity. Recent progress in high resolution crossed molecular beam scattering experiments now allows the detailed probing of the dynamics of various bimolecular gas phase reactions. For example, the products rovibrational state distribution, state-resolved differential and integral cross sections, the structure of the transition state, atomistic insights of the reactive mechanisms and energy flow can be investigated [18–21]. An example is the F+CHD_3 reaction for which it was found that the C-H stretch excitation favors the DF+CHD_2 product channel. Simulations were able to explain the mechanisms behind the counter-intuitive finding. The ability of experimental apparatus to tackle reactive systems with increasing complexity creates the need for theoretical tools to follow suit to back and interpret the experimental findings [22–24]. Furthermore, accurate simulations of reactions which cannot yet be probed with state-resolved precision by experiments are highly desirable.

As a consequence of the quantum nature of molecular reactive scattering events, quantum effects can have a strong impact on the dynamics of chemical reactions [25–29]. In spite of the fact that the quantum mechanical foundations underpinning the theoretical treatment of chemical reactions are established, it is very difficult to elucidate to which extent quantum effects govern the dynamics. Thus, their inclusion in computer simulations is necessary to achieve accurate predictions and a fundamental understanding for a wide range of reactive systems [30]. However, quantum simulations are very challenging due to the exponential scaling of their computational cost with the number of nuclei and electrons.

Very often, nuclear and electronic dynamics can be solved separately by employing the Born–Oppenheimer (BO) approximation which is at the foundation of

most molecular reactive scattering simulations and has been pivotal for many advances in chemical physics [31]. It allows to first solve the electronic part of the Schrödinger equation to extract the electronic ground-state adiabatic (or BO) potential energy surface (PES). From the PES, a wealth of information about the nuclear dynamics can be obtained such as the locations and energies of the reaction barrier, minimum energy paths and even valuable understanding of the reaction mechanisms. There is a variety of chemical reactions (e.g., electrochemical, ion-molecule and photochemical reactions in particular) where nonadiabatic electronic transitions may occur and thus cannot be described with a single adiabatic PES [32]. This thesis focuses on gas phase neutral-neutral chemical reactions involving atoms and molecules and involving only a single adiabatic PES.

In this context, the nuclear motion is left to be solved based on the PES corresponding to the reaction of interest. The determination of such PESs is crucial for the elucidation of simple chemical reactions as no matter how precise the propagation of the nuclei might be, an inaccurate PES would hinder greatly any realistic dynamics. Their deduction started with the use of semi empirical approximations and progressed to more advanced first principle electronic structure methods [33]. However, it becomes increasingly difficult with the number of electrons to obtain accurate PESs. Recent advances in ab-initio electronic structure calculations [34–37] and fitting procedures [38–40] of ab-initio data has allowed the obtention of accurate PESs for a wide range of chemical reactions within "chemical" accuracy. Nevertheless, as quantum scattering simulations are still far away from tackling even hexatomic systems, a great part of the challenge of simulating chemical reactive mechanisms lies in the latter. Ideally, a quantum treatment of the nuclear coordinates is in order due to the presence of nuclear quantum effects (NQEs). They can be seen as the discrepancies between the results from the classical propagation of the assumed point-like nuclei and quantum simulations based on the same PES. One notable NQE present in chemical reactions is zero-point energy (ZPE) effects. They arise from the zero-point energy contained in each vibration of the reactants, the products and also in the molecular configurations during the reaction. Consequently, reaction threshold energies can be very different from classical predictions alongside the overall reactivity as ZPE effects enforce a certain minimum vibrational energy which the products must have. Besides, ZPE cannot leak to other vibrational degrees of freedom while energy can leak between vibrational modes in

classical simulations. Another important NQE is tunneling which can allow reactions to occur at energies below the barrier height. It is especially relevant for light nuclei and at low temperatures as it is related to the wave nature of the atoms and the tendency to penetrate into energy barriers [26].

The computational effort for quantum methods scales exponentially with respect to the number of nuclei. It was not until the 1970s that the first rigorous quantum calculations could be undertaken to tackle the dynamics of the simplest chemical reactions. The first rigorous full-dimensional state-to-state quantum calculations were published in 1976 for the H+H_2 reaction using an analytical PES [41]. The accurate treatment of more complicated and general atom-diatom reactions was only performed more than a decade later with more modern techniques and computer technology [42]. Today, quantum treatment of atom-diatom reactions is considered essentially solved as the simulations match state-of-the-art experimental results [43–46]. Later, only from the 1990s onwards could tetratomic reactions be studied accurately without any dynamical approximations [17]. State-resolved quantum simulations for the hexatomic H+CH_4 reaction were reported in 2014, albeit for a vanishing total angular momentum and still requiring months of computer time [47]. This was achieved using the multi-configuration time-dependent Hartreee (MCTDH) approach [48, 49]. As of now, even with the advent of increasingly powerful and faster computers, full-dimensional quantum simulations remain prohibitively expensive for systems consisting of more than five atoms. As the number of degrees of freedom and product channels increases considerably with the number of atoms, it is not expected that in the near future full-dimensional quantum simulations will be achievable for hexatomic reactions and beyond.

The only alternative to retain quantum scattering simulations while rendering the simulations feasible is to employ reduced dimensional models (RD) or to constrain the dynamics to fixed values of physical quantities such as the total angular momentum. Even though there are accurate RD approaches, they remain non-systematic as they have to be developed for each system specifically [47, 50–60, 60–63]. Also, RD approaches will eventually face the same faith as full-dimensional treatments with larger systems and inevitably become computationally infeasible [38].

The nature of these impracticalities greatly incentivized the development of simulation techniques that remain numerically affordable and scalable. Classical and quasiclassical trajectories (CT and QCT) methods constitute such approaches and

have been widely used to study chemical reactions. CT mainly consists in propagating the atoms with the classical equations of motions using an adiabatic PES. As a consequence, the CT method does not describe state-resolved behaviour nor NQEs. The QCT method employs classical dynamics and a specific initial states preparation that imposes quantal rovibrational energies for the reactants (producing the so-called quasi-classical trajectories) [64–68]. This approach allows full-dimensional, effective and detailed simulations, albeit with a classical description of the atoms evolving on a potential energy surface. Along with being very efficient and conceptually simple simulation tools, classical dynamics can provide accurate and intuitive analysis of the mechanistic dynamics. Also, QCT simulations are prone to lead to relatively accurate results for high energies and in the presence of heavy atoms as NQEs can be less dominant. For various reactions, the QCT method provides accurate quantitative products state and energy distrubutions. Other successes of QCT include the exposure of the steering dynamics for the H+CHD_3 reaction, the identification of "roaming" reactions and the cause of reactivity depression for the reaction H+CD_4 at high collision energies [69], just to name a few among a wealth of mechanistic information [64–67, 70, 71]. However, QCT suffers from the absence of intrinsic descriptions of nuclear quantum effects. In particular, but not limited to, it can allow zero-point vibrational energies to leak into other unbound internal DOFs or vibrational modes, it neglects quantum tunneling and, it can lead to product states which do not respect zero-point energy constraints. In the presence of sizable polyatomic reactants, a large amount of ZPE can leak into the reaction coordinates which can in turn lead to an underestimation of the reaction threshold and overestimation of the overall reactivity [72, 73]. Also, information about the vibrational specificity of the target molecule can be greatly compromised, as seen in methane dissociation on metals [74]. Recent developments have introduced extra procedures [75–77] which can to a certain degree mitigate the absence of ZPE effects while keeping QCT efficient. *Post-hoc* procedures that discard ZPE violating classical trajectories along with binning techniques have been developed to account for ZPE effects. However, these procedures do not provide an inherent description of quantum phenomena.

Since the 1980s, the path integral molecular dynamics approach (PIMD) has allowed the inclusion of nuclear quantum effects in simulations of static thermodynamical properties of quantum systems [78, 79]. These simulations techniques

are based on the so-called "classical isomorphism" between the quantum mechanical partition function of particles and the classical partition function of necklaces consisting of classical replicas (or beads) of the atoms joined by harmonic springs. This approach allows via ensemble configurational averages for the accurate computation of time-independent quantum thermal expectation values while retaining computational efficiency and scalability, albeit in an extended phase space. Fictitious momenta for the beads can also be introduced to employ molecular dynamics as a sampling tool to facilitate the exploration of the configuration space. In 2004, Manolopoulos et al. demonstrated using simulations that ring polymer molecular dynamics (RPMD) can be used to compute approximate Kubo-transformed real-time correlation functions (TCF) [80]. These dynamical quantities appear in a variety of approximate treatments of real-time quantum dynamics. In particular RPMD was shown to provide consistently improved results over classical MD. Ten years later, RPMD's relevance for real-time dynamics was theoretically justified as an approximation to Matsubara dynamics [81, 82]. RPMD has stood out in the last two decades thanks to its various successful applications. Indeed, RPMD has shown great potential by successfully computing thermal rate constants for a variety of bimolecular reactions even at a much smaller computational cost than accurate, fully converged quantum mechanical (QM) calculations [83–88]. Also, RPMD can predicts accurately diffusion coefficients and to some degree vibrational spectra [85, 86, 89–94]. For thermal equilibrium applications, RPMD is almost immune to the shortcomings associated with the ZPE leakage from classical dynamics. It captures ZPE constraints and describes tunneling contributions to the reactivity. The classical, trajectory based nature of the simulation, albeit in the ring polymer phase space, allows to probe directly the atomistic dynamics and extract detailed dynamical knowledge. Despite of these accomplishments, RPMD cannot describe real-time coherences and suffers from the spurious-mode effect when calculating vibrational spectra above certain frequencies [91–93].

Up to recently, no information on state-selectivity nor microcanonical quantities for chemical reactions could yet be retrieved. The energy dependence of cross sections, reaction probabilities and general state-resolved information remained out of the scope of RPMD. Only the use of initial thermal states were so far justified and considered. Very recently (2016), the theoretical justification of the introduction of specific non-equilibrium (NE) conditions within RPMD (NE-RPMD) was reported [95]. The NE conditions consist of a sudden change of external potential

or an initial momentum impulse, i.e., a "kick". The latter NE condition provides a pragmatic possibility to employ RPMD beyond the canonical ensemble and initial thermal states. The possibility of extending RPMD towards the detailed study of the dynamical properties of chemical reactions for which quantum treatments are infeasible is a promising prospect.

In this thesis, this promising step is addressed and the work done towards extending the capabilities of NE-RPMD to initial state-resolved bimolecular reactions is performed. It provides a new and efficient approach to include NQEs within a full-dimensional treatment of reaction dynamics and prospectively enables the computation of state-resolved microcanonical properties for molecular reactive systems containing many atoms.

.

Organization of the thesis

In **Chapter 2** I begin by outlining the quasi-classical trajectory method and introducing the theoretical concepts behind the ring polymer molecular dynamics approach and its recent developments. **Chapter 3** describes succinctly the newly developed approach and its first applications. **Chapters 4** and **5** describe further generalizations and applications. Finally, **Chapter 6** provides the conclusion and an outlook to close the thesis.

Chapter 2

Theoretical framework

This chapter presents the basic theoretical background for understanding the method developed during this thesis. First, as our approach depends on the Born-Oppenheimer approximation, the concept of adiabatic potential energy surfaces (PES) is explained. Subsequently, the main features of the quasi-classical trajectory method (QCT) are explained, followed by a discussion about the applicability and robustness of QCT. This is motivated for benchmark purposes as our results will be compared with QCT predictions in **Chapters 3**, **4** and **5**. Thereafter, I proceed by presenting the theoretical foundations and an overview of several properties of the path integral and ring polymer molecular dynamics approaches (PIMD and RPMD). After that, I introduce an extension of RPMD for non-equilibrium dynamics (NE-RPMD) that will be used throughout this thesis. Finally, the current scope of RPMD and NE-RPMD will be reviewed and discussed to get **Chapter 3** underway.

In this chapter, the Cartesian coordinate system is characterized by the mutually orthogonal unit vectors $\mathbf{e_x}$, $\mathbf{e_y}$ and $\mathbf{e_z}$. The coordinate symbol $\bar{\mathrm{X}}$ refers to the center of mass of the molecule X. The dynamics are always assumed non-relativistic, involving distinguishable particles or nuclei and evolving on a single adiabatic potential denoted as V.

2.1 Adiabatic potential energy surface

Chemical dynamics is intrinsically of quantum nature [96] and therefore, the task of modeling the physical processes occurring in chemical reactions would ideally require the solution of the time-dependent Schrödinger equation for the electrons and nuclei involved. This problem is impossibly difficult with the exception of the

simplest systems such as the hydrogen atom [97,98]. Nevertheless, in many chemical processes and practically without loss of accuracy, one can make this problem considerably more feasible by employing the Born-Oppenheimer (BO) approximation [31].

The BO approximation relies on the assumption that the electronic motion and the nuclear motion in molecules can be separated. This is in most cases valid as the nuclei are much more massive than the electrons. With this assumption, the electronic wavefunction should evolve from the reactant electronic configuration to the product electronic configuration on a time scale that is much smaller compared to the nuclear dynamics through the transition state. [99]. This way, the total wave function Ψ_{tot} can be expressed as a product of two wave functions. Specifically, one wave function describes the nuclei, referred by $\chi(\hat{\mathbf{R}})$, and another describes the electrons, referred by $\psi(\hat{\mathbf{R}}, \hat{\mathbf{r}})$, for the electronic coordinates $\hat{\mathbf{r}}$ and the fixed nuclear coordinates $\hat{\mathbf{R}}$, such that

$$\Psi_{\text{tot}}\left(\hat{\mathbf{R}}, \hat{\mathbf{r}}\right) = \chi(\hat{\mathbf{R}})\psi(\hat{\mathbf{R}}, \hat{\mathbf{r}}). \tag{2.1}$$

The BO approximation allows to solve $\psi(\hat{\mathbf{R}}, \hat{\mathbf{r}})$ by first fixing the nuclear positions $\mathbf{R}$ and then solving the electronic part independently. In practice, this amounts to solving the electronic eigenstates for a large number of nuclear configurations. This results in the determination of an effective adiabatic potential energy surface (PES) depending solely on the nuclear coordinates $\mathbf{R}$. Such PESs are specific for each system and their electronic characteristics.

In this thesis and for the systems treated in **Chapters 3**, **4** and **5** the nuclei are assumed to follow a single adiabatic PES associated to the electronic ground state. This constitutes an excellent approximation for many reactive systems and collision energies of chemical interest with almost no impact on the accuracy of the simulations [100]. Detailed description of the BO approximation, its validity, generalization and the problem of deriving corrections to it are thoroughly discussed in the literature [101]. Various semi-empirical methods were originally employed to obtain approximate description of these potentials, mostly until the 1990s [102]. The construction of more accurate potential energy surface (PES) from accurate *ab initio* calculations followed [103]. For the rest of the thesis, V refers to a single adiabatic PES.

Assuming that an accurate PES is provided, propagating the nuclear motion can

be computationally very expensive and remains infeasible if one wants to simulate rigorously the quantum dynamics of chemical reactions involving more than five atoms [47]. A widely employed alternative approach that scales appropriately with the size of the system is the quasiclassical trajectory approach (QCT).

2.2 Quasiclassical trajectory method

Even though the dynamics of chemical processes take place on a microscopic scale where quantum effects can be dominant, many such phenomenon can to a good approximation be accurately simulated using classical dynamics [71, 104, 105]. Historically, the first classical simulations were performed for unimolecular and bimolecular systems [106]. For classical simulations, it is not clear how to initialize a molecule in a specific rovibrational configuration and neither is the comparison of the simulation results with the quantum mechanical counterpart. The most widely employed method which allows comparisons to be made between classical and quantum reactive scattering results is the quasiclassical trajectory method (QCT). The first QCT applications to gas-phase triatomic reactions with the description of quantal intramolecular vibrational dynamics date back to 1965 [64, 107]. Upon the determination of the PES, the first step in QCT simulations is the selection of initial conditions for the ensemble of trajectories to be computed depending on the quantum states we want to mimic classically.

2.2.1 Initial conditions for QCT simulations

Vibrational motion initialization

In quantum mechanics, the bound eigenstates of a system can only have certain discrete energy values. This is the case for the periodic motion of molecular vibrations. An approximate quantization rule for a one-dimensional periodic system is given by the well-kown Bohr-Sommerfeld quantization rule. It states that the corresponding action variable (or integral variable) I statisfies

$$I \doteq \frac{1}{\pi}\int_{q_<}^{q_>} d\,q\sqrt{2\mu[E-V(q)]} = (\nu+1/2)\hbar, \tag{2.2}$$

where V is the potential, μ is the reduced mass, $q_>$ and $q_<$ are the turning points of the motion and ν is a non-negative integer. The establishment of this formula is a delicate problem and has been considered in detail in the literature [108]. For one-dimensional systems, Eq. (2.2) has been worked out for many types of potential to very good approximations [109]. For complex molecules that are in general multidimensional non-separable systems, we have the following straightforward generalization of Eq. (2.2)

$$\mathcal{I}_i = (\nu_i + 1/2)\,\hbar \quad , i = 0, 1, 2, \ldots \tag{2.3}$$

where the $\mathcal{I}_i$'s are the action variables or adiabatic invariants of the system and the ν_i's are non-negative integers. Thus, the direct generalization can only be carried out by finding the action-angle variables of multidimensional non-separable systems. This is in general impossible without employing numerical methods or the techniques of perturbation theory [109].

The QCT method circumvents this difficulty for complex molecules by initially considering the harmonic approximation of the molecular potential. This way, the quantization rule in Eq. (2.2) can be carried out exactly for each independent vibrational motion. This forms the basis of the normal mode (NM) sampling procedure. The separable harmonic Hamiltonian H^0 can be written as

$$H^0 = \sum_{i=1}^{f} \left(\frac{P_i^2}{2} + \frac{\Omega_i^2 {Q_i}^2}{2} \right), \tag{2.4}$$

where P_i, Q_i are the mass-scaled momentum and position normal modes, ω_i is the harmonic frequency of the ith mode and f the number of vibrational modes. The f angle variables (ϕ_i, $i = 1, \ldots, f$) correspond to the phases of the harmonic oscillators and the f action variables to the contour integrals over the periodic motions $I_i = \oint P_i \, \mathrm{d}Q_i$ with $i = 1, \ldots, f$. Following the quantization scheme of Eq. (2.3) leads to have for each mass-scaled normal modes the coordinates

$$P_i = \left(\frac{\Omega_i I_i}{\pi} \right)^{1/2} \cos\phi_i, \quad Q_i = \left(\frac{I_i}{\Omega_i \pi} \right)^{1/2} \sin\phi_i, \tag{2.5}$$

where $\phi_i \in [0, 2\pi]$ is a random phase. Once the normal mode coordinates are sampled, the Cartesian coordinates are obtained by inverse transformation. The purpose of this sampling scheme is the determination of an ensemble of internal classical configurations corresponding to pre-selected vibrational eigenstates for the reactant molecules. The expression "quasiclassical" refers to this first step (also further steps can be added later) in which the molecule internal motion is prepared. These configurations will then be used as initial conditions for the vibrational motion. The assumption that molecular zero-point and excited motion can be described by the normal mode approximation holds in general to some extent [110]. It can be problematic in the presence of a strongly anharmonic potential and for higher excited states where the difference between the harmonic and correct quantum energy is large. These points and possible circumventions are discussed at the end of this chapter.

The initialization of excited rotational states is not covered in this thesis. Procedures to initialize quantal rotational motion accordingly with different degrees of elaboration can be found in the literature [111, 112].

Beyond the preparation of the vibrational states of the reactants, it is necessary to prepare the initial relative momentum and relative position of the reactants in order to study their reactive collisions.

Collision initialization

This thesis considers two reactants, a polyatomic molecule T and an atom X. The center of mass of the reactant molecule T is fixed at the origin of the coordinate system. The collision axis passes through the origin and points in the direction of the x-axis with unit vector $\boldsymbol{e_x}$. The coordinate system is oriented such that the vector joining the atom X and the center of mass of T lies in the $x-y$ plane. For each trajectory, T is randomly rotated around its center of mass and for a given impact parameter b we have for the position coordinates of the center of mass of T denoted $\bar{\mathbf{Q}}_{\mathrm{T}}$, and for the position coordinates of the atom X denoted $\mathbf{Q}_{\mathrm{X}}$,

$$\bar{\mathbf{Q}}_{\mathrm{T}} = \mathbf{0}, \quad \mathbf{Q}_{\mathrm{X}} = b\,\mathbf{e_y} - \sqrt{\rho_0^2 - b^2}\;\mathbf{e_x}, \tag{2.6}$$

where ρ_0 is the initial distance between X and the center of mass of T. The value of ρ_0 is required to be large enough so that the interaction potential between X and

T is initially negligible. Smaller ρ_0 values can be used to save computing time if suitable. This can be the case for high collision energies trajectories where the initial asymptotic regime plays a smaller role in the dynamics.

The momentum of the center of mass of T denoted by $\bar{\mathbf{P}}_{\mathrm{T}}$, and for the momentum of the atom X denoted by $\mathbf{P}_{\mathrm{X}}$, are set so that

$$\mathbf{P}_{\mathrm{tot}} = \mathbf{P}_{\mathrm{X}} + \bar{\mathbf{P}}_{\mathrm{T}} = \mathbf{0} \quad \text{and} \quad \mathbf{P}_{\mathrm{rel}} = \mu_{\mathrm{X,T}} \boldsymbol{V}_{\mathrm{rel}} = \sqrt{2\mu_{\mathrm{X,T}} E_{\mathrm{col}}}\, \mathbf{e}_{\mathbf{x}}, \tag{2.7}$$

where $\boldsymbol{V}_{\mathrm{rel}}$ is the relative velocity between the reactants, $\mu_{X,T} = \frac{m_{\mathrm{X}} m_{\mathrm{T}}}{m_{\mathrm{X}} + m_{\mathrm{T}}}$ is the reduced mass of the combined system and E_{col} is the initial collision energy between the two reactants.

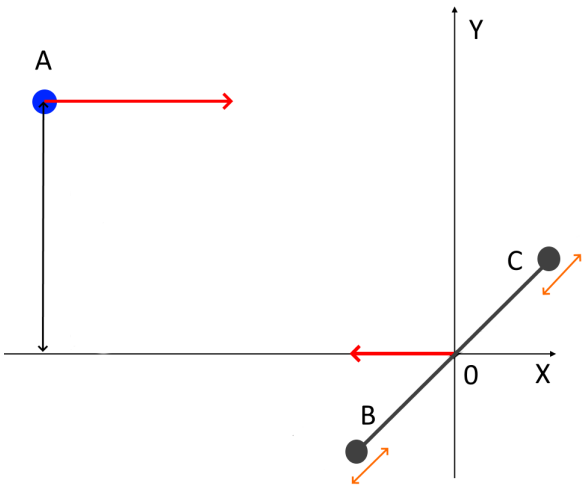

FIGURE 2.1: Illustration of the initial conditions for a triatomic system A+BC. The orange arrows indicate the motion along the vibrational mode. The red arrows indicate the translational motion of the reactants.

Once the initialization of the reactants' vibrational motion and collision is done, the time evolution is governed solely by the classical equations of motion for the point-like nuclei using the adiabatic PES V.

With the initial conditions defined as above, it is explained in the following section how to compute integral cross sections employing QCT.

2.2.2 Integral cross section

A major attribute of QCT is the efficient computation of reactivity dependencies on the collisional energy, the initial state of the reactants and the final states of the products. Such detailed information is contained in the integral cross section (ICS). It can be measured in sophisticated molecular beam experiments and is one of the most precise measurable quantity on chemical reactivity [17].

The reaction probability P_r of X and T (averaged over the different orientations of T) depends on the vibrational state of T labelled by the vector $\boldsymbol{\nu}$, the impact parameter b and the collision energy E_{col}. Having determined the fraction of reactive trajectories N_r among a total of N_{tot} trajectories, we have $P_r(E_{\text{col}}, \boldsymbol{\nu}, b) = N_r(E_{\text{col}}, \boldsymbol{\nu}, b)/N_{\text{tot}}(E_{\text{col}}, \boldsymbol{\nu}, b)$. The integral cross section $\sigma\left(E_{\text{col}}, \boldsymbol{\nu}\right)$ is then calculated as

$$\sigma\left(E_{\text{col}}, \boldsymbol{\nu}\right) = \int_0^{b_{\max}} P_r\left(E_{\text{col}}, \boldsymbol{\nu}, b\right)\, 2\pi\, b\, db, \tag{2.8}$$

where $b_{\max}$ is the maximal impact parameter beyond which no reaction occurs.
As a more convenient alternative to the direct integration of Eq. (2.8), the ICS can be evaluated using Monte Carlo techniques [113]. The simplest approach states that if $b^2/b_{\max}^2$ is sampled uniformly in the interval $(0, 1)$ for each trajectory, Eq. (2.8) can be computed as

$$\sigma\left(E_{\text{col}}, \boldsymbol{\nu}\right) = \pi b_{\max}^2 \lim_{N_{\text{tot}} \to \infty} \frac{N_r\left(E_{\text{col}}, \boldsymbol{\nu}\right)}{N_{\text{tot}}}. \tag{2.9}$$

The error in computing the ICS using this formula is proportional to $N_{\text{tot}}^{-\frac{1}{2}}$. It decreases rapidly at first and then in a slower fashion with N_{tot}. Thus, to obtain an accurate estimate is not too requiring compared to reaching high accuracy.

2.2.3 Product states considerations and binning techniques

The previous formula for the ICS in Eq. (2.9) does not consider the product states characteristics (beyond the fact that a reaction has occurred or not). However, the classical propagation of the nuclei ignores ZPE effects beyond the initial conditions. As a consequence, reactive QCT trajectories lead to products states covering a continuous range of internal vibrational energy. These energies can be far from the allowed quantum values and even below the zero-point energy value. To mitigate these side effects, binning techniques that can "filter" the products states have been

proposed. I briefly describe the two main binning techniques and their advantages and limitations.

A common feature of these procedures is the determination of non-integer classical harmonic action number for each vibrational mode of the product molecules. This procedure is by nature approximate and involves several steps. Briefly stated, the angular momentum of the molecule is first removed. Then, for each trajectory, a normal mode displacement within the harmonic approximation is extracted for each vibrational mode. From the normal mode coordinates, a classical harmonic action number ν'_k is determined for each normal mode k. A detailed description of this procedure can be found in the literature [76]. Finally, the closest integer quantum number n_k for each ν'_k is assigned leading to a vector $\boldsymbol{n}$.

For a given collision energy, the state-resolved probability for a collision to lead to a product with vibrational state $\boldsymbol{\nu}_f$ given the initial conditions $\boldsymbol{\nu}_i$ is

$$P_r(E_{\text{col}}, \boldsymbol{\nu}_i \to \boldsymbol{\nu}_f) = \frac{N_r\left(E_{\text{col}}, \boldsymbol{\nu}_i \to \boldsymbol{\nu}_f\right)}{N_{\text{tot}}}. \tag{2.10}$$

The question now is what is the best way to compute $P_r\left(E_{\text{col}}, \boldsymbol{\nu}_i \to \boldsymbol{\nu}_f\right)$ given a sample of product states each characterized by the non-integers ν'_k, labelled now as $\boldsymbol{\nu}'$. The straightforward approach is the so-called histogram binning (HB) procedure which assumes that

$$P_r^{\text{HB}}\left(E_{\text{col}}, \boldsymbol{\nu}_i \to \boldsymbol{\nu}_f\right) = \frac{N_r\left(E_{\text{col}}, \boldsymbol{\nu}_i \to \boldsymbol{\nu}_f = \boldsymbol{n}\right)}{N_{\text{tot}}}. \tag{2.11}$$

The issue of HB is that P_r^{HB} can be non-zero for energetically forbidden states and does not account for the discrete values of the vibrational quantum numbers. A widely used variant of the HB is the ZPE-corrected HB where products states with internal energies below the zero-point value are simply discarded.

An alternative technique is the Gaussian binning approach (GB). It assigns a Gaussian weight to each trajectory such that for each product $\boldsymbol{p}$ and each mode k the closer is $\nu'_{\boldsymbol{p},k}$ to its nearest integer, the larger is the associated weight. Details of such binning processes vary considerably as they are prone to some arbitrariness such as the width of the Gaussian weights and which products are considered. Examples and applications are given in Refs. [75,76,114]. However, when the number of vibrational modes is large, converging the GB simulations requires a very large number of trajectories as each trajectory is weighted by a product of Gaussian

weights. Moreover, applications of the GB shows that it does not lead systematically to more accurate ICS compared to HB or ZPE-corrected HB. This is especially the case around the reaction threshold energy [115].

2.2.4 Discussion

The quasiclassical trajectory method is one of the most popular tools to study molecular reaction dynamics. On the condition that an accurate PES is available, QCT allows for the efficient simulation of almost any chemical reaction owing to its favorable scalability with the number of atoms. Although nuclear quantum effects are not described in the dynamics (besides the correct initial vibrational and rotational quantum energies for the reactants), QCT can provide valuable atomistic insights into the reaction dynamics. It is especially valuable in the presence of complex reactions where QCT provided crucial insights into underlying mechanisms [69,71,116]. Moreover, QCT can yield reliable quantitative results if the spread of the nuclei coordinates covered by wave packets is small. This is typically the case when the collision energy is high and in the presence of heavy atoms [69,115].

QCT is relatively accurate for describing mode specificity for many polyatomic reactions. The normal mode sampled excited states are to some extent robust so that they usually live (on average) long enough for most practical purposes. However, substantial energy leakage can occur. This is problematic at very low collision energies for which the propagation time is long. The recently introduced adiabatic switching procedure for QCT has proven to lead to more accurate and stationary initial states [117]. Nevertheless, the leakage of energy between vibrational modes in the reactants is still present as the dynamics are classical. Also, zero-point energy can flow to the reaction coordinates during the collision [118]. This is exemplified in the reaction H+CH_4 and H+CHD_3 where QCT overestimates the reactivity [119].

Additionally, the final rovibrational energies of the collision products can take forbidden values. As discussed before, binning techniques can be used to mitigate such outcomes. However, while being mostly *ad-hoc*, such procedures do not systematically improve the results even though they usually predict reaction thresholds more accurately. On top of that, elaborate binning techniques such as GB become very expensive for complex molecules to reach appreciable convergence [77].

Besides, tunneling effects which can be dominant at low energies and in the presence of light atoms are absent in classical simulations. This fact coupled with

the absence of ZPE effects can produce undesired falsely accurate results as ignoring both effects can lead to error compensation [115].

Nuclear quantum effects are important factors to take into account when studying chemical reactions. Even more so if we are after the detailed knowledge of reactive mechanisms and state-selective reactivity information. Among prominent NQEs, tunneling and ZPE effects are the most common and can have great impact on the outcome of a wide range chemical reactions. Unfortunately, NQEs are either very or prohibitively expensive to describe using full-dimensional or reduced-dimensional quantum reactive scattering approaches for systems beyond 5 atoms. In this regard, alternative and efficient approaches to describe NQEs in chemical reactions are in high demand.

Path integral approaches provide an efficient way to describe approximately quantum dynamics at thermal equilibrium (using RPMD) and in the presence of specific non-equilibrium initial conditions (using NE-RPMD). The purpose of the rest of this chapter is to present the basics of ring polymer molecular dynamics (RPMD) and non-equilibrium ring polymer molecular dynamics (NE-RPMD). The conceptualization of the work done in this thesis finds its origin in the following theoretical content.

2.3 Path integral description of quantum statistics

This section discusses in some details the main aspects of the path integral molecular dynamics (PIMD) approach. PIMD allows for the efficient computation of static properties of quantum systems at equilibrium. The approach is based on the classical isomorphism allowing an exact path integral description of quantum systems governed by the quantum Boltzmann operator. The following section serves as a basis for the introduction of the ring polymer molecular dynamics (RPMD) approach.

2.3.1 The classical isomorphism

It is possible to map the expression of the quantum mechanical partition function $Z = \mathrm{tr}[e^{-\beta\hat{H}}]$ onto the expression of a classical partition function in an extended phase space. For clarity we start by considering a non-relativistic atom in one spatial dimension at inverse temperature β governed by a potential V. The properties that will be derived here are directly generalizable to multiple particles in multiple dimensions. The Hamiltonian reads

$$\hat{H} = \frac{\hat{p}^2}{2m} + V(\hat{q}) \doteq \hat{T} + \hat{V}. \tag{2.12}$$

The quantum partition function Z, with the trace operator expanded over the position eigenstates, reads

$$Z = \mathrm{tr}[e^{-\beta\hat{H}}] = \int dq \, \langle q|e^{-\beta(\hat{T}+\hat{V})}|q\rangle. \tag{2.13}$$

Using the Trotter identity [120]

$$e^{-\beta(\hat{T}+\hat{V})} = \lim_{n\to\infty} \Omega^n \;\text{ with }\; \Omega = e^{-\frac{\beta}{2n}\hat{V}} e^{-\frac{\beta}{n}\hat{T}} e^{-\frac{\beta}{2n}\hat{V}}, \tag{2.14}$$

and inserting $n-1$ times the identity operator $\hat{I} = \int dq|q\rangle\langle q|$ in the integrand of Eq. (2.13) leads to the expression

$$\begin{aligned} Z &= \lim_{n\to\infty} \int dq^{(1)} \cdots dq^{(n)} \left\langle q^{(1)}|\Omega|q^{(2)}\right\rangle \left\langle q^{(2)}|\Omega|q^{(3)}\right\rangle \left\langle q^{(3)}|\cdots|q^{(n)}\right\rangle \left\langle q^{(n)}|\,\Omega\,|q^{(1)}\right\rangle \\ &= \lim_{n\to\infty} \int dq^{(1)} \cdots dq^{(n)} \left[\prod_{k=1}^{n} \left\langle q^{(k)}|\Omega|q^{(k+1)}\right\rangle\right]_{q^{(1)}=q^{(n+1)}} . \end{aligned} \tag{2.15}$$

The superscript notation (k) will turn out to be practical when later multiple atoms are considered. To evaluate[1]

$$\left\langle q^{(k)}|\,\Omega\,|q^{(k+1)}\right\rangle = e^{-\frac{\beta}{2n}V\left(q^{(k)}\right)} \left\langle q^{(k)}\left|e^{-\frac{\beta}{n}\hat{T}}\right|q^{(k+1)}\right\rangle e^{-\frac{\beta}{2n}V\left(q^{(k+1)}\right)}, \tag{2.16}$$

$\hat{T} = \hat{p}^2/(2m)$ is written via its spectral decomposition using momentum eigenstates $|p\rangle$ so that

$$\left\langle q^{(k)}|\Omega|q^{(k+1)}\right\rangle = \int dp\, e^{-\beta p^2/(2mn)} e^{-\frac{\beta}{2n}V\left(q^{(k)}\right)} \left\langle q^{(k)}\mid p\right\rangle \left\langle p\mid q^{(k+1)}\right\rangle e^{-\frac{\beta}{2n}V\left(q^{(k+1)}\right)} \tag{2.17}$$

$$= \left(\frac{m\,n}{2\pi\beta\hbar^2}\right)^{1/2} \exp\left[-\frac{m\,n}{2\beta\hbar^2}\left(q^{(k)}-q^{(k+1)}\right)^2 - \frac{\beta}{2n}\left(V\left(q^{(k)}\right)+V\left(q^{(k+1)}\right)\right)\right]. \tag{2.18}$$

Thus, the partition function Z (Eq. (2.13)) can be written as

$$\begin{aligned} Z &= \lim_{n\to\infty} \left(\frac{m\,n}{2\pi\beta\hbar^2}\right)^{n/2} \int d\mathbf{q} \exp\left(-\frac{\beta}{n}\sum_{k=1}^{n}\left[\frac{m\omega_n^2}{2}\left(q^{(k)}-q^{(k+1)}\right)^2 + V\left(q^{(k)}\right)\right]\right) \\ &\doteq \lim_{n\to\infty} \left(\frac{m\,n}{2\pi\beta\hbar^2}\right)^{n/2} \int d\mathbf{q}\, e^{-\beta_n\phi_n(\mathbf{q})} \\ &\doteq \lim_{n\to\infty} Z_n, \end{aligned} \tag{2.19}$$

where $\mathbf{q}$ is the vector $\left(q^{(1)},\ldots,q^{(n)}\right)^T$ with the notation $q^{(1)} = q^{(n+1)}$, $\omega_n = n/(\beta\hbar) \doteq 1/(\beta_n\hbar)$ and $\phi_n(\mathbf{q}) = \sum_{k=1}^{n}\left(\frac{m\omega_n^2}{2}\left(q^{(k)}-q^{(k+1)}\right)^2 + V\left(q^{(k)}\right)\right)$. In Eq. (2.19) Z is expressed as a classical partition function involving an infinite dimensional phase space. For finite n the paritition function Z_n converges to Z with an error of the order $|Z-Z_n| = \mathcal{O}(1/n^2)$ [121]. This so-called classical isomorphism opens up the

[1]The Trotter formula introduces an error only of order $(\beta/n)^3$ for each evaluation of the matrix element in Eq. (2.16). In contrast, the high-temperature expansion error is of order β^3.

possibility to relate equilibrium quantum many-body theory to classical statistical mechanics in an extended phase space. The quantum partition function expressed in Eq. (2.19) and thermal expectation values for position dependent operators can at this stage be computed employing Monte Carlo sampling techniques[2] [122].

The fictional classical system implied by $\phi_n(\mathbf{q})$ can be interpreted as n replicas (also termed beads) of the original system joined by harmonic springs together forming a closed ring polymer like a necklace. The classical partition function Z_n thus describes a ring polymer (RP) with a canonical distribution at n times the physical temperature. The periodic condition on the beads reflects the fact that the trace operation has to be performed for computing the partition function. The RP structure arises in the discretized path integral classical description of the matrix elements of the quantum Boltzmann operator $e^{-\beta\hat{H}}$ with each bead corresponding to a "slice" of the Boltzmann operator arising with the factorization of the kinetic energy operator in Eq. (2.17). The force constant of the springs is $m\omega_n^2 = \frac{m\,n}{2\pi\beta\hbar^2}$. Thus, the springs become stiffer with higher temperature so that in the limit $\beta \to 0$ the ring polymer shrinks to a point particle. This leads to purely classical dynamics. The finite spatial extension of the ring polymers accounts for the spatial fluctuations due to the quantum mechanical fluctuation at finite temperature.

Once the isomorphism has been established, it is left to find how to calculate the quantities of interest from the ring polymer coordinates. In a similar fashion as done in the derivation of the partition function, it is possible to write for the expectation value of a position dependent operator $A(\hat{q})$

$$\langle A(\hat{q})\rangle = \frac{1}{Z}\,\mathrm{tr}\left[e^{-\beta\hat{H}}A(\hat{q})\right] \tag{2.20}$$

$$= \frac{1}{Z}\,\mathrm{tr}\left[\left(e^{-\beta_n\hat{H}}\right)^{k-1}A(\hat{q})\left(e^{-\beta_n\hat{H}}\right)^{n+1-k}\right] \tag{2.21}$$

$$\overset{n\to\infty}{=} \frac{1}{Z_n}\int dq^{(1)}\ldots\int dq^{(n)}\left\langle q^{(1)}\left|e^{-\beta_n\hat{H}}\right|q^{(2)}\right\rangle\ldots\left\langle q^{(n)}\left|e^{-\beta_n\hat{H}}\right|q^{(1)}\right\rangle A\left(q^{(k)}\right). \tag{2.22}$$

[2]This constitutes the Path Integral Monte Carlo approach (PIMC).

Using the cyclic relabelling of the position coordinates, one obtains

$$\langle A(\hat{q})\rangle = \lim_{n\to\infty} \frac{1}{Z_n}\left(\frac{m\,n}{2\pi\beta\hbar^2}\right)^{n/2} \int d\mathbf{q} e^{-\beta_n \phi_n(\mathbf{q})} \mathcal{A}_n(\mathbf{q}), \tag{2.23}$$

where

$$\mathcal{A}_n(\mathbf{q}) \doteq \frac{1}{n}\sum_{k=1}^{n} A\left(q^{(k)}\right), \tag{2.24}$$

is the *path integral estimator* (or simply *estimator*) of the operator $\hat{A}$. In section 2.3.2 important estimators will be discussed. In practice, appreciable convergence is achieved for a reasonable number of beads depending on the system, the temperature and the observable. In general, the lower the temperature and the higher the frequencies of the physical potential, the higher is the needed number of beads to converge Eq. (2.23). Fig. 2.2 illustrates the classical isomorphism for a single atom.

The present result states that static equilibrium properties can be computed (exactly if $n \to \infty$) via a classical integral involving a configurational average over an extended phase space with the effective potential $\phi_n(\mathbf{q})$. In other words, the task of computing Eq. (2.24) now amounts to generating configurations consistent with a probability distribution $\propto e^{-\beta_n\phi_n}$ and averaging over the values that the estimator takes over these configurations.

FIGURE 2.2

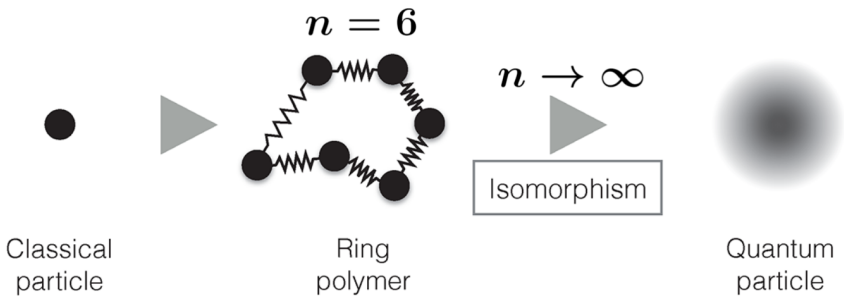

In 1984, Parrinello and Rahman [78] suggested the introduction of artificial momenta for each bead in order to allow the use of molecular dynamics (MD) as a

sampling tool to explore the RP phase space. In other words, the statistical sampling of the configurations of the classical problem established by $\phi_n(\mathbf{q})$ can be performed by generating ring polymer trajectories assuming ergodicity [123, 124].
The momenta are introduced using the identity

$$1 = \left(\frac{\beta_n}{2\pi m'}\right)^{n/2} \int d\mathbf{p} \exp\left[-\beta_n \sum_{k=1}^{n} \frac{\left(p^{(k)}\right)^2}{2m'}\right], \tag{2.25}$$

where $\mathbf{p}$ is the vector $\left(p^{(1)}, \ldots, p^{(n)}\right)^T$ and m' is some arbitrary mass associated to the beads of the ring polymer. This expression is inserted into Eq. (2.19) and Eq. (2.23) to yield

$$Z_n = \frac{1}{(2\pi\hbar)^n} \int d\mathbf{p} \int d\mathbf{q} e^{-\beta_n H_n(\mathbf{p},\mathbf{q})}, \tag{2.26}$$

and

$$\langle A(\hat{q})\rangle = \frac{1}{(2\pi\hbar)^n Z_n} \left(\frac{m}{m'}\right)^{n/2} \int d\mathbf{p} \int d\mathbf{q} e^{-\beta_n H'_n(\mathbf{p},\mathbf{q})} \mathcal{A}_n(\mathbf{q}) \doteq \langle \mathcal{A}_n(\mathbf{q})\rangle_n, \tag{2.27}$$

where H'_n is

$$H'_n(\mathbf{p},\mathbf{q}) = \sum_{k=1}^{n} \left(\frac{(p^{(k)})^2}{2m'} + \frac{1}{2} m\omega_n^2 \left(q^{(k)} - q^{(k+1)}\right)^2 + V\left(q^{(k)}\right)\right), \tag{2.28}$$

with $q^{(1)} = q^{(n+1)}$. Classical dynamics with the conjugate variables $(q^{(k)}, p^{(k)})$ for $k = 1, \ldots, n$ can be performed using H'_n as the Hamiltonian of the dynamics to sample the ring polymer phase space. The use of bead momenta leads to dynamics in a ring polymer phase space consisting of $f = 2 \times D \times N \times n$ degrees of freedeom (d.o.f.), where N is the number of atoms in the system and D is the number of spatial dimensions. So far, the generated trajectories do not hold any real dynamical meaning and are just a computational tool. The procedure is valid for any choice of mass m', albeit with differences in the efficiency of the sampling [125].

In this thesis, the mass is chosen such that $m' = m$, where m is the actual physical mass of the particle. It will be shown in Sec. 2.4 that this choice is linked to the ring polymer molecular dynamics approach (RPMD). With this choice, H_n is the ring polymer Hamiltonian and the corresponding distribution

$$\rho_n(\mathbf{p},\mathbf{q}) = \frac{1}{(2\pi\hbar)^n Z_n} e^{-\beta_n H_n(\mathbf{p},\mathbf{q})} \tag{2.29}$$

is the ring polymer Boltzmann distribution (or ring polymer distribution) for n beads. From now on, averages with respect to the distribution ρ_n will be denoted $\langle . \rangle_n$ (cf. Eq. (2.27) with $m' = m$). The ring polymer trajectories are integrated from the phase space points $(\mathbf{q}(0), \mathbf{p}(0))$ to $(\mathbf{q}(t), \mathbf{p}(t))$ using

$$\frac{d\mathbf{p}(t)}{dt} = -\frac{\partial H_n\left(\mathbf{p}(t), \mathbf{q}(t)\right)}{\partial \mathbf{q}(t)} \quad \text{and} \quad \frac{d\mathbf{q}(t)}{dt} = \frac{\partial H_n\left(\mathbf{p}(t), \mathbf{q}(t)\right)}{\partial \mathbf{p}(t)}, \tag{2.30}$$

i.e. for $k = 1, \ldots, n$,

$$\begin{aligned} \frac{dq^{(k)}}{dt} &= \frac{\partial H_n\left(\mathbf{p}, \mathbf{q}\right)}{\partial p^{(k)}} = \frac{p^{(k)}}{m}, \\ \frac{dp^{(k)}}{dt} &= -\frac{\partial H_n\left(\mathbf{p}, \mathbf{q}\right)}{\partial q^{(k)}} = -m\omega_n^2\left[2q^{(k)} - q^{(k+1)} - q^{(k-1)}\right] - \frac{\partial V\left(q^{(k)}\right)}{\partial q^{(k)}}, \end{aligned} \tag{2.31}$$

with $q^{(0)} \equiv q^{(n+1)} = q^{(1)}$.

The numerical implementation of the equations of motion in Eq. (2.31) will be discussed in details in Sec. 2.4.3. The use of the ring polymer trajectories constitutes the path integral molecular dynamics approach (PIMD) and is an attractive alternative to Monte Carlo techniques. However, most ring polymer systems are nonergodic[3] [126]. The RP dynamics can be attached to a thermostat[4] so that the RP trajectories adequately and efficiently sample the phase space [121]. The implementation of the Langevin thermostat for PIMD is explained in Appendix B.

The generalization of the ring polymer Hamiltonian H_n to an arbitrary number N of particle in three dimensions corresponding to the Hamiltonian

$$\hat{H} = \sum_{i=1}^{N} \frac{\hat{\mathbf{p}}_i^2}{2m_i} + \hat{V}\left(\mathbf{q}_1, \ldots, \mathbf{q}_N\right) \tag{2.32}$$

is

$$H_n(\mathbf{p}, \mathbf{q}) = \sum_{i=1}^{N}\sum_{k=1}^{n}\left(\frac{\left(\mathbf{p}_i^{(k)}\right)^2}{2m_i} + \frac{1}{2}m_i\omega_n^2\left(\mathbf{q}_i^{(k)} - \mathbf{q}_i^{(k+1)}\right)^2\right) + \sum_{k=1}^{n} V\left(\mathbf{q}_1^{(k)}, \ldots, \mathbf{q}_N^{(k)}\right), \tag{2.33}$$

[3]The high frequency modes of the ring polymer are usually far out of resonance with the external potential so that the energy exchange between the modes is very slow or non-existent.

[4]The periodic resampling of the bead momenta according to the RP Boltzmann distribution during the propagation is the simplest example of such a procedure.

where the three-dimensional vector $\mathbf{q}_i^{(k)}$ refers to kth bead of the ith particle and similarly for the momenta. This notation is used for the rest of the thesis. Fig. 2.3 illustrates how the interaction between two atoms is described via the interaction between two corresponding ring polymers (the interaction via V is represented by a dotted line) according to Eq. (2.33). The internal spring interaction is represented in the figure by the black springs. The ring polymer equations of motion lead each bead of each atom to interact via the physical potential V with the corresponding bead (of same index) of the other atoms bijectively. Thus, a given bead interacts through the physical potential with the $N-1$ other corresponding beads while also interacting through the spring term with its neighbouring beads of the same atom.

FIGURE 2.3: Sketch of the ring polymer representation (right) of a quantum system (left) consisting of two interacting particles.

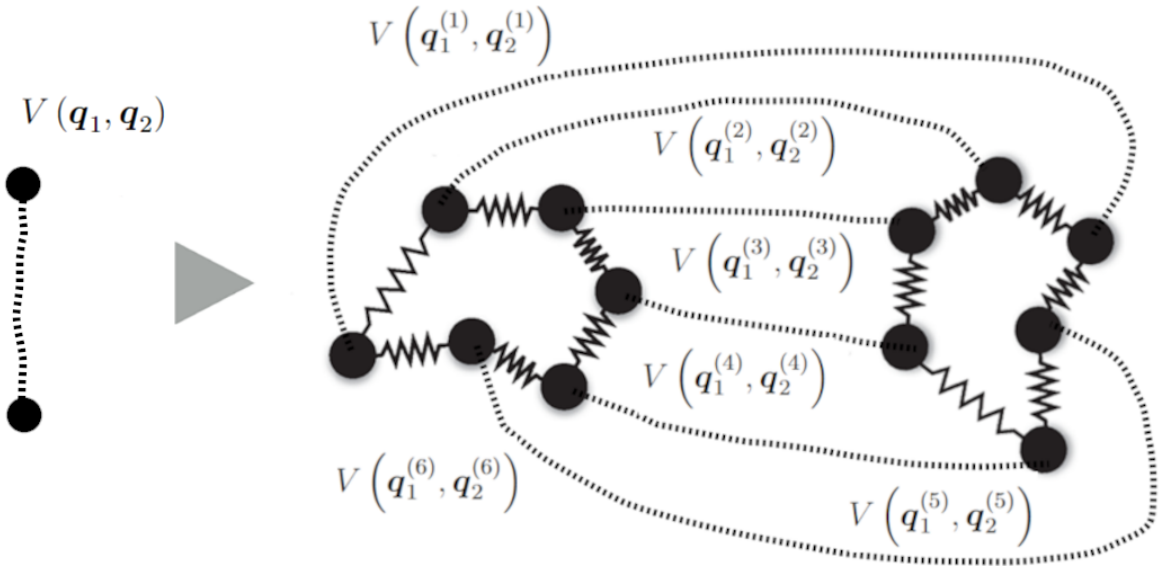

It is worthwhile to note at this point that the usual quantities (e.g. the total energy, kinetic energy and action) can have different meaning in PIMD. In particular, H_n does not correspond to the expression for the total energy of the ring polymer system but to its action. In this thesis, it is sufficient to take note of the latter subtlety. A detailed discussion about this shift of vocabulary can be found in section D of Ref. [127]. The next section explains how to compute the energy in PIMD.

2.3.2 Path integral estimators

In quantum mechanics, observables can be computed with operators but it is not apparent how a specific operator can be expressed within the classical isomorphism. To compute expectation values of an observable, the correct expression of its path integral expression, the estimator, has to be derived and averaged according to the ring polymer distribution. Thus, estimators play a key role in path integral calculations. Estimators are not unique and are strongly correlated to the choice of Hamiltonian employed to compute the static properties (e.g. using PIMD or PIMC). Also different estimators can have the same average value but converge more or less rapidly with the number of beads and sampled ring polymer configurations.

The simplest case is the estimator for the potential energy and more generally any observable that depends strictly on the position of the atoms. This could be the bond length or a molecular configuration. We have seen already the case of expectation values of general position dependent operators in Sec. 2.3.1. The expectation value of the potential $\langle V(\hat{q})\rangle$ reads

$$\begin{aligned}\langle V(\hat{q})\rangle &= \lim_{n\to\infty} \frac{1}{(2\pi\hbar)^n Z_n} \int d\mathbf{p} \int d\mathbf{q} e^{-\beta_n H_n(\mathbf{p},\mathbf{q})} \frac{1}{n}\sum_{k=1}^{n} V\left(q^{(k)}\right) \\ &= \lim_{n\to\infty} \langle \mathcal{V}_n(\mathbf{q})\rangle_n,\end{aligned} \tag{2.34}$$

where $\mathcal{V}_n(\mathbf{q}) = \frac{1}{n}\sum_{k=1}^{n} V\left(q^{(k)}\right)$ is the path integral estimator of the potential operator $V(\hat{q})$. The estimator of the potential energy turns out to be intuitive and unambiguous.

The simplest form of the total energy estimator can be obtained via direct temperature differentiation of the partition function

$$E = \langle \hat{H}\rangle = \lim_{n\to\infty}\left(\frac{-\partial \ln Z_n}{\partial\beta}\right) \approx -\frac{1}{Z_n}\left(\frac{\partial Z_n}{\partial\beta}\right), \tag{2.35}$$

yields

$$E = \lim_{n\to\infty} \frac{1}{(2\pi\hbar)^n Z_n} \int d\mathbf{p} \int d\mathbf{q} e^{-\beta_n H_n(\mathbf{p},\mathbf{q})} \mathcal{E}_n(\mathbf{p},\mathbf{q}), \tag{2.36}$$

with

$$\mathcal{E}_n(\mathbf{p},\mathbf{q}) = \frac{1}{n}\sum_{k=1}^{n}\frac{(p^{(k)})^2}{2m} - \frac{1}{n}\sum_{k=1}^{n}\frac{m\omega_n^2}{2}\left(q^{(k)} - q^{(k+1)}\right)^2 + \frac{1}{n}\sum_{k=1}^{n} V\left(q^{(k)}\right). \tag{2.37}$$

The kinetic energy estimator can now be extracted using $\mathcal{T}_n$ since $\mathcal{E}_n \equiv \mathcal{T}_n + \mathcal{V}_n$ we have

$$\mathcal{T}_n(\mathbf{p},\mathbf{q}) = \frac{1}{n}\sum_{k=1}^{n}\frac{(p^{(k)})^2}{2m} - \frac{1}{n}\sum_{k=1}^{n}\frac{m\omega_n^2}{2}\left(q^{(k)} - q^{(k+1)}\right)^2. \tag{2.38}$$

Eq. (2.38) constitutes the so-called "primitive" kinetic energy estimator. These estimators are special because they are functions of both coordinate and momentum coordinates and can be evaluated via cyclic (using ring polymers) path integrals. More general momentum dependent coordinates are more complicated to derive and generally involve open-chain ring polymers [127]. These are not discussed here. Nevertheless, it is shown in the next chapter that they can be computed naturally withing the framework of ring polymer molecular dynamics. The drawback of the primitive energy estimator is that it converges very slowly. This is because each averaged term in Eq. (2.38) scales linearly with n, thus leading the variance to also grow linearly with n. The number of beads necessary to converge PIMD results depend on the observable, the temperature and the system. A widely used minimum value for n is $\hbar\beta\omega_{\text{max}}/2$ where ω_{max} is the highest frequency present in the physical system. This criterion can be interpreted as constraining the average distance between neighboring beads to be shorter than the characteristic length of the potential [128].

There are other equivalent (leading to the same average value) energy estimators where the ill-behaved terms are eliminated and that converge much faster [129]. In this thesis, only the primitive form of the energy estimator involving explicitely the momentum coordinates $\mathcal{E}_n(\mathbf{p},\mathbf{q})$ is considered. This is because the estimator needs to account for non-equilibrium conditions which will be employed later in **Chapters 3**, **4** and **5**. Thus, only the most general (but also crude) momentum and position dependent expression of the energy estimator can be used to account for the non-equilibrium dynamics.

The kinetic energy estimator is rather counter-intuitive as it is the *difference* between the sum of all the kinetic energies of the beads $U_n^{\text{kin}}(\boldsymbol{p}) = \frac{1}{n}\sum_{k=1}^{n}\frac{(p^{(k)})^2}{2m}$ and the energy contained in the springs $U_n^{\text{springs}}(\boldsymbol{q}) = \frac{1}{n}\sum_{k=1}^{n}\frac{m\omega_n}{2}(q^{(k)}-q^{(k+1)})^2$. It is possible for the kinetic energy estimator to take negative values even though the averaged values over many ring polymer configurations will always lead to positive values. It is instructive to compute the average value of the kinetic energy estimator in the case of the harmonic potential. For a one-dimensional system with a potential of

the form $V(q) = \frac{m\omega^2}{2}q^2$ we have[5]

$$\langle U_n^{\text{kin}}(\boldsymbol{p})\rangle_n = \frac{n}{2\beta}, \tag{2.39}$$

$$\langle U_n^{\text{springs}}(\boldsymbol{q})\rangle_n = \frac{n}{2\beta} - \frac{\hbar\omega}{4}\coth(\beta\omega/2) + O(1/n^2), \tag{2.40}$$

so that $\langle \mathcal{T}_n\rangle_n \overset{n\to\infty}{=} \frac{\hbar\omega}{4}\coth(\beta\omega/2)$. It also possible to show[6] that $\langle \mathcal{V}_n\rangle_n \overset{n\to\infty}{=} \frac{\hbar\omega}{4}\coth(\beta\omega/2)$. As one can see from Eqs. (2.39) and (2.40), half of the quantum thermal energy is contained in the springs. This is the simplest manifestation of the fact that the internal ring polymer structure accounts for the ZPE effects [7].

There exist relatively intuitive coordinates within the ring polymer phase space. They are the so-called position and momentum " centroid" coordinates. The following example illustrates the concept of centroid as it is helpful for the understanding of the next Chapters.

Example : ***Several properties of the "free" ring polymer and its centroids.***
In this example a free ring polymer ($V = 0$) in one spatial dimension consisting of n beads at inverse temperature β with the physical mass m associated to the momenta is considered. The centroid momentum and position vector coordinates $\boldsymbol{q}^c, \boldsymbol{p}^c$ read

$$\boldsymbol{q}^c = \frac{1}{n}\sum_{k=1}^{n}\boldsymbol{q}^{(k)}, \quad \boldsymbol{p}^c = \frac{1}{n}\sum_{k=1}^{n}\boldsymbol{p}^{(k)}. \tag{2.41}$$

The averaged kinetic energy estimator for n beads in the free case is[8]

$$\begin{aligned}\langle \mathcal{E}_n\rangle_n &= \left\langle \frac{1}{n}\sum_{k=1}^{n}\left(\frac{\left(\boldsymbol{p}^{(k)}\right)^2}{2m} - \frac{m\omega_n^2}{2}(\boldsymbol{q}^{(k)} - \boldsymbol{q}^{(k+1)})^2\right)\right\rangle_n \\ &= \left\langle \frac{(\boldsymbol{p}^c)^2}{2m}\right\rangle_n = \frac{1}{2\beta}.\end{aligned} \tag{2.42}$$

This implies that the entire energy of the free ring polymer is contained on average in its centroid momentum. Also, it has the same average kinetic energy of a classical particle at reciprocal temperature β. The standard deviation of the position and

[5] See the fourth property of Appendix A for the proof.
[6] See the third property of Appendix A for the proof.
[7] Note that PIMD cannot be applied for arbitrary potentials as $V(\boldsymbol{q})$ must be differentiable.
[8] See the second property in Appendix A for details.

momentum of the beads is given by

$$\Delta q \doteq \left\langle \frac{1}{n}\sum_{k=1}^{n}\left|\mathbf{q}^{(k)}-\mathbf{q}^{c}\right|^{2}\right\rangle^{1/2}, \quad \Delta p^{c} \doteq \sqrt{\left\langle (\boldsymbol{p}^{c})^{2}\right\rangle}, \tag{2.43}$$

respectively. Δq can be interpreted as the average spatial extension of the ring polymer. It is possible to show that for any number of beads

$$\Delta q = \frac{1}{2}\sqrt{\frac{\hbar^{2}\beta}{m}}, \quad \Delta p^{c} = \sqrt{m/\beta}. \tag{2.44}$$

It is observed that Δq is proportional to the thermal de Broglie wavelength $\lambda(\beta) = \sqrt{\frac{2\pi\hbar^{2}\beta}{m}}$. This stems from the ring polymer description of the spatial spreading of a thermal wave packet. One can interpret the centroid coordinates of the ring polymer as the "most classical" coordinates in the ring polymer phase space. Indeed, the momentum fluctuation term Δp^{c} is equal to the average momentum of the free classical point particle of mass m at inverse temperature β.

2.4 Ring polymer molecular dynamics

In the previous section, we saw that PIMD involves artificial momenta to allow the use of molecular dynamics simulations to sample ring polymer configurations. The present section shows that, remarkably, the ring polymer phase space with the choice of masses $m_i' = m_i$ associated to the momenta, can be used to compute approximately *dynamical* quantum properties for systems at thermal equilibrium. This constitutes the ring polymer molecular dynamics (RPMD) approach. It will be explained how RPMD emerges as a practical approximation of Matsubara dynamics. Matsubara dynamics was recently derived as a very general form of quantum-Boltzmann-conserving classical dynamics theory that approximates Kubo-transformed time-correlation functions (TCFs) [81]. This section begins by explaining the particularity of the Kubo-transformed TCFs and its connection to the classical isomorphism.

2.4.1 Kubo-transformed time-correlation functions

So far, only static properties were discussed. The natural connection to dynamical properties is made by stating that static equilibrium ensemble averages of a product of two operators are equilibrium time-correlation functions (TCF) at $t = 0$. TCFs provide a link between theory and experiments for dynamical properties and arise in linear response theory [130]. From the previous section, it is known that RPMD is exact at $t = 0$ for the evaluation of the commonly used "standard" quantum TCF $C_{AB}(t)$ of two position dependent operators, $\hat{A}$ and $\hat{B}$, within a canonical ensemble which reads

$$C_{AB}(t) = \frac{1}{Z} \operatorname{tr}\left[e^{-\beta\hat{H}}\hat{A}e^{i\hat{H}t/\hbar}\hat{B}e^{-i\hat{H}t/\hbar}\right]. \tag{2.45}$$

In general, for $t > 0$ $C_{AB}(t)$ takes complex values and does not satisfy the detailed-balance condition ($C_{AB}(t) \neq C_{BA}(-t)$) which has to be respected by an approach employing classical dynamics. Consequently, RPMD cannot describe $C_{AB}(t)$ for $t > 0$. If RPMD approximates quantum dynamics, it naturally should approximate to some extent some kind of equilibrium quantum TCFs for $t > 0$ or at least in the vicinity of $t = 0$. A better suited candidate is the Kubo-transformed time-correlation function [131] which also arises naturally in the quantum generalisation of linear response theory [132]. The Kubo TCF, denoted as $K_{AB}(t)$, is an equivalent symmetrized form of Eq. (2.45) and reads

$$K_{AB}(t) = \frac{1}{Z\beta}\int_0^\beta d\lambda \operatorname{tr}\left[e^{-(\beta-\lambda)\hat{H}}\hat{A}e^{-\lambda\hat{H}}e^{i\hat{H}t/\hbar}\hat{B}e^{-i\hat{H}t/\hbar}\right]. \tag{2.46}$$

$K_{AB}(t)$ only takes real values and satisfies the detailed-balance condition [81]. Also, no information about the dynamics is lost by computing $K_{AB}(t)$ instead of $C_{AB}(t)$ as both are related by their Fourier transforms $\widetilde{K}_{AB}(\omega)$ and $\widetilde{C}_{AB}(\omega)$ such that

$$\widetilde{C}_{AB}(\omega) = \frac{\beta\omega\hbar}{1 - e^{-\beta\omega\hbar}}\widetilde{K}_{AB}(\omega). \tag{2.47}$$

Moreover, it is possible to show that

$$\lim_{t\to 0} K_{AB}(t) = \lim_{n\to\infty} \langle A_n(\mathbf{q})B_n(\mathbf{q})\rangle_n, \tag{2.48}$$

where

$$\langle A_n(\mathbf{q})B_n(\mathbf{q})\rangle_n = \frac{1}{(2\pi\hbar)^n Z_n}\int d\mathbf{p}\int d\mathbf{q}\, e^{-\beta_n H_n(\mathbf{p},\mathbf{q})}A_n(\mathbf{q})B_n(\mathbf{q}), \tag{2.49}$$

with $A_n(\mathbf{q}) = \frac{1}{n}\sum_{k=1}^{n} A(q^{(k)})$ and same for $B_n(\boldsymbol{q})$ [80].

Taking the dynamics of the ring polymers literally to compute $K_{AB}(t)$ for $t > 0$ such that

$$K_{AB}(t) \simeq \frac{1}{(2\pi\hbar)^n Z_n} \int d\mathbf{p}_0 \int d\mathbf{q}_0 e^{-\beta_n H_n(\mathbf{p}_0,\mathbf{q}_0)} A_n(\mathbf{q}_0)\, B_n(\mathbf{q}(t))\,, \tag{2.50}$$

with $(\mathbf{p}_0, \mathbf{q}_0)$ the initial conditions was first considered in an *ad hoc* manner by Manolopoulos and Craig in 2004 [80]. Their related paper reported simulation results showing that RPMD yields superior TCF results compared to classical simulations. Subsequently, various applications of RPMD followed (thermal rates, diffusion coefficients, vibrational spectra) [83, 84].

Kubo TCFs of certain non-local operators such as the velocity operator can be computed naturally within the RPMD approach. Appendix C illustrates the case of the velocity autocorrelation function.

The subject of the next section is the theoretical derivation of RPMD that was first established in 2015.

2.4.2 Theoretical justification of RPMD

The derivation of RPMD requires a certain amount of technicalities which have little relevance for the rest of the thesis. Thus, this subsection discusses only qualitatively the nature of the derivation and what information is provided from it. For the shorter and self-contained detailed explanation, the reader is referred to the very well written review of RPMD by Prof. Stuart C. Althorpe in Ref. [133]. For the complete derivation of RPMD, the reader is referred to Refs. [81, 82].

Recent works from Hele *et al.* have established a natural connection between RPMD and Matsubara dynamics [82]. Matsubara dynamics approximates the quantum Kubo-transformed time-correlation function $K_{AB}(t)$ in Eq. (2.46). For simple systems, Matsubara dynamics gives time-correlation functions which are in close agreement with the exact quantum results [81]. In a nutshell, Matsubara dynamics are classical dynamics that satisfies quantum Boltzmann statistics. However, it is not a practical method for realistic systems due to the sign problem emerging from the presence of the Matsubara phase. Removing parts of the Matsubara Liouvillian in order to remove the Matsubara phase leads to RPMD. Thus, RPMD emerges as a

practical approximation of Matsubara dynamics. What is learned from the derivation is now stated succinctly below. Starting with the beneficial properties, RPMD

1. is exact in the high temperature limit $\beta \to 0$
2. is exact in the short time limit $t \to 0$
3. is exact in the harmonic limit for linear operators
4. computes exactly $K_{1B}(t) = \frac{1}{Z}\,\mathrm{tr}\left[e^{-\beta\hat{H}}\hat{B}\right]$

The last point states that RPMD is consistent at all times with the quantum Boltzmann statistics.

As mentioned above, the derivation of RPMD relies on the speculative choice of discarding parts of the Matsubara Liouvillian. Thus, it is difficult to forecast the error in the dynamics for realistic systems. Nevertheless, the derivation can shed light on parts of the inherent drawbacks of RPMD. In particular, RPMD does not describe interference effects because Matsubara dynamics are themselves classical. Also, it can be shown that the discarded part of the Matsubara Liouvillian does not act directly on the *centroids* dynamics. Thus, with the exception of the harmonic regime with linear operators, it is expected that with time this can lead to an appreciable error in the dynamics. Other consequences are that RPMD is expected to break down more rapidly for non-linear operators and in the presence of strongly anharmonic potentials. Indeed, strong anharmonicities in the potential and notably the non-linear character of operators promote the coupling of the centroid and non-centroid dynamics and thus should lead to more inaccuracies. In a nutshell, regarding the disadvantageous properties, RPMD

1. does not describe interference effects and lacks phase information
2. loses accuracy in the presence of non-linear operators
3. is expected to accumulate errors with time.

The theoretical justification of RPMD does not provide clear information on the extent of its accuracy. Thus, in the absence of a more complete theoretical backing, the capabilities of RPMD can be benchmarked via applications.

Before discussing applications of RPMD, the details of the numerical implementation of the ring polymer equations of motion are explained in the following section.

2.4.3 Implementation of the propagation of the ring polymers

This section focusses on a one-dimensional system consisting of N atoms with masses m_i. All the derivations below generalize immediately to multi-dimensional systems.

To propagate the ring polymers the RP equations of motion given in Eq. (2.31) with the ring polymer Hamiltonian given in Eq. (2.33) need to be integrated. However, the ring polymers' internal motion can contain very high frequency modes due to the spring constant $\omega_n = n/(\beta\hbar)$. Thus, a straightforward integration of Eq. (2.31) can require a very small time step which would render the simulations impractical. To circumvent this problem, one can propagate the internal RP modes separately by decoupling the spring terms dynamics [121]. The procedure is based on the transformation of Cartesian coordinates to the RP normal mode coordinates (see also Appendix A). This way, the ring polymer Hamiltonian can be split into a free part H_n^0 and an interaction part V_n. The RP phase space evolves during the time step Δt according to the propagator $e^{-\Delta t L}$ where $L = L_0 + L_V$ and L_0 and L_V are the Liouvillians associated with H_n^0 and V_n, respectively. The propagator expanded up to the second order in time reads

$$e^{-\Delta t L} = e^{-(\Delta t/2) L_V} e^{-\Delta t L_0} e^{-(\Delta t/2) L_V} + \mathcal{O}(\Delta t^2\, L_V). \tag{2.51}$$

This product splits the propagation into internal RP modes and external potential contributions [134]. To simplify the integration of the evolution generated by $H_n^0(\mathbf{p}, \mathbf{q})$ the transformation from the Cartesian bead representation $(\mathbf{q}, \mathbf{p})$ to the normal mode representation $(\tilde{\mathbf{q}}, \tilde{\mathbf{p}})$ is performed

$$\tilde{p}_i^{(k)} = \sum_{j=1}^{n} p_i^{(j)} C_{jk} \quad \text{and} \quad \tilde{q}_i^{(k)} = \sum_{j=1}^{n} q_i^{(j)} C_{jk}, \tag{2.52}$$

where for an even number of beads the transformation matrix C is

$$C_{jk} = \begin{cases} \sqrt{1/n}, & k = 0 \\ \sqrt{2/n}\cos(2\pi jk/n), & 1 \le k \le n/2 - 1 \\ \sqrt{1/n}(-1)^j, & k = n/2 \\ \sqrt{2/n}\sin(2\pi jk/n), & n/2 + 1 \le k \le n - 1 \end{cases}. \tag{2.53}$$

With the normal mode coordinates $H_n^0(\mathbf{p},\mathbf{q})$ reads

$$H_n^0(\mathbf{p},\mathbf{q}) = \sum_{i=1}^{N}\sum_{k=0}^{n-1}\left(\frac{\left[\tilde{p}_i^{(k)}\right]^2}{2m_i} + \frac{1}{2}m_i\omega_k^2\left[\tilde{q}_i^{(k)}\right]^2\right), \tag{2.54}$$

with

$$\omega_k = 2\omega_n \sin(k\pi/n). \tag{2.55}$$

Note that in the normal representation, the sum over k runs from 0 to $n-1$. It is now possible to exploit the diagonalized form of the the free ring polymer Hamiltonian to integrate the normal modes basis analytically and then include the integration of the physical potential. In details, this is done by employing a modified Velocity-Verlet algorithm [121] in accordance to the splitting of the propagator in Eq. (2.51). The evolution algorithm for a single time step Δt consists of five operations that are

$$p_i \leftarrow p_i - \frac{\Delta t}{2}\frac{\partial V(q_i)}{\partial q_i}, \tag{2.56}$$

$$\tilde{p}_j \leftarrow \sum_i p_i C_{ij} \quad \tilde{q}_j \leftarrow \sum_i q_i C_{ij}, \tag{2.57}$$

$$\begin{pmatrix}\tilde{p}_j\\ \tilde{q}_j\end{pmatrix} \leftarrow \begin{pmatrix}\cos\omega_j\Delta t & -m\omega_j\sin\omega_j\Delta t\\ [1/m\omega_j]\sin\omega_j\Delta t & \cos\omega_j\Delta t\end{pmatrix}\begin{pmatrix}\tilde{p}_j\\ \tilde{q}_j\end{pmatrix}, \tag{2.58}$$

$$p_i \leftarrow \sum_j C_{ij}\tilde{p}_j \quad q_i \leftarrow \sum_j C_{ij}\tilde{q}_j, \tag{2.59}$$

$$p_i \leftarrow p_i - \frac{\Delta t}{2}\frac{\partial V(q_i)}{\partial q_i}. \tag{2.60}$$

The first step involves the evolution of the ring polymer momenta during $\Delta t/2$ under the exclusive influence of $V_n(\mathbf{q})$. The second step is a transformation to the normal mode coordinates. The third step consists of an exact evolution during Δt of the bead normal modes under the sole influence of $H_n^0(\mathbf{q},\mathbf{p})$. The fourth step is an inverse transformation to the bead coordinates. The fifth step is the same as the first one. The integration remains symplectic and conserves the phase-space volume. Note that for $n = 1$ the algorithm reduces to the standard velocity Verlet method for classical systems. For any number of beads the integration error term remains of the order $O(\Delta t^2)$. In practice, the extra steps to perform the normal mode transformation and inverse transformation require negligible computational effort compared to the evaluation of the potential energy surface V.

To generate PIMD trajectories, it is possible to combine the above algorithmic steps with a simple white noise Langevin thermostat. This amounts to add a few computationally cheap extra steps. These steps are explained in Appendix B.
Fig. 2.4 illustrates the contrast beween RPMD and PIMD trajectories.

FIGURE 2.4: Representation of configurations generated via a thermostatted RP trajectory (black upper line). Each configuration corresponding to a point of the black line is a valid initial configuration to use in RPMD. Real-time RP trajectories (yellow lower lines) starting from these points are propagated without thermostat, strictly using Eq. (2.31).

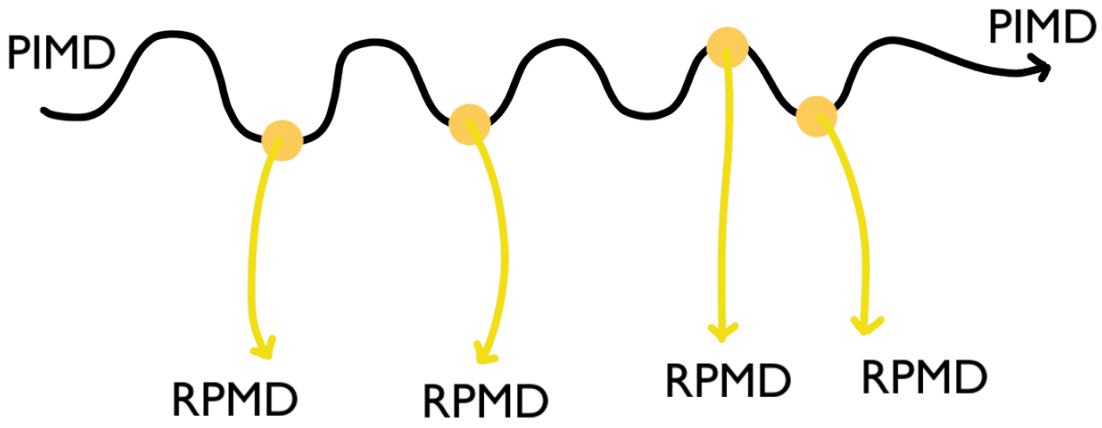

The next section focuses on RPMD thermal rates results. In anticipation of the study of reactive dynamics using RPMD in the next chapters, it is relevant to discuss earlier works studying thermally induced reaction rates using RPMD. Thermal rates provide precise kinetic informations about chemical reactions and thereby are a firm test of the RPMD approach. The following is also insightful in anticipation of potential microcanonical extensions of RPMD.

2.4.4 RPMD for chemical reaction rates

RPMD has proven to be an efficient tool to compute accurately thermal rate coefficients for many chemical reactions for which quantum mechanical approaches are computationally very expensive [88, 135–138]. To illustrate the connection between RPMD and thermal rate coefficients, we focus on one-dimensional bimolecular reactions. The exact formula for the thermal rate constant $k(\beta)$ can be rewritten in

terms of the Kubo-transformed flux-side time correlation function[9] so that

$$k(\beta) = \frac{1}{Z_r(\beta)} \lim_{t\to\infty} K_{Fh}(t), \tag{2.61}$$

with

$$\hat{h} = \theta(\hat{q} - q^\dagger) \text{ and } \hat{F} = \frac{i}{\hbar}[\hat{H}, \hat{h}] \tag{2.62}$$

the side operator and flux operator, respectively. $\theta(q)$ is the Heaviside step function. $q^\dagger$ is a dividing "surface" that separates reactant and product regions. The limit $t \to$ "∞" means that the system is propagated long enough to unequivocally define the trajectories outcomes. $Z_r(\beta)$ is the reactant partition function.

The computation of Eq. (2.61) using RPMD is a priori problematic and could lead to noticable inaccuracies for the two following reasons. First, the operators $\hat{h}$ and $\hat{F}$ are highly non-linear so that the condition of better accuracy with linear operators is far removed. Second, the need to compute the long-time limit of $K_{Fh}(t)$ is a priori prone to generate inaccuracies, since RPMD validity is expected to deteriorate with time.

In spite of these expected difficulties, studies have shown that RPMD yields accurate thermal rate coefficients for various reactions even at very low temperatures. In this context, it has been demonstrated that RPMD captures ZPE effects and prevents ZPE leakage [139,140]. It also produces very satisfying results when tunneling effects dominate the reactivity [141, 142]. The success of the RPMD rate theory at describing tunneling effects can be in part attributed to its connection to semiclassical instanton theory [135]. Moreover, RPMD yields accurate thermal rate results for more complex reactions [143].

It is worthwhile to compare the expressions of the RPMD and classical thermal rate constants. The corresponding classical expression of Eq. (2.62) is

$$K_{Fh}^{\mathrm{CL}}(t) = \frac{1}{2\pi\hbar} \int dp_0 \int dq_0 e^{-\beta H(p_0, q_0)}\, \delta\left(q_0 - q^\dagger\right) \frac{p_0}{m}\, \theta\left(q(t) - q^\dagger\right), \tag{2.63}$$

with $\delta\left(q_0 - q^\dagger\right)\frac{p_0}{m}$ (δ is the Dirac delta function), $\theta\left(q(t) - q^\dagger\right)$, q_0, p_0 and $q(t)$ are the classical analogues of the flux and side operators, initial position, initial momentum and position of the atom at time t, respectively. To compute $K_{Fh}^{\mathrm{CL}}(t)$ is to correlate the position and velocity of the atom at time t from an initial thermal equilibrium

[9] This formalism allows for the extraction of kinetic properties without having to consider all possible state-specific reaction probabilities.

distribution in which the atoms are positioned at the dividing surface for the reaction.

In RPMD, it reads

$$K_{Fh}^{\mathrm{RP}}(t) = \lim_{n\to\infty} \frac{1}{(2\pi\hbar)^n} \int dp_0 \int dq_0 e^{-\beta_n H_n(p_0,q_0)}\, \delta\left(q_0^c - q^\dagger\right) \frac{p_0^c}{m}\, \theta\left(q^c(t) - q^\dagger\right), \qquad (2.64)$$

with q_0^c, p_0^c and $q^c(t)$ defined similarly as in the classical case but considering the centroid coordinates. It is observed that $K_{Fh}^{\mathrm{RP}}(t)$ is similar to $K_{Fh}^{\mathrm{CL}}(t)$. The only differences are

- the classical coordinates are substituted in RPMD by the centroid coordinates
- the initial bead configurations are sampled according to the ring polymer Boltzmann distribution with certain initial constraints on the position centroids
- the ring polymer is propagated using the ring polymer equations of motion
- at least $n > \beta\hbar\omega_{\mathrm{max}}$ beads are needed to converge the calculations [128, 144]

Thus, it is possible to bridge classical and quantum results in the case of thermal rates in a natural way by employing RPMD. These analogies between the classical and RPMD calculations will in part motivate the content of Sec. 2.4.7 when introducing non-equilibrium initial conditions on the centroids.

Summary:
Previously in PIMD, the ring polymer trajectories were used as a sampling tool to compute the values of static equilibrium properties. In RPMD, trajectories are propagated from an initial equilibrium configuration without any thermalization protocol (i.e. resampling the momenta or attaching a thermostat would uncorrelate the dynamics) and are taken literally as real-time approximation of quantum dynamics. This leads to quantum-Boltzmann-conserving classical dynamics, albeit in an extended ring polymer phase space. In several successful applications, RPMD incorporates almost perfectly ZPE effects and to a good approximation tunneling effects. The cost of RPMD is about n times the cost of the corresponding classical simulation. The computational cost of RPMD scales much more slowly with the number of atoms than any quantum mechanical treatment making it applicable to

large systems. However, as discussed in the context of the derivation from Matsubara dynamics, RPMD describes the dynamics only approximately.

So far, the use of RPMD has only been justified for thermal equilibrium conditions. Thus, microcanonical magnitudes such as integral cross sections and its dependencies on the rovibrational states of reactants and products have until recently not been addressed with this method. In the next section, an extension of RPMD to non-equilibrium conditions is introduced that is at the basis for the other chapters of the thesis.

2.4.5 Non-equilibrium RPMD

The non-equilibrium time-dependent expectation value of the form

$$\langle \hat{B} \rangle(t) = \mathrm{tr}\left[e^{-\beta \hat{H}^{(0)}} e^{i\hat{H}^{(1)}t/\hbar} \hat{B} e^{-i\hat{H}^{(1)}t/\hbar} \right], \tag{2.65}$$

with $\hat{H}^{(0)} \neq \hat{H}^{(1)}$ is considered. To simplify the following discussion, we consider a single atom in one spatial dimension. The argument can be directly generalized to multiple atoms and dimensions.

The Hamiltonians

$$\hat{H}^{(0)} = \frac{(\hat{p} - \Delta p)^2}{2m} + V(\hat{q}) \quad \text{and} \quad \hat{H}^{(1)} = \frac{\hat{p}^2}{2m} + V(\hat{q}). \tag{2.66}$$

describe a momentum shift (or kick) as the eigenfunctions of the two Hamiltonians are related by the factor $e^{i\Delta p\, q/\hbar}$. Fig. 2.5 illustrates the initial impulse applied to a ring polymer.

By employing the same procedure as mentioned in Sec. 2.4.2 it is possible to recover the RPMD approximation for the case of the Kubo-transformed non-equilibrium TCF[10] and thereby also for the non-equilibrium time-dependent expectation value $\langle \hat{B} \rangle(t)$ [95]. Thus, we have

$$\langle \hat{B} \rangle(t) \approx \frac{1}{(2\pi\hbar)^n} \int d\mathbf{q} \int d\mathbf{p} e^{-\beta_n H_n^{(0)}(\mathbf{p},\mathbf{q})} B_n\left(\mathbf{p}(t), \mathbf{q}(t)\right), \tag{2.67}$$

[10] No general transformation between Kubo-transformed non-equilibrium TCFs and standard non-equilibrium TCFs has yet been established.

where B_n refers to the estimator of the operator $\hat{B}$ and

$$H_n^{(0)}(\mathbf{p},\mathbf{q}) = \sum_{k=1}^{n} \frac{\left(p^{(k)} - \Delta p\right)^2}{2m} + \sum_{k=1}^{n} \left[\frac{m\omega_n^2}{2} \left(q^{(k)} - q^{(k+1)}\right)^2 + V\left(q^{(k)}\right) \right], \tag{2.68}$$

and the evolution of the coordinates $(\mathbf{p}(t), \mathbf{q}(t))$ is governed by

$$H_n^{(1)}(\mathbf{p},\mathbf{q}) = \sum_{k=1}^{n} \frac{\left(p^{(k)}\right)^2}{2m} + \sum_{k=1}^{n} \left[\frac{m\omega_n^2}{2} \left(q^{(k)} - q^{(k+1)}\right)^2 + V\left(q^{(k)}\right) \right]. \tag{2.69}$$

Thus, the momentum shift Δp initially appearing in Eq. (2.66) is effectively translated in RPMD by an initial shift of the momentum centroid. An interesting fact is that more general changes to the Hamiltonian (corresponding to more involved non-equilibrium initial conditions) besides a momentum rescaling ($p \to \alpha p$) or a sudden switch of potential would not lead to the usual form of the ring polymer Hamiltonian $H_n^{(0)}$ and the connection to Matsubara dynamics would not be maintained [95]. As in the equilibrium case, NE-RPMD is exact in the high temperature limit. When applied to the calculations of non-equilibrium TCFs, NE-RPMD and RPMD have in common their exactness for the limit $t = 0$ (also for non-linear operators) and for harmonic potentials (with linear operators). Also, the accuracy of NE-RPMD has been shown to be similar to the one of RPMD when computing TCFs [95].

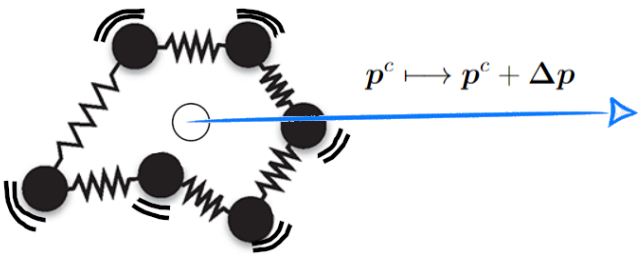

FIGURE 2.5: A ring polymer characterized by an arbitrary momentum impulse $\boldsymbol{\Delta p}$ applied on its centroid. The sampling of the internal fluctuations remains the same and depends on β and H_n.

2.4.6 Status of β

For thermal applications of RPMD, β is well-defined. Its value alongside the number of beads n and the external potential characterize completely the distribution of the initial conditions. Also, β plays a particularly crucial role in the dynamics since its value influences the harmonic springs between the beads. In the case of an initial momentum impulse, Δp constitutes an extra parameter independent of the ring polymer Boltzmann distribution. Consequently, the initial state becomes non-thermal, with β only influencing the internal motion of the ring polymers. This leads β to, a priori, hold the status of parameter as it cannot be interpreted as the reciprocical temperature in that context. The consequences of the non-equilibrium conditions on the status and values of β have not yet been understood.

There have been several applications of NE-RPMD employing the initial momentum kick and the sudden change of potential. However, several of these studies employ reasonable but not well-founded and fixed values for β [95, 145, 146]. This is problematic as NE-RPMD results are very sensitive to the choice of β. Thus, this adds a certain degree of arbitrariness to the simulations results. Several ansätze consider matching β with the total initial energy of the system considered ($\beta = 1/E$) [147]. However, it generally leads to very low β such that the ring polymers' behavior is almost classical. A recent work by Miller *et al.* addressed the question of β in the case of a one dimensional Eckhart barrier potential model. However, the reported β ansatz does not include vibrational aspects and relies on an equilibrium expression of the energy estimator [148].

Desired attributes of β

One expects that β should decrease if the initial momentum impulse is increased since the dynamics progressively becomes more classical with higher momenta. In the limit $\Delta p \to \infty$, β should vanish so that the ring polymers shrink to classical point-like atoms. Also, assuming that Δp is finite, β should be sufficiently large to describe the quantum statistics of the internal motion in molecules correctly. The specific dependencies on the parameters of the problem remain unknown.

2.4.7 Direct trajectory approach

As shown for the computation of thermal rates, RPMD can provide an efficient way to bridge the gap between classical and quantum dynamics. With the justification of the use of non-equilibrium initial conditions, a wide range of possibilities is now available for exploration. NE-RPMD can be potentially exploited to approximately include NQEs in various non-equilibrium chemical processes.

For thermal rates, the classical and RPMD approaches are in direct analogy (see Eqs. (2.63) and (2.64)). Thus, it is worthwhile to explore similar connections in the context of non-equilibrium situations. In particular, this thesis considers realistic systems with atoms and molecules that have specific positions, momenta, vibrational states for a molecule, and that interact with each other via a collision. The simplest case consists of atoms that are assumed to be initially far away from each other (so that $V(\boldsymbol{q}) = 0$) at the positions $\boldsymbol{q}_I$ and having specific momenta $\boldsymbol{p}_I$. With $B(\hat{\boldsymbol{q}})$ an operator having for its argument the position of the atoms $\boldsymbol{q}$, the NE-RPMD "direct trajectory" approach to compute the time-dependent expectation value $\langle \hat{B} \rangle(t)$ reads

$$\lim_{n\to\infty} \frac{1}{(2\pi\hbar)^n Z_n} \int \mathrm{d}\mathbf{p}_0 \int \mathrm{d}\mathbf{q}_0 \, \mathrm{e}^{-\beta_n H_n^{(0)}(\mathbf{p}_0,\mathbf{q}_0)} B_n(\boldsymbol{q}(t)) \, \delta(\boldsymbol{q}^c(0) - \boldsymbol{q}_I) \, \delta(\boldsymbol{p}^c(0) - \boldsymbol{p}_I), \quad (2.70)$$

with $\boldsymbol{q}^c(t)$ and $\boldsymbol{p}^c(t)$ referring to the coordinates of the position and momentum centroids at time t. $H_n^{(0)}$ accounts for the initial momenta impulses such that $\boldsymbol{p}^c(t = 0) = \boldsymbol{p}_I$ and the coordinates $\boldsymbol{q}(t)$ are propagated using the ring polymer Hamiltonian $H_n^{(1)}$ for multiple atoms. $\mathrm{d}\mathbf{p}_0 \, \mathrm{d}\mathbf{q}_0$ is a phase space element over the initial ($t = 0$) conditions. As shown in Appendix A, the internal energy of the individual and initially free ring polymer vanishes and the total energy reduces to the kinetic energy of the centroids. Thus, the initial average state of the ring polymers can be defined with the momentum impulses and initial positions of the centroids. This corroborates the microcanonical classical description of the system at $t = 0$. It follows a physically intuitive practical approach to compute Eq. (2.70): the centroids of the ring polymers are initialized accordingly, then the internal (non-centroid) bead motion is sampled according to the ring polymer Boltzmann distribution and lastly the estimator values for $B(\hat{q})$ at time t are averaged over many ring polymer trajectories. This is in direct analogy with the calculation of non-equilibrium TCFs using

RPMD with initial momentum kicks [95]. However, it is not straightforward to generalize this approach to model more complex systems comprised of molecules with specific initial ro-vibrational states.

Discussion:
NE-RPMD considered as a tool to approximate to some undefined extent quantum dynamics might appear plain compared to wave-function methodologies. Nevertheless, it might capture the essential quantum effects in several non-equilibrium chemical processes. RPMD has been successfully applied in various regimes between its exact limits, and it shares the same theoretical grounds with its non-equilibrium extension. Also, RPMD handles all degrees of freedom equally and thus is full-dimensional. Thus, it is worthwhile to explore the capabilities of NE-RPMD to model the dynamics of chemical reactions. In particular, it is worthwhile to first look at reactions whose kinetics (thermal rate coefficients) are well-described by RPMD.

The next Chapters (4, 5 and 6) consist of published papers that extended non-equilibrium RPMD to the study of state-resolved reactive molecular dynamics.

Chapter 3

Nuclear quantum effects in state-selective scattering from ring polymer molecular dynamics

This chapter is centered on the following publication, of which I am the first author, and has been included verbatim:
"Nuclear quantum effects in state-selective scattering from ring polymer molecular dynamics", Marjollet, A., Welsch, R., J. Chem. Phys. **152**, 194113 (2020) [149].
It is reproduced with the permission of AIP Publishing for the purpose of this thesis. My contributions include the investigation and theoretical work, programming the simulation tools, data analysis and writing the article.

This Chapter presents ICS results obtained by applying our developed NE-RPMD approach to the triatomic Mu/H/D+H_2 reactions with H_2 either in its ground ($v = 0$) or first vibrational excited state ($v = 1$). This work constitutes the first benchmarking of the method and also the first extraction of ICS employing NE-RPMD. The reactions H/D+$H_2(v = 0, 1)$, for which the exact quantum results and QCT ICS results are very close over a wide range of collision energies, were chosen for preliminary benchmarking purposes. Furthermore, the method is applied to the reaction Mu+$H_2(v = 0, 1)$ in which the ZPE and tunneling effects influence greatly the ICS results in the case of the ground state and the first vibrational excited state H_2 reactant, respectively. This is due to the Muonium being a very light atom (around 0.113 the mass of hydrogen). We report an ansatz for the choice of β based on physically sound assumptions. We also analyze the the ring polymer reactants' configurations around the transition state for the Mu+$H_2(v = 1)$.

3.1 Introduction

Bimolecular reactions in the gas phase or chemisorption of a molecule onto a surface are important classes of reactions with relevance to many areas of chemistry, e.g., atmospheric and interstellar chemistry, combustion and catalysis [2,8,150–152]. State-selective measurements and simulations of these processes provide a detailed understanding of the reaction dynamics and help us understand the flow of energy in chemical reactions. The detailed understanding of the reaction dynamics can lead to efficient ways for controlling and steering these reactions. While impressive measurements can already provide detailed information for polyatomic systems, [18, 150, 151, 153–159] a full-dimensional quantum-dynamical description of state-selective scattering remains a great challenge. The biggest system treated today is the $H+CH_4 \rightarrow H_2+CH_3$ reaction [48,49,160–164] which was simulated employing the quantum transition state concept [165–171] and the multi-configurational time-dependent Hartree approach [172–179] for the wavepacket propagation. However, these simulations are very involved and intricate, require many prerequisites, e.g., a fitted potential energy (PES) surface that can be evaluated efficiently [38, 47] and an appropriate curvilinear coordinate system, [60] and take up many months of simulation time for each specific reaction.

Therefore, most reactive scattering simulations employ the quasiclassical trajectory (QCT) approach [64–66]. In this approach, all nuclei are treated classically and evolve on an accurate PES or based on gradients obtained from on-the-fly ab initio calculations [180]. Suitable initial conditions for each trajectory are chosen to include the correct amount of zero-point energy (ZPE) and the correct amount of additional energy for a vibrational (or rotational) excitation. This approach has been very successful for the description of bimolecular and gas-surface reactions, in particular, for energies well above the threshold. A great advantage of the QCT approach is its numerical efficiency as only Newton's equations of motion have to be solved. This allows for the treatment of large systems and it is even possible to perform QCT simulations while evaluating the potential energy and gradients on-the-fly. However, QCT simulations suffer from the ZPE leakage problem and also do not respect ZPE constraints of the products. Due to the classical nature of the simulation, any ZPE put into a certain degree of freedom initially can artificially leak out into other degrees of freedom, in particular the reaction coordinate, and help to overcome the barrier. Additionally, in QCT the products can violate ZPE

constraints by having less energy than the ZPE would require, which can lead to many additional reactive trajectories. Both these problems can lead to an increased reactivity in QCT compared to quantum simulation [181]. Furthermore, QCT simulations do not include tunneling effects, which can lead to underestimation of the cross-section, in particular close to the threshold energy and in systems where protons are transferred as part of the reaction [115]. These problems can be manifest in a single reaction when looking at the reactivity of different initial vibrational states.

Various methods have emerged that approximately include nuclear quantum effects in classical-like simulations. Among the most used ones is the ring polymer molecular dynamics (RPMD) approach [80, 87, 128, 144]. RPMD is based on the imaginary-time path-integral formalism that maps a quantum Boltzmann distribution onto a set of classical replicas in phase space joined by harmonic springs, which is known as ring polymer. Dynamical quantities such as real-time correlation functions, are obtained from classical dynamics in this extended ring polymer phase space. RPMD is exact in the high-temperature, short-time and harmonic limits. It incorporates ZPE effects and does not suffer from ZPE leakage [139, 140, 145]. Furthermore, it can incorporate some tunneling effects due to the extension of the ring polymer that can stretch over a barrier and thus lower the effective barrier height [182]. RPMD has been especially successful for the calculations of thermal rate constants in the form of RPMD rate theory [83, 84, 128, 144, 182]. RPMD rate theory is particularly efficient as it allows for the calculation of thermal rate constant based on dynamics around the barrier region without the need to resolve the initial or final ro-vibrational states. Employing RPMD rate theory to various isotopologues of the $H+H_2$ reaction, it was impressively shown that it incorporates ZPE effects as well as tunneling [139, 182]. The original RPMD formulation is restricted to the simulation of equilibrium correlation functions. Recently, it was shown that RPMD can be effectively used to calculate correlation functions and expectation values associated with non-equilibrium initial conditions, e.g., for the case of an initial momentum kick [95]. As the RPMD approach with equilibrium and non-equilibrium initial conditions can be obtained from Matsubara dynamics [81] in similar ways, both exhibit the same well-known properties, e.g., it being exact in the high-temperature and classical limits, for dynamics in harmonic potentials and conserving the average energy of the springs [95]. Further numerical tests showed that one can expect similar accuracy of RPMD for calculations with equilibrium

and non-equilibrium initial conditions [95]. Very recently, the non-equilibrium initial conditions have been used to obtain microcanonical rate constants from RPMD simulations, [145, 148] however, initial state-selectivity could not be addressed in these works.

In this manuscript we describe an efficient approach to combine QCT simulations with the RPMD approach to obtain initial state-selective cross sections for bimolecular and molecule-surface reactions, which include several non-classical effects. These advantages of the method are exemplified using isotopic variants of the H+H_2 reaction. In particular, the Mu+H_2 reaction serves as a benchmark as it highlights both the missing ZPE constraints as well as the missing tunneling contributions in QCT simulations [115]. The RPMD approach respects ZPE constraints and based on RPMD simulations of non-reactive polyatomic systems, we expect it to not suffer from ZPE leakage. Furthermore, the method only slightly overestimates the exact reactive cross section for Mu+$H_2(v = 1)$, where tunneling through the $v = 1$ adiabatic barrier is present [115]. Section 3.2 describes the details of the method. Section 3.3 presents results obtained for Mu/H/D+$H_2(v = 0, 1)$. Conclusions and an outlook are given in Section 3.4.

3.2 Method

To perform state-selective scattering calculations within the RPMD approach we follow the idea of quasiclassical trajectories (QCT). For illustrative purposes, let us consider an atom+diatom reaction A+BC. The generalization to polyatomic reactions is discussed further below. For the initialization of the diatomic molecule BC we proceed in two steps, first we employ the harmonic approximation with ω the vibrational frequency of BC to sample the initial ring polymer configurations for the vibrational normal mode of BC from the well-known Boltzmann distribution of a harmonic system. Corresponding Cartesian coordinates for the beads are obtained by inverse normal mode transformation. Sampling the normal mode guarantees that the molecule will not undergo spurious rotations or center of mass motion. These configurations represent a system containing the ZPE with additional thermal energy. By employing the path integral approach we obtain correct initial quantum fluctuations for the position and momentum normal mode of BC. To obtain reliable scattering results, $\beta = \frac{1}{k_B T}$ has to be chosen high enough in order to

make the contribution of the additional thermal energy to the reaction dynamics negligible. The choice of β is discussed below.

Vibrationally excited states are mimicked by modifying the initial position and momentum of the ring polymer centroids, $\bar{Q}$, $\bar{P}$, to add the correct amount of vibrational energy since the initial sampling already contains the correct amount of ZPE. This step is again inspired by the QCT approach. To this end, we add to the mass scaled positions and momentum centroid of the ring polymer representing the vibrational mode of BC the following quantities:

$$K_Q = \sqrt{\frac{2v}{\omega}}\cos(\phi), \quad K_P = \sqrt{2v\omega}\sin(\phi), \tag{3.1}$$

where $\phi \in [0, 2\pi]$ is a random phase and v the vibrational quantum number. Following this step, the mass scaled position and momentum fluctuations for each bead $k \in [1, n]$ are

$$\langle Q_v^2 \rangle_k = \frac{1}{2\omega}\coth(\frac{\beta\omega}{2}) + \frac{v}{\omega}, \quad \langle P_v^2 \rangle_k = \frac{\omega}{2}\coth(\frac{\beta\omega}{2}) + v\omega. \tag{3.2}$$

The initial ring polymer configurations of BC are then used in the scattering calculations. To this end, we directly switch to the full PES. In order to avoid extra fictitious vibrational energy introduced by the direct switching, we discard configurations with interatomic distances smaller than d_{min}. d_{min} can be chosen based on the initial distances of vibrationally excited BC in QCT simulations. Upon switching we have good stability of BC's internal energy around its harmonic energy value $\omega(v + \frac{1}{2})$. This constitutes a reliable and consistent approximation in the case of a diatomic molecule with reasonable masses. This approach can be generalized to any polyatomic molecule by employing the normal modes of the respective molecule. Finally, the initial relative centroid velocities of BC are 'kicked' towards A along the x axis

$$\bar{\boldsymbol{V}}_B = \bar{\boldsymbol{V}}_C = -\frac{\boldsymbol{P}_{rel}}{m_B + m_C}, \tag{3.3}$$

where m_B and m_C are the masses of B and C, respectively, and the relative momentum set as $\boldsymbol{P}_{\text{rel}} = \sqrt{2\mu E_{\text{col}}}\boldsymbol{\kappa}$, where E_{col} and μ are the collision energy and the reduced mass of the system, respectively, and $\boldsymbol{\kappa}$ the unit vector along the x axis.

The atom A is initialized far away from BC with the distance of the centroid of A to the centroid of the center of mass of BC equal to

$$d(A, BC) = d(A, BC)_{\text{QCT}} + R_A^g + \max(R_B^g, R_C^g), \tag{3.4}$$

where $d(A, BC)_{\text{QCT}}$ is the distance that would be used for a standard QCT simulation, and $R_i^g, i = A, B, C$ is the radius of gyration of the ring polymer for atom A, B and C, respectively. The centroid of the ring polymer representing atom A is then displaced away from the molecular axis of BC according to the impact parameter b as in QCT. The initial centroid velocity of A is set to

$$\bar{\boldsymbol{V}}_A = \frac{\boldsymbol{P}_{rel}}{m_A}. \tag{3.5}$$

The initial non-centroid modes of the ring polymer for atom A are drawn from a free ring polymer distribution along the direction of propagation $\boldsymbol{\kappa}$.

Integral cross sections for a given total energy $E_{\text{tot}} = E_{\text{col}} + \omega(v + \frac{1}{2})$ are obtained following the QCT approach as

$$\sigma(E_{tot}) = \pi b_{\text{max}}^2 \frac{N_R(E_{\text{tot}})}{N(E_{\text{tot}})}, \tag{3.6}$$

where $N(E_{\text{tot}})$ and $N_R(E_{\text{tot}})$ are the number of total and reactive trajectories, respectively, and b_{max} is chosen so that no reaction occurs for $b > b_{\text{max}}$ [66]. The number of reactive trajectories is obtained by evaluating suitable distances criteria that distinguish the products.

β is set depending on the initially chosen collision energy (E_{col}) and the energy added to BC by our vibrational excitation scheme ($E_v = \omega v$) as

$$\beta = \frac{2(\frac{m_{\text{tot}}}{\mu} - 2)}{\pi(E_c + E_v)}, \tag{3.7}$$

where m_{tot} is the total mass of the system. The above choice of β corresponds to an average of β_{A} and β_{BC}. Here β_{A} and β_{BC} are chosen such that the average relative velocities of A and BC match the corresponding QCT values in the center of mass reference frame. For higher collision energies, this can lead to low values of β resulting in non-negligible effects due to the additional thermal energy. Therefore, we set a lower cutoff value so that $\beta = \beta_-$ if $\beta < \beta_-$. A more detailed discussion of the

choice and further tests of the robustness are beyond the scope of this manuscript and will be part of a forthcoming publication. Possible generalizations of the approach are discussed at the end of the manuscript.

3.3 Results

As a benchmark system we choose the triatomic reaction of Mu/H/D + H_2(v=0,1). In particular, the reaction of Mu+H_2 exemplifies the problems of QCT simulations. For the reaction of Mu with H_2 in its ground vibrational state, the ZPE constraints problem is dominant and QCT simulations find a threshold of about 0.2 eV lower than exact quantum dynamics simulations [115]. Yet, for the reaction of Mu with vibrationally excited H_2, QCT results find a threshold of about 0.15 eV higher than exact quantum dynamics simulations due to the absence of any tunneling in the QCT simulations [115]. We employ the BKMP2 PES [183], a modified Velocity-Verlet integrator with a timestep of 0.02 fs, 40000 trajectories per collision energy, β_- = 300 a.u. and a ratio of $\frac{n}{\beta\omega_{H_2}} > 4$, which guarantees convergence with the number of beads. d_{min} is set to 1.078 Bohr. The QCT distance between A and BC is $d(A,BC)_{\text{QCT}} = 12$ Bohr. Please note that the maximal impact parameter is typically slightly higher in the RPMD simulations than in the QCT simulations. However, at low collision energies close to the classical threshold it can be up to a factor of 1.5 higher than in the QCT simulations.

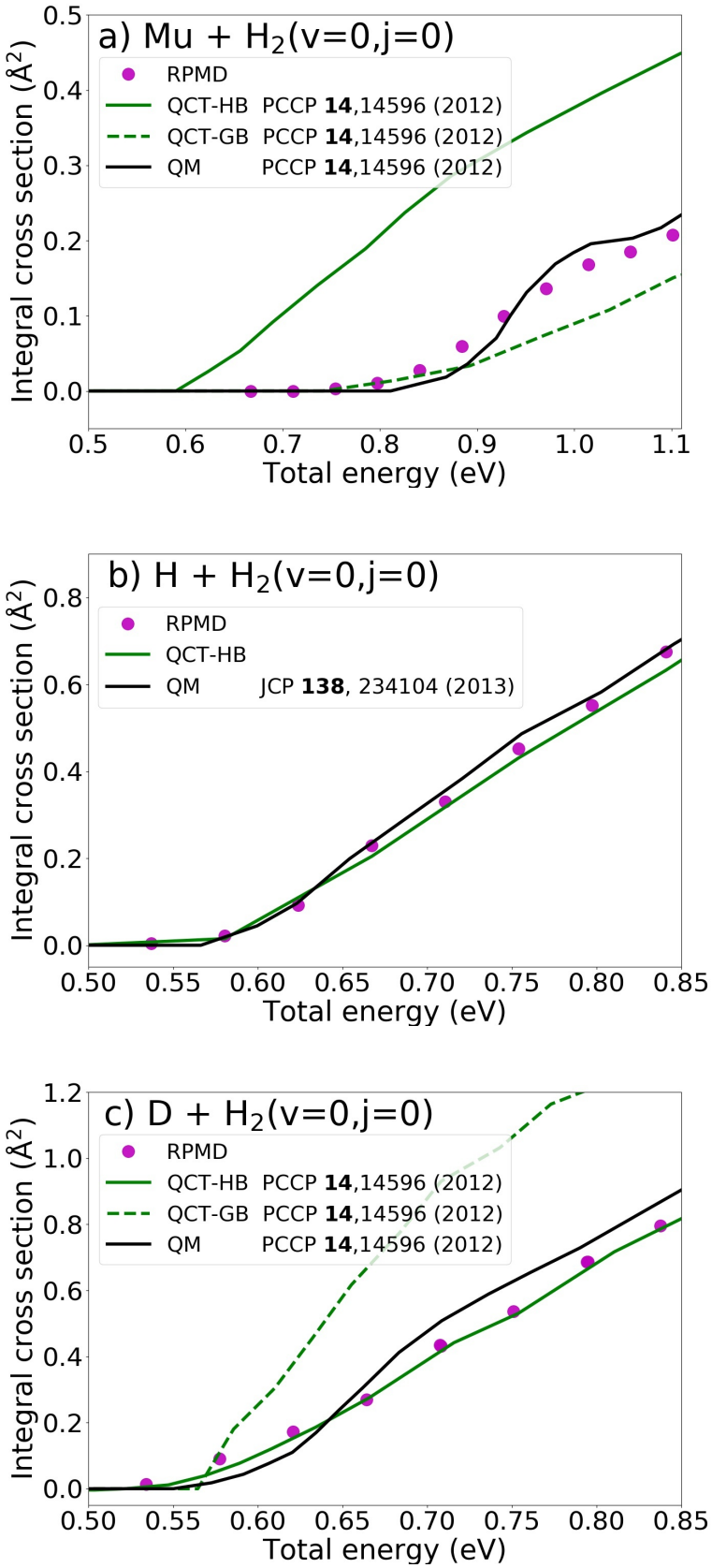

FIGURE 3.1: Integral cross sections for the reaction of Mu/H/D + $H_2(v = 0)$ calculated using RPMD. Reference quantum dynamics results and QCT results are taken from Refs. [115] and [184].

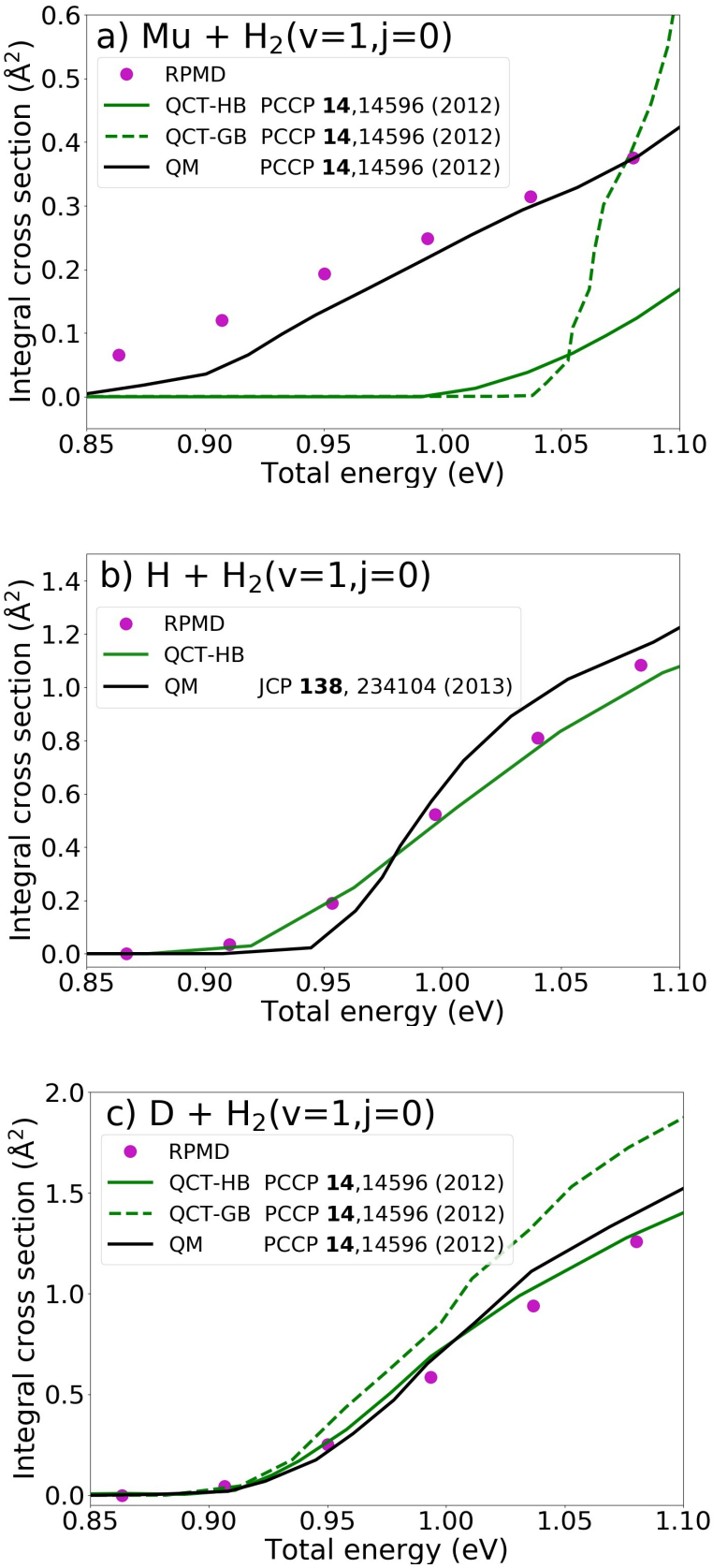

FIGURE 3.2: Integral cross sections for the reaction of Mu/H/D + $H_2(v = 1)$ calculated using RPMD. Reference quantum dynamics results and QCT results are taken from Refs. [115] and [184].

First, we focus on the reactivity of Mu/H/D with H_2 in its vibrational ground state. Fig. 3.1 presents the integral cross section of the Mu/H/D + $H_2(v{=}0)$ reactions. For the Mu+H_2 reaction (panel a), it can be seen that the proposed RPMD scattering approach very well reproduces the exact QM calculations from Ref. [115]. The straight forward QCT calculations employing histogram binning (HB), i.e., treating every trajectory equally, however, show a much lower threshold for reactivity compared to the QM calculations due to leakage of ZPE, which is well documented in literature [115]. Please note, that this problem can partly be circumvented employing Gaussian binning (GB) [185,186] as seen in Fig. 3.1 a). GB diminishes the contribution to the cross section for trajectories that violate the ZPE condition, i.e., where the resulting diatom has less internal energy than required from the quantum mechanical ZPE. Yet, it can be seen that the GB results underestimate the cross sections away from the threshold, whereas the proposed approach closely reproduces the exact results. In panels b) and c) of Fig. 3.1 it can be seen that RPMD can reproduce the QM integral cross sections for the H+$H_2(v{=}0)$ and D+$H_2(v{=}0)$ reactions very well. For these two cases the QCT simulations also perform well.

Second, we investigate the integral cross sections for the same reactions but employing vibrationally excited H_2, v=1. The resulting cross sections are displayed in Fig. 3.2. Again, the proposed RPMD scattering approach very well reproduces all QM integral cross sections. For this case both QCT variants (HB, GB) cannot reproduce the exact QM results for the Mu+H_2 reaction and display a higher threshold for reactivity. This is due to the missing tunneling contributions through the $v = 1$ adiabatic barrier in the QCT calculations [115]. This problem is mitigated in the RPMD simulations, as some quantum contributions are included due to the finite extension of the ring polymers.

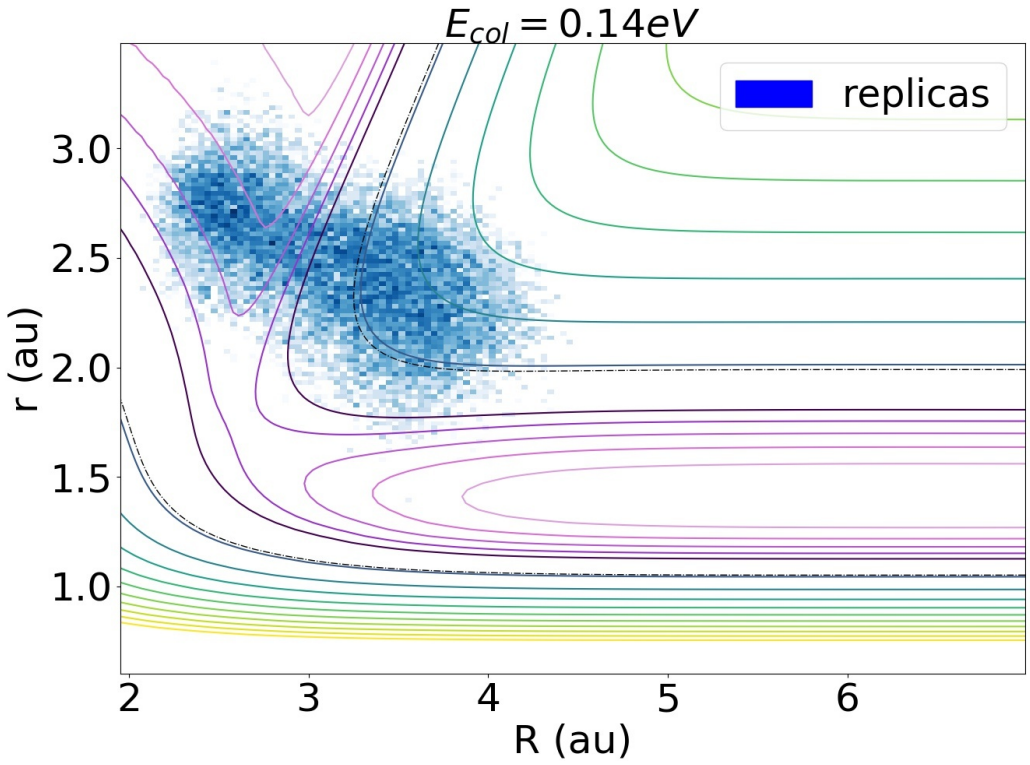

FIGURE 3.3: Density of the ring polymer beads for the Mu+$H_2(v = 1)$ reaction for reactive trajectories at the time of barrier crossing at $E_{\text{col}} = 0.14$ eV and for impact parameters $b < 3$ au. r refers to the H_2 distance and R to the distance of Mu to the center of mass of H_2. The PES for the system is plotted for comparison with the remaining coordinates relaxed.

The classically forbidden contributions in RPMD can be best seen by inspecting plots of the ring polymer density during the barrier crossing given in Fig. 3.3. The figure displays the density of the beads for all reactive ring polymer trajectories for a collision energy of 0.14 eV and impact parameters $b < 3$ au at about the time of the barrier crossing. It can be clearly seen that the ring polymer "cuts the corner" through a higher energy region to allow for reactivity. This region is never reached by QCT trajectories due to insufficient energy in the system, yet in the extended ring polymer phase space it is possible as the ring polymer is never completely located in the higher energy region but some beads are always in the lower energy regions on both sides of the barrier, which lowers the effective (i.e., averaged) energy of the full ring polymer when corner cutting.

3.4 Conclusion

In this manuscript, we focused on the description of triatomic systems and a first approach to combine QCT with RPMD for state-selective scattering simulations and many generalizations and extensions of the approach have to be left for future work. First of all, the current approach to initiate the vibrational excitation is described for triatomics, but is readily generalized to any polyatomic system including gas-surface reactions. Even better inital energies are obtained in QCT by employing the adiabatic switching procedure. This procedure cannot be generalized to the present approach right away and has to be left for further development. Furthermore, the initialization of distinct rotational or ro-vibrational states and the analysis of distinct ro-vibrational final states to obtain state-to-state cross sections have to be left for future work. Lastly, also non-adiabatic effects can be important in many bimolecular reactions [187, 188]. Several approaches have been proposed to include the treatment of non-adiabatic effects within RPMD [189–191]. It has to be explored, which of these approaches performs best for reactive scattering problems. The presented approach for choosing β in the current context of microcanonical RPMD and initial state-specificity is a first attempt, which can be reasonably motivated and provides good results for integral cross sections. However, more detailed investigation of its reliability and robustness as well as the investigation of other approaches for choosing β should be pursued. To this end, one can, for example, learn from the attempt to tune β for the computation of microcanonical rates for the one-dimensional Eckart model potential [148]. While RPMD rate theory is the preferred, much more efficient and direct way to obtain thermal rate constants, we think that due to good agreement with the exact quantum simulations, one can expect to also obtain reasonable thermal rate constants from calculations following our approach. However, as we have to introduce several additional steps compared to standard RPMD rate theory (e.g., non-equilibrium initial conditions), the results will most likely not match perfectly.

In conclusion, we have presented an efficient way to obtain initial state-selective cross-sections for bimolecular gas-phase and gas-surface reactions. The proposed approach combines the ideas of quasiclassical trajectories with the ring polymer molecular dynamics method. We showed that this combination is possible and can alleviate several problems intrinsic to the QCT approach, i.e., the problem of ZPE constraints and the neglect of tunneling contributions, which was discussed

employing the prototypical Mu/H/D+H_2(v=0,1) reactions. The new approach is easily implemented, numerically efficient and significantly improves the accuracy of QCT simulations.

Chapter 4

State-selective cross sections from ring polymer molecular dynamics

This chapter is centered on the following publication of which I am the first author, and has been included verbatim:
"State-selective cross sections from ring polymer molecular dynamics", Marjollet, A., Welsch, R., Int J Quantum Chem. **121**:e26447 (2021) [192].
It is reproduced with permission of the International Journal of Quantum Chemistry for the purpose of this thesis. My contributions include the investigation and theoretical work, programming the simulation tools, data analysis and writing the article.

This chapter presents the application of our developped NE-RPMD method to triatomic reactions and provides an in-depth analysis of its applicability and robustness for a wider range of collision energies and more reactions. The ansatz for β is also refined as to be better adapted for high collision energies. The stability of the excited vibrational state is analyzed and compared with the exact quantum value for the BMPK2 PES. To further explore its applicability, the method is applied for the computation of initial state-resolved integral cross sections for the F, Cl+$H_2(\nu = 0, 1)$ reactions. The theoretical part behind the initialization is presented in detail. This work constitutes the starting point from which NE-RPMD can be extended to more complex and intricate systems. In this chapter, the reduced Planck constant $\hbar$ is set to 1.

4.1 Introduction

The detailed study and understanding of reaction processes is a central challenge of chemical physics and theoretical chemistry. Chemisorption of a molecule onto a surface or bimolecular reactions in the gas phase are two important classes of reactions studied. Their detailed understanding is of relevance in many areas, e.g., atmospheric and interstellar chemistry, combustion and catalysis [2, 8, 68, 150–152, 193–196]. The most detailed results, initial state-selected and fully quantum state resolved reaction probabilities and cross sections, can be computed from full-dimensional quantum dynamics simulations for reactions involving only few atoms. The biggest system treated today is the $H+CH_4 \rightarrow H_2+CH_3$ reaction [48, 49, 160, 161, 163, 164]. To this end, the multi-configurational time-dependent Hartree approach [172, 175–177, 179, 197] was employed for the wavepacket propagation and reaction probabilities were obtained using the quantum transition state concept [165–171, 198]. However, these simulations are numerically very expensive and take up many months of simulation time for each reaction. They also require fitted or interpolated potential energy surfaces (PES) that can be evaluated efficiently and dedicated curvilinear coordinate systems with complicated kinetic energy operators [38, 47, 60].

To avoid the high numerical cost of rigorous, full-dimensional quantum scattering simulations, many reactive scattering calculations employ the quasiclassical trajectory (QCT) approach [64–67, 70, 71]. QCT treats all nuclei classically evolving on accurate PES or using gradients from on-the-fly ab initio calculations [180]. Initial conditions are chosen to mimic the quantum state under investigation. This is done by adding the correct amount of zero-point energy (ZPE) and energy for rovibrational excitations to the system. The QCT approach has been employed successfully to study many bimolecular and gas-surface reactions in detail. Reactions with many degrees of freedom, even including surface motion, as well as reaction with several heavy atoms can be investigated and understood by employing QCT simulations [71, 105, 116, 199, 200]. For example, effects such as the depression of reactivity at high collision energies were studied in detail [69]. The most accurate results are obtained for energies well above the threshold as tunneling is often not important for these cases. Due to the purely classical dynamics involved, the QCT approach is numerically very efficient and large systems can be treated. Yet, due to the classical nature of the QCT simulations, quantum effects such as ZPE effects

and tunneling are not systematically taken into account. Please note, that there exist many advanced procedures for QCT which can remedy those effects [75–77]. However, QCT simulations can be inaccurate for particular cases where quantum effects become important. For these cases, the inaccuracies can often be traced back to the following three points. First, the classical nature of the simulations allows any zero-point energy put into a certain degree of freedom initially to artificially leak out into any other degree of freedom. If the energy leaks into the reaction coordinate it can increase the reactivity in the QCT calculations. In certain cases this may lead to an increase of the reactivity compared to rigorous quantum calculations [72, 73]. Second, classical simulations do not respect ZPE constraints for the products which can allow forbidden product outcomes and can lead to an overestimation of the reactivity. Third, the QCT simulations do not include tunneling effects. This can lead to an underestimation of the cross-sections, particularly when the reaction includes a proton transfer and in the threshold region. Different problems can be manifest in a single reaction when looking at the reactivity of different initial vibrational states [201].

The approximate inclusion of nuclear quantum effects (NQE) like ZPE and tunneling into classical-like dynamics simulations has been a very active field of research. Various efficient methods along this way have emerged. One of the widely used approaches is the ring polymer molecular dynamics (RPMD) approach [80, 83–88]. In RPMD, an initial quantum Boltzmann distribution is represented by an ensemble of discrete representations of the imaginary-time path integral, the so-called ring polymer. Each ring polymer consists of classical replicas (termed beads) of the system joined by harmonic springs. Real-time correlation functions are then obtained from classical dynamics of these ring polymers, i.e., classical dynamics in an extended ring polymer phase space. RPMD has several appealing features. It is exact in the short-time, classical and high-temperature limits [80, 202]. Exact correlation functions can also be obtained for harmonic potentials. ZPE effects are incorporated through the harmonic springs connecting the beads and RPMD therefore respects ZPE constraints and does not suffer from ZPE leakage [139, 140, 145]. Also tunneling effects are incorporated due to the finite extension of the ring polymer, which can stretch over a barrier and therefore lower its effective height [83, 84, 135, 136, 143]. Originally, RPMD was formulated for the calculation of real-time correlation functions associated with equilibrium initial conditions. This allowed the efficient calculation of thermal rate constants,

[83, 84, 88, 135–138, 143, 203–206] diffusion coefficients, [85, 86, 89, 90] and, to some extent, vibrational spectra [91–94]. Recently, an approach to obtain quantities associated with different non-equilibrium initial conditions, e.g., a momentum kick or a vertical excitation, within the RPMD framework was proposed [95]. It was shown that RPMD can be obtained from the more general Matsubara dynamics framework [81, 82]. Despite its success, RPMD also suffers from several drawbacks. Due to the classical nature of the dynamics simulations, it cannot describe real-time coherences. Furthermore, when calculating vibrational spectra it suffers from the spurious-mode effect [91–93].

Very recently, the non-equilibrium initial conditions have been used to obtain microcanonical rate constants from RPMD simulations, however, initial state selectivity could not be addressed in these works [145, 148]. We have proposed an efficient approach that combines the RPMD approach with QCT simulations to obtain initial state-selective cross sections for bimolecular reactions [149]. Initial state-selective cross sections for the Mu/H/D+H_2(ν=0,1) reactions were calculated close to the threshold energy. It was shown that the approach approximately incorporates ZPE constraints and includes some tunneling contributions. In this manuscript we explore the approach in more detail. In particular, we test the robustness of our approach with respect to the choice of the ring polymer parameters (n, β) and the vibrational excitation scheme. Integral cross-sections for the five X+H_2, X=Mu,H,D,F,Cl reactions are studied for H_2 in its ground state as well as vibrationally excited state and for a wide range of collision energies.

4.2 Theory

4.2.1 Quasiclassical trajectory method

QCT has been widely reviewed and thus we will only give a brief overview of the approach here [65, 68, 196]. We focus on general triatomic systems A + BC(ν, j) and mostly follow Ref. [64]. The molecule BC is initially in a ro-vibrational state with vibrational and rotational quantum numbers ν and j, respectively. Quasiclassical initial positions and momenta mimicking state (ν, j) are obtained as follows: the center of mass of BC is set at the origin of the coordinate system. The intramolecular distance $r = |\boldsymbol{r}|$, where $\boldsymbol{r}$ is the vector between B and C, is set to either of the classical turning-point values r_+ or r_- corresponding to the energy of the ro-vibrational state,

$E_{\nu,j}$. The total internal molecular momentum $\boldsymbol{P} = \mu_{\mathrm{BC}}(\boldsymbol{v_C} - \boldsymbol{v_B})$, where μ_{BC} is the reduced mass of BC, is set so that that $P^2 = j(j+1)/r_{\pm}^2$ and $\boldsymbol{P}\cdot\boldsymbol{r} = 0$. BC is arbitrarily oriented along $\boldsymbol{r} \times \boldsymbol{\kappa}$ where $\boldsymbol{\kappa}$ is the unit vector along the x-axis. A vibrational phase is added by propagating BC for a random fraction of its vibrational period and finally BC is randomly oriented. The procedure described above is restricted to diatomic molecules. For polyatomic molecules one can initialize the vibrational state via normal mode sampling [117, 207]. Initial position and momenta of each mass-weighted normal mode are chosen as

$$Q_i = \sqrt{\frac{2\nu_i + 1}{\omega_i}}\cos(\phi_i), \quad P_i = \sqrt{(2\nu_i + 1)\omega_i}\sin(\phi_i), \tag{4.1}$$

where ν_i is the quantum vibrational number corresponding to the ith mode and $\phi_i \in [0, 2\pi]$ a random phase. One can then adiabatically switch the system to the full potential for better vibrational state accuracy [117]. Cartesian coordinates are then obtained by inverse normal mode transformation.

The atom A is initially placed at a fixed distance from the center of mass of BC. The distance is chosen such that there is no interaction between A and BC. The impact parameter b is chosen so that b^2/b_{max}^2 is uniformly sampled in $[0, 1]$, where b_{max} is the maximum impact parameter so that no reactions occur for any $b > b_{\mathrm{max}}$. To initiate the reaction the relative momentum between A and BC is set as $\boldsymbol{P}_{\mathrm{rel}} = \sqrt{2\mu E_{\mathrm{col}}}\boldsymbol{\kappa}$ where E_{col} and μ are the collision energy and the reduced mass of the system, respectively. The system is then propagated solving Newton's equations of motion.

Integral cross sections (ICSs) for a given total energy E_{tot} are obtained as

$$\sigma(E_{\mathrm{tot}}) = \pi b_{\mathrm{max}}^2 \frac{N_{\mathrm{R}}(E_{\mathrm{tot}})}{N(E_{\mathrm{tot}})}, \tag{4.2}$$

where N and N_{R} are the number of total and reactive trajectories respectively [64]. The number of reactive trajectories is obtained by evaluating suitable distances criteria that distinguish the products.

4.2.2 Ring polymer molecular dynamics

RPMD is based on the ring polymer extended phase space used to represent imaginary-time path integrals. For a quantum mechanical system the canonical partition function Z at inverse temperature $\beta = 1/k_B T$ can be computed as

$$Z = \mathrm{tr}\left[e^{-\beta\hat{H}}\right] = \lim_{n\to\infty} \frac{1}{(2\pi)^n} \int d\boldsymbol{p} \int d\boldsymbol{q} e^{-\beta_n H_n^{\mathrm{RP}}(\boldsymbol{p},\boldsymbol{q})} = \lim_{n\to\infty} Z_n, \tag{4.3}$$

with n the number of replicas in the ring polymer, $\beta_n = \beta/n$ and the ring polymer Hamiltonian H_n^{RP} reads

$$H_n^{\mathrm{RP}}(\boldsymbol{q},\boldsymbol{p}) = \sum_{i=1}^{N}\sum_{k=1}^{n}\left(\frac{(\boldsymbol{p}_i^k)^2}{2m_i} + \frac{m_i}{2\beta_n^2}(\boldsymbol{q}_i^{k+1} - \boldsymbol{q}_i^k)^2\right) + \sum_{k=1}^{n} V(\boldsymbol{q}_1^k,\ldots,\boldsymbol{q}_N^k), \quad \boldsymbol{q_i^{n+1}} = \boldsymbol{q_i^1}. \tag{4.4}$$

where N is the number of atoms, $\boldsymbol{q}_i^k$ and $\boldsymbol{p}_i^k$ the position and momentum vectors of the kth bead for the ith atom and V the molecular potential interaction [78]. The Boltzmann distribution in the ring polymer phase space can be effectively sampled using molecular dynamics.
The quantum mechanical Kubo-transformed equilibrium real-time correlation function

$$\bar{C}_{AB}(t) = \frac{1}{\beta Z}\int_0^\beta \mathrm{tr}\left[e^{-\lambda\hat{H}}\hat{A}e^{-(\beta-\lambda)\hat{H}}e^{i\hat{H}t}\hat{B}e^{-i\hat{H}t}\right]d\lambda, \tag{4.5}$$

with $\hat{A}$ and $\hat{B}$ arbitrary operators, is approximated within RPMD as

$$\bar{C}_{AB}^{\mathrm{RP}}(t) = \lim_{n\to\infty}\frac{1}{Z_n}\int d\boldsymbol{q}_0 \int d\boldsymbol{p}_0 e^{-\beta_n H_n^{\mathrm{RP}}(\boldsymbol{q}_0,\boldsymbol{p}_0)} A_n(\boldsymbol{q}_0,\boldsymbol{p}_0) B_n(\boldsymbol{q}_t,\boldsymbol{p}_t), \tag{4.6}$$

with $(\boldsymbol{q}_t, \boldsymbol{p}_t)$ propagated with H_n^{RP} and

$$A_n(\boldsymbol{q},\boldsymbol{p}) = \frac{1}{n}\sum_{k=1}^{n} A(\boldsymbol{q}_1^k,\ldots,\boldsymbol{q}_N^k,\boldsymbol{p}_1^k,\ldots,\boldsymbol{p}_N^k) \tag{4.7}$$

where $A(\boldsymbol{q}_1^k,\ldots,\boldsymbol{q}_N^k,\boldsymbol{p}_1^k,\ldots,\boldsymbol{p}_N^k)$ is the classical function corresponding to $\hat{A}$ evaluated at the kth bead coordinates. RPMD is exact in the short time, high temperature

and harmonic oscillator limits. Additionally, it has been shown that RPMD can be derived from Matsubara dynamics [81,82].
Recently, it has been shown that RPMD can be used to approximate non-equilibrium correlation functions and expectation values [95], e.g. for cases with an initial momentum impulse or "kick". The non-equilibrium expectation value

$$\langle \hat{A}(t) \rangle = \frac{1}{Z} \operatorname{tr} \left(e^{-\beta \hat{H}_0} e^{i\hat{H}_1 t} \hat{A} e^{-i\hat{H}_1 t} \right), \tag{4.8}$$

with

$$\hat{H}_0 = \sum_{i=1}^{N} \left(\frac{(\hat{\boldsymbol{p}}_i - \Delta\hat{\boldsymbol{p}}_i)^2}{2m_i} + V(\hat{\boldsymbol{q}}_i) \right), \quad \hat{H}_1 = \sum_{i=1}^{N} \left(\frac{\hat{\boldsymbol{p}}_i^2}{2m_i} + V(\hat{\boldsymbol{q}}_i) \right), \tag{4.9}$$

is approximated as

$$\langle A(t) \rangle = \lim_{n\to\infty} \frac{1}{Z_n} \int d\boldsymbol{q}_0 \int d\boldsymbol{p}_0 e^{-\beta_n H^{\mathrm{RP}}_{0,n}(\boldsymbol{q}_0,\boldsymbol{p}_0)} A_n(\boldsymbol{q}_t, \boldsymbol{p}_t), \tag{4.10}$$

with $(\boldsymbol{q}_t, \boldsymbol{p}_t)$ propagated with $H^{\mathrm{RP}}_{1,n}$.

4.3 Methodology

4.3.1 Initial state-selected scattering within RPMD

Initialization of BC

The initialization of BC mimicking the initial quantum state is done in two steps. Please note, that for the initialization we employ the harmonic approximation for the PES of isolated BC

$$V_0(Q) = \frac{1}{2}\omega^2 Q^2, \tag{4.11}$$

where ω and Q are the harmonic frequency and corresponding mass-weighted normal mode coordinate of BC. We will discuss the approach for a diatomic molecule here. The generalization to polyatomic molecules is discussed further below.
In the first step, initial ring polymer configurations for the mass-weighted normal mode are obtained by sampling the well-known thermal distribution for a harmonic potential. Cartesian coordinates for the beads are obtained by inverse normal mode

transformation. Sampling the normal mode guarantees that the molecule will not undergo spurious rotations or center of mass motion and that it will have the correct vibrational zero-point energy (ZPE). Yet due to sampling the initial Boltzmann distribution BC will have some additional thermal energy contributions. The thermal contributions will be minimized by choosing a low initial temperature, i.e., high β value, for the RPMD simulations. The detailed choice of β will be discussed later in Sec. 4.3.1. By employing the path integral approach we obtain correct mass-weighted initial quantum fluctuations for the position Q and momentum P. For each bead $k \in [1, n]$, we obtain

$$\langle Q^2 \rangle_k = \frac{1}{2\omega} \coth\left(\frac{\beta\omega}{2}\right), \quad \langle P^2 \rangle_k = \frac{\omega}{2} \coth\left(\frac{\beta\omega}{2}\right), \tag{4.12}$$

In the second step, to mimic a vibrationally excited state, we modify the initial position and momentum of the ring polymers' centroids to add the correct amount of vibrational energy. This step is inspired by the QCT approach described in Sec. 4.2.1. Please note that the initial sampling already contains the correct amount of ZPE and we only need to add additional vibrational energy. In this step we employ mass-weighted normal modes (of the system) and ring polymer normal modes: $\widetilde{Q}^k, \widetilde{P}^k$, $k \in [0, n-1]$. To the position and momentum centroids ($k = 0$) we add the following quantities:

$$K_Q = \sqrt{\frac{2\nu}{\omega}} \cos(\phi), \quad K_P = \sqrt{2\nu\omega} \sin(\phi), \tag{4.13}$$

with $\phi \in [0, 2\pi]$ a random phase. The resulting effect can be analyzed employing the primitive path integral energy estimator $\mathcal{E}_0$, which reads

$$\begin{aligned} \langle \mathcal{E}_0 \rangle &= -\frac{\partial \ln(Z_n)}{\partial \beta} \\ &= \langle \frac{1}{n} \sum_{i=1}^{N} \sum_{k=1}^{n} \left[\frac{\left|\boldsymbol{p}_i^k\right|^2}{2m_i} - \frac{1}{2} m_i \left(\frac{n}{\beta}\right)^2 \left(\boldsymbol{q}_i^k - \boldsymbol{q}_i^{k+1}\right)^2 \right] + \frac{1}{n} \sum_{k=1}^{n} V\left(\boldsymbol{q}_1^k, \ldots, \boldsymbol{q}_N^k\right) \rangle, \end{aligned} \tag{4.14}$$

where $N = 2$ for the case of the diatomic molecule BC. Since we employ a harmonic potential for the initialization, we can diagonalize the estimator employing mass-weighted normal modes (of the system) and ring polymer normal modes. The

estimator then reads

$$\mathcal{E}_0 = \frac{1}{n}\sum_{k=0}^{n-1}\left(\frac{1}{2}(\widetilde{P}_0^k)^2 + \frac{1}{2}(\omega^2 - \omega_k^2)(\widetilde{Q}_0^k)^2\right). \tag{4.15}$$

Adding the two quantities given in Eq. (4.13) to the path integral centroids, the path integral energy estimation reads

$$\mathcal{E}_0 = \frac{1}{n}\sum_{k=0}^{n-1}\left(\frac{1}{2}(\widetilde{P}_0^k + \delta_{k\,0}\sqrt{n}K_P)^2 + \frac{1}{2}(\omega^2 - \omega_k^2)(\widetilde{Q}_0^k + \delta_{k\,0}\sqrt{n}K_Q)^2\right). \tag{4.16}$$

Separating the centroids contributions we obtain

$$\mathcal{E}_0 = \frac{1}{n}\sum_{k=1}^{n-1}\left(\frac{1}{2}(\widetilde{P}_0^k)^2 + \frac{1}{2}(\omega^2 - \omega_k^2)(\widetilde{Q}_0^k)^2\right) + \frac{1}{2n}(\widetilde{P}_0^0 + \sqrt{n}K_P)^2 + \frac{1}{2n}\omega^2(\widetilde{Q}_0^0 + \sqrt{n}K_Q)^2, \tag{4.17}$$

and when averaging over the initial distribution we obtain

$$\langle\mathcal{E}_0\rangle = \frac{\omega}{2} + \langle(\widetilde{P}_0^0 K_P + \omega^2\widetilde{Q}_0^0 K_Q)\rangle + \frac{1}{2}(K_P^2 + \omega^2 K_Q^2), \tag{4.18}$$

where the second term on the right hand side vanishes since $\langle\widetilde{Q}_0^0\rangle = \langle\widetilde{P}_0^0\rangle = 0$. Therefore the averaged value of the energy estimator is

$$\langle\mathcal{E}_0\rangle = \omega\left(\frac{1}{2} + \nu\right). \tag{4.19}$$

The mass-weighted position and momentum fluctuations for each bead $k \in [1, n]$ are

$$\langle Q_\nu^2\rangle_k = \frac{1}{2\omega}\coth\left(\frac{\beta\omega}{2}\right) + \frac{\nu}{\omega}, \quad \langle P_\nu^2\rangle_k = \frac{\omega}{2}\coth\left(\frac{\beta\omega}{2}\right) + \nu\omega, \tag{4.20}$$

The initial ring polymer positions and velocities of BC are then used in the scattering calculations. To this end, one can directly switch to the full PES, which can depend on the anharmonicity of the full PES, or one can employ an adiabatic switching procedure to obtain more accurate initial configurations [117]. However for the direct switching, in some cases the intramolecular distance of BC will be too small at the time of the switch due to the anharmonicity of the full PES, therefore providing non-negligible extra vibrational energy which can influence the reactivity at very low collision energies. We discard those trajectories where the centroid distance for

BC falls below $d_{\text{min}}^{\nu=1}$, corresponding to the lower initial length of excited BC in QCT at the time of the switch.This ad hoc discarding procedure is performed to limit the inaccuracies from the direct switching approximation, but is not an intrinsic limitation of the overall approach as discussed later. The center of mass motion of BC is set following the QCT approach via a "kick" to the velocity centroids

$$\bar{\boldsymbol{V}}_{\text{B}} = \bar{\boldsymbol{V}}_{\text{C}} = -\frac{\boldsymbol{P}_{\text{rel}}}{m_{\text{B}} + m_{\text{C}}}, \tag{4.21}$$

which induces a center of mass motion without perturbing the internal dynamics of BC. The centroid of the center of mass of BC is initially set at the origin of the coordinate system. For the initialization of a polyatomic molecule the generalization is straightforward. We sample in the same way each normal mode independently, set its centroid center of mass at rest and its angular momentum to zero using a standard iterative modification to the velocities routinely employed in QCT simulations

$\bar{\boldsymbol{V}} \leftarrow \bar{\boldsymbol{V}} - \boldsymbol{\Omega} \times \bar{\boldsymbol{Q}}$,

to each ring polymer centroid of the molecule to compute the angular velocity $\boldsymbol{\Omega}$ with $\bar{\boldsymbol{Q}}$ and $\bar{\boldsymbol{V}}$ the centroid position and centroid velocity vector. Direct switching is then performed. Employing adiabatic switching for polyatomic systems will be the focus of a forthcoming study.

Initialization of A

A is initialized far away from the position of BC with its non-centroid ring polymer normal modes sampled from the free ring polymer distribution along the direction of the initial QCT momentum kick $\boldsymbol{\kappa}$. Then the initial centroid position of A is set similar as in QCT with an extra increment to the initial distance between the reactants due the finite spatial extension of the ring polymers. The initial distance between the centroid of A and the centroid of the center of mass of BC $d(\text{A}, \text{BC})$ is set to

$$d(\text{A}, \text{BC}) = d(\text{A}, \text{BC})_{\text{QCT}} + R_{\text{A}}^{g} + \max(R_{\text{B}}^{g}, R_{\text{C}}^{g}), \tag{4.22}$$

where $d(\text{A}, \text{BC})_{\text{QCT}}$ is the distance choice for QCT simulations and R_{A}^{g},R_{B}^{g},R_{C}^{g} are the radiuses of gyration for the ring polymer of A, B and C, respectively. Lastly the momentum centroid is then "kicked" following the QCT approach. The initial centroid velocity is set to

$$\bar{\boldsymbol{V}}_{\text{A}} = \frac{\boldsymbol{P}_{\text{rel}}}{m_{\text{A}}}. \tag{4.23}$$

Reactions and cross sections

After initializing both reaction partners we propagate the system solving the classical equations of motions in the extended ring polymer phase space. Considering the distances between the centroids of the ring polymers representing the different atoms the trajectories are distinguished between reactive and non-reactive. Cross sections are then obtained following the QCT approach (see Eq. (4.2)) as

$$\sigma_{\nu,j}(E_{\text{tot}}) = \pi b_{\text{max}}^2 \frac{N_{\text{R}}(E_{\text{tot}})}{N(E_{\text{tot}})},$$

where N and N_{R} are the number of total and reactive trajectories, respectively, and $E_{\text{tot}} = E_{\text{col}} + E_{\text{reac}}$ and E_{reac} is the total internal energy of the reactants. In this work, we focus on X+H_2 reactions and vibrational excitation and always set the angular momentum of H_2, j, to zero and employ the harmonic approximation. Therefore we have $E_{\text{reac}} = E_{H_2} = \omega_{H_2}(\nu + 0.5)$. This constitutes a reliable and consistent approximation in the case of a diatomic molecule as we shall see later with the results for classical-like systems such as $D + H_2(\nu = 0, 1)$.

Choice of β

We touched on the importance of β for the current approach above. Here, we motivate the choice of β for the present approach. The decision is guided by four main considerations.

First, since the choice of β will influence the additional thermal energy in the initialization of the molecule, it should therefore be high enough to limit those thermal contributions. As the system is expected to behave classically when the collision energy becomes large, β should reach a lower limit, β_-. Second, the dynamics of the ring polymer will be influenced by the choice of β through the spring constants and therefore β should be set such that the energy and momentum of each reactant reflect the temperature associated with β.

Third, β should be inversely proportional to the additional energy we give to the system in the initialization process through kicking the centroids, which comprise initiating the collision process and adding vibrational excitation.

Fourth, when $\nu = 0$ we assume that β lies in the interval $[\beta_A, \beta_{BC}]$ for $m_{BC} > m_A$

(and inversely otherwise) with

$$\beta_{\mathrm{A}} = \alpha \frac{m_{\mathrm{tot}}/m_{\mathrm{BC}}}{E_{\mathrm{col}}}, \quad \beta_{\mathrm{BC}} = \alpha \frac{m_{\mathrm{tot}}/m_{\mathrm{A}}}{E_{\mathrm{col}}}, \tag{4.24}$$

where β_X is obtained via equating $|\bar{\boldsymbol{V}}_X|$ with a typical thermal speed corresponding to different values of α ($\alpha = \frac{4}{\pi}$ for the mean of the magnitude, $\alpha = \frac{3}{2}$ for the root mean square and $\alpha = 1$ for the most probable magnitude) at inverse temperature β_X for a mass m_X.

To obtain a common β for all the ring polymers, we choose β as an average of both values,

$$\beta = \frac{1}{2}(\beta_{\mathrm{A}} + \beta_{\mathrm{BC}}), \tag{4.25}$$

following a symmetry argument since in the center of mass frame we have $|p_A| = |p_{BC}|$.
So far our choice of β for a given initial collision energy and vibrational state reads

$$\beta = \begin{cases} \frac{\alpha}{2} \frac{m_{\mathrm{tot}}/\mu}{(E_{\mathrm{c}}+\nu\omega)}, & \text{if } \beta > \beta_{-}. \\ \beta_{-}, & \text{otherwise}, \end{cases} \tag{4.26}$$

where $\alpha \in \{\frac{4}{\pi}, \frac{3}{2}, 1\}$. This is the ansatz we used in our previous work (with $\alpha = \frac{4}{\pi}$ and $\beta_{-} = 300$) [149]. Inducing a lower cut-off for β is necessary for high collision energies.

In our previous work β_{-} was chosen to a fixed value so that the extra thermal energy contributions remained within 1% of the ZPE of H_2. This can result in an abrupt cut-off. Nevertheless we can avoid this abrupt cut-off by imposing the thermal contribution to the internal energy of the H_2 vibrational energy to be within a few percent of the total energy instead of H_2's vibrational energy. This way β will monotonically decrease with the total energy instead of meeting a fixed cut-off value. Doing so improves slightly the results for the H/D+$H_2(\nu = 1; j = 0)$ ICSs around the threshold energy values. We limit the thermal contributions below $p\%$ of the total energy and thus:

$$\beta_{-} = \frac{1}{\omega} \log \frac{\omega - pE_{\mathrm{tot}}}{pE_{\mathrm{tot}}}, \tag{4.27}$$

where $E_{\mathrm{tot}} = E_{\mathrm{col}} + E_{\mathrm{H_2}}$ and $E_{\mathrm{H_2}}$ is the total internal energy of H_2. In this work, we

focus on vibrational excitation and always set the angular momentum of H_2 to zero and therefore have $E_{H_2} = \omega_{H_2}(\nu + 0.5)$.
This choice can lead to high values of β at very low collision energies for $\nu = 0$, which is only desired for the cases where there is a large increase of ZPE from reactants to products, i.e., for cases where there is a large decrease in "non-ZPE energy" for a given total energy, e.g., for reactions like Mu+H_2. In these cases one requires a large value of β to describe the product side of the reaction well. However, for cases where the ZPE does not change much or where it decreases, the values of β employed are too large. We therefore correct our ansatz by only keeping the terms $2 + \frac{m_{\mathrm{BC}}}{m_{\mathrm{A}}}$ from $\frac{m_{\mathrm{tot}}}{\mu}$ for such systems when $m_{\mathrm{A}} > m_{\mathrm{BC}}$ and $\nu = 0$. This modification is a first attempt at obtaining a reliable and systematic choice of β for our approach and will require further study and possibly adjustments. For vibrationally excited systems the change of ZPE is typically small compared to the vibrational energy added to the system and thus we do not employ this modification. All things considered we have:

$$\beta_{\nu=0} = \begin{cases} \beta_- & \text{if } \beta < \beta_- \text{ else} \\ \frac{\alpha}{2}\frac{2+\frac{m_A}{m_{BC}}+\frac{m_{BC}}{m_A}}{E_{\mathrm{c}}} & \text{if } m_A \leq m_{BC}, \\ \frac{\alpha}{2}\frac{2+\frac{m_{BC}}{m_A}}{E_{\mathrm{c}}} & \text{if } m_A > m_{BC}, \end{cases} \qquad \beta_{\nu\geq 1} = \begin{cases} \beta_- & \text{if } \beta < \beta_- \text{ else} \\ \frac{\alpha}{2}\frac{m_{\mathrm{tot}}/\mu}{(E_{\mathrm{c}}+\nu\omega)}. \end{cases} \tag{4.28}$$

The β profiles for the systems studies in this manuscript are shown in Fig. 4.1. The range of collision energies employed in this work is between 0.08 eV and 1.55 eV and the centroid kick (see Eq. (4.13) with $\nu = 1$) vibrational excitation energy of H_2 is 0.55 eV.

4.4 System details

We use our method to compute initial state-resolved integral cross sections (ICSs) for the following triatomic systems: D+$H_2(\nu = 0, 1)$, H+$H_2(\nu = 0, 1)$, Mu+$H_2(\nu = 0, 1)$, Cl + $H_2(\nu = 0, 1)$ and F + $H_2(\nu = 0, 1)$, with the mass of Mu mass being 0.113 m_{H}. In all cases the angular momentum of H_2 is set to zero and β is chosen according to Eq. (4.28) (equivalently Eq. (4.26) for the systems Mu/H/D+H_2) with $\alpha = \frac{4}{\pi}$. The employed harmonic frequency of H_2 (ω_{H_2}) is 4407 cm^{-1}. For H_2 (BKMP2 PES) the difference between the exact energies for the vibrational ground and excited

states and their harmonic counterparts are around 20 cm^{-1} and 250 cm^{-1}, respectively. Thus only a very small error is introduced for the ground state while for the excited state this error might play a small role around the threshold for the systems Cl/F+$H_2(\nu = 1)$ which will be discussed in the results part. Unless explicitly specified otherwise, the number of beads n employed throughout this work is expressed as an integer multiple of the dimensionless quantity $\lceil \beta\omega_{H_2} \rceil$, where $\lceil x \rceil$ gives the least integer greater or equal to x. $\lceil \beta\omega \rceil$ is often used in PIMD or RPMD simulations as an indicator of the minimum value for n such that the approximation in Eq. (4.3) can be justified. We set $p = 0.01$ for β_- so that the thermal contributions never exceed 1% of the total energy. For our simulations, the lowest value of β is reached for $\nu = 0$ at $E_{\text{tot}} = 1.4$ eV where $\beta = \beta_- = 181$. An upper limit for β, $\beta_{max} = 1500$, is introduced for computational convenience. As for $d_{min}^{\nu=1}$, the lower intermolecular distance corresponding to a vibrationally excited H_2, it is set to 1.078 bohr.
To study the D/H/Mu+H_2 systems we employ the BKMP2 PES [208]. The minimal initial distance between the reactants is 10 bohr. The maximal impact parameter in the QCT-RPMD simulations is typically about a factor of 1.3 for Mu+H_2 and 1.1 for D/H+H_2 larger than in the respective QCT simulations at the lowest collision energies when there is still reactivity in both cases. For each collision energy the integral cross sections are computed via running 40000 trajectories per collision energy using a modified Velocity-Verlet integrator with a time step of 0.02 fs. To study the systems $Cl + H_2$ and $F + H_2$ we employ the Capecchi-Werner (CW) PES and the Li-Werner-Alexander-Lique (LWAL) PES, respectively [209, 210]. As for the maximal impact parameters, in the QCT-RPMD simulations it is noticeably higher than QCT for Cl+$H_2(\nu = 1)$ by a factor of 1.5 at most and typically a factor of 1.15 for F+$H_2(\nu = 0)$. The highest difference is found for the reaction F+$H_2(\nu = 1)$ where QCT-RPMD trajectories at $E_{\text{col}} = 0.3$ eV can react for impact parameters as high as 8 bohr corresponding to a factor of 3 compared to QCT. The initial distance between the reactants is set to 10 and 12 bohr for Cl/F+H_2, respectively. The same number of trajectories are run per collision energy with the same integrator, this time with a time step of 0.05 fs. In Fig. 4.1 we plot the profiles of our choice of β for each system and vibrational state of H_2 over the total energy.

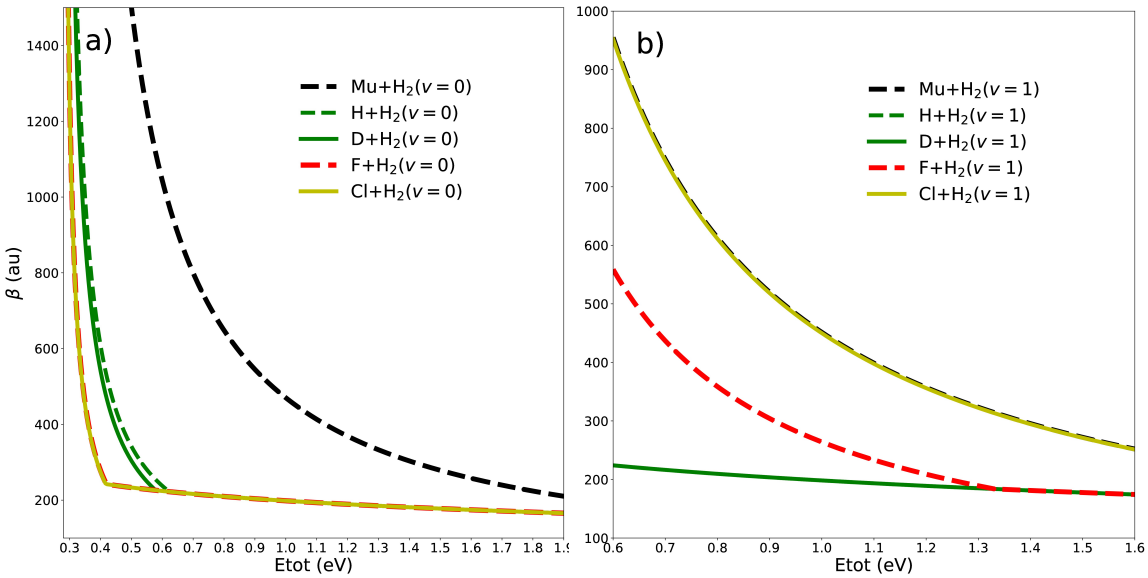

FIGURE 4.1: β values for each reactive system treated.

4.5 Results

In this section, we will discuss the results of the proposed approach for five different triatomic reactions: Mu/H/D+$H_2(\nu = 0, 1)$ and Cl/F+$H_2(\nu = 0, 1)$. Yet, before we go into the details of the specific reactions, we will investigate the robustness of our vibrational excitation scheme, the choice of β as well as the convergence with the number of beads. To this end, we employ the Mu+$H_2(\nu = 0, 1)$ reaction as a test case, as this reaction shows the biggest difference between exact quantum dynamics and QCT.

4.5.1 Convergence studies

First, let us consider the robustness of the proposed scheme to mimic the vibrational states $\nu = 0, 1$ of H_2. To this end, we investigate the time-evolution of the primitive internal energy estimator averaged over the ring polymer configurations, initialized as described in the "Initialization of BC" subsection and then propagated on the full PES. In this case, the second reactant is placed very far away from H_2 such that there is no interaction during the full simulation. The primitive internal energy

estimators for H_2 reads

$$\langle E_\nu^{\mathrm{RP}}(\boldsymbol{q},\boldsymbol{p})\rangle = \left\langle \frac{1}{n}\sum_{i=1}^{N}\sum_{k=1}^{n}\left(\frac{(\boldsymbol{p}_i^k)^2}{2m_i} - \frac{m_i}{2\beta_n^2}(\boldsymbol{q}_i^{k+1}-\boldsymbol{q}_i^k)^2\right) + \frac{1}{n}\sum_{k=1}^{n} V(\boldsymbol{q}_1^k,\ldots,\boldsymbol{q}_N^k)\right\rangle, \tag{4.29}$$

where $\langle \ldots \rangle$ is an average over the initial conditions. Here, we use 50 000 different initial conditions. We consider the primitive estimator regardless of the slow convergence since both virial variations are not suited for the $\nu = 1$ initialization due to the absence of suitable kinetic term to take into account the centroid stretch in Eq. (4.15). The time evolution $\langle E_\nu^{\mathrm{RP}}(\boldsymbol{q},\boldsymbol{p})\rangle(t)$ is shown in Fig. 4.2. For the ground state $\nu = 0$ (blue and green lines) we observe almost stable average energy upon switching to the full PES at $t = 0$. As for the excited state $\nu = 1$, yellow lines, we observe a small dependence on β. For $\beta = 200$, we find a stable average energy around the harmonic value. For $\beta = 300$ we find small jumps to lower energies at $t = 0$. This difference is due to the coupling of the beads with the now much more energetic centroids and the abrupt nature of the potential switch for which the direct use of the same estimator before and after the instantaneous switch makes the evaluation of the energy approximate.

We also observe a very small energy damping coming from the centroids of around 3 cm^{-1} every 10 fs, which is too slow to interfere with the reaction process in the time frame of our simulations, typically which is less than 250 fs. The damping also indicates that the leakage of energy from the centroid to the beads due to the anharmonicity of the potential is very small. Second, we study the influence of β on the calculated cross sections. In Fig. 4.3 a) we display the integral cross sections for Mu+$H_2(\nu = 0)$ in the vicinity the exact threshold energy for a fixed value of β. For each β the ICS curve behaves quite differently which indicates, as expected, the necessity to select β depending on the total energy of the system. The fact that the ICS calculated with $\beta = 200$ does not coincide with the one from QCT-HB calculations is a confirmation that some non-classical effects are still encompassed for this case even at higher collision energies. As we higher β the ICS curves match the quantum threshold better for $E_{\mathrm{tot}} < 0.9$ eV and then tend to underestimate more and more the reactivity for higher total energy. This indicates that higher β values capture better the low energy reactivity and inversely so. A similar test for the system Mu + $H_2(\nu = 1)$ is shown in Fig. 4.3 b). The same qualitative behavior of the ICS with respect to β is observed.

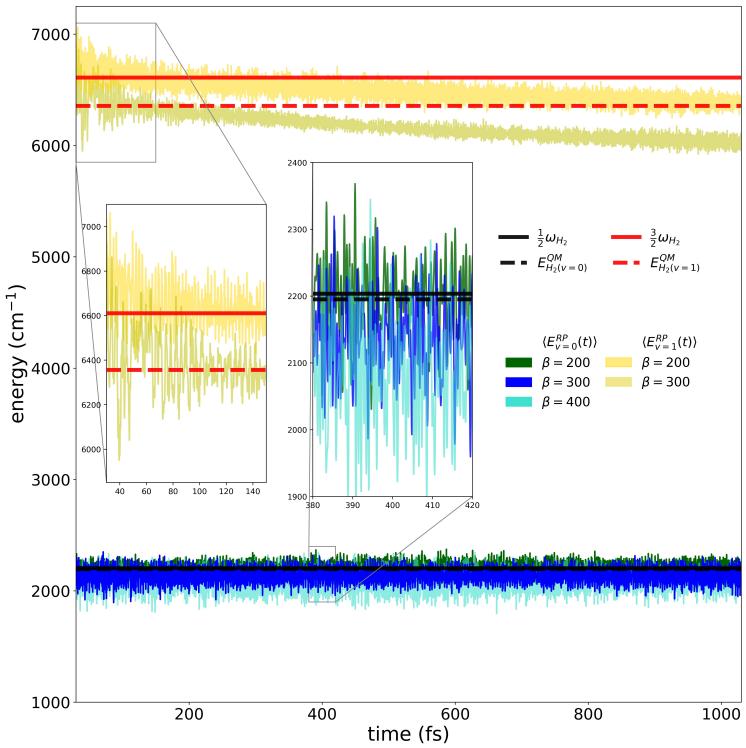

FIGURE 4.2: Energy estimators $\langle E^{\mathrm{RP}} \rangle$ for $H_2(\nu = 0, 1)$ as a function of time. Reference values for the harmonic regime and exact energy levels of $H_2(\nu = 0, 1)$ are indicated as solid and dashed lines, respectively.

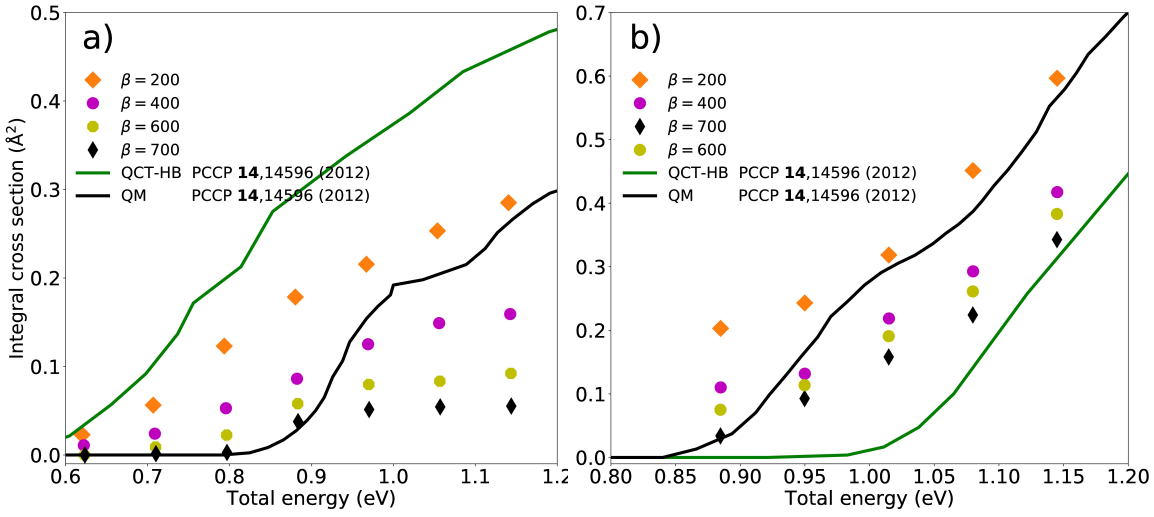

FIGURE 4.3: a) Mu + $H_2(\nu = 0; j = 0)$ and b) Mu + $H_2(\nu = 1; j = 0)$ QCT-RPMD ICSs for several fixed values of β with $n = 4\lceil \beta\omega_{\omega_{H_2}} \rceil$ where $\lceil \beta\omega_{\omega_{H_2}} \rceil$ refers to the least integer i such that $i \geq \beta\omega_{\omega_{H_2}}$. The corresponding numbers of beads used for $\beta = 200, 400, 600, 700$ are 16, 32, 48 and 56, respectively.

Third, we test the convergence of the scattering results with the number of beads employed. Fig. 4.4 a) and 4.4 b) present cross sections computed with different values of β ($\beta = 200, 700$ and β according to Eq. (4.26) with $\alpha = \frac{4}{\pi}$) for different numbers of beads. We observe graphical convergence with $n \geq 3n_r$ resulting in less than 100 beads for all cases considered here (see Table 4.1). The biggest differences of about 23% can be observed around the threshold at $E_{col} \approx 1.05$ eV for $\nu = 0$ and also around the threshold for the $\nu = 1$ case with a difference of around 20% at $E_{col} \approx 0.2$ eV. The presence of convergence with the number of beads shows that the method is consistent throughout its different steps.

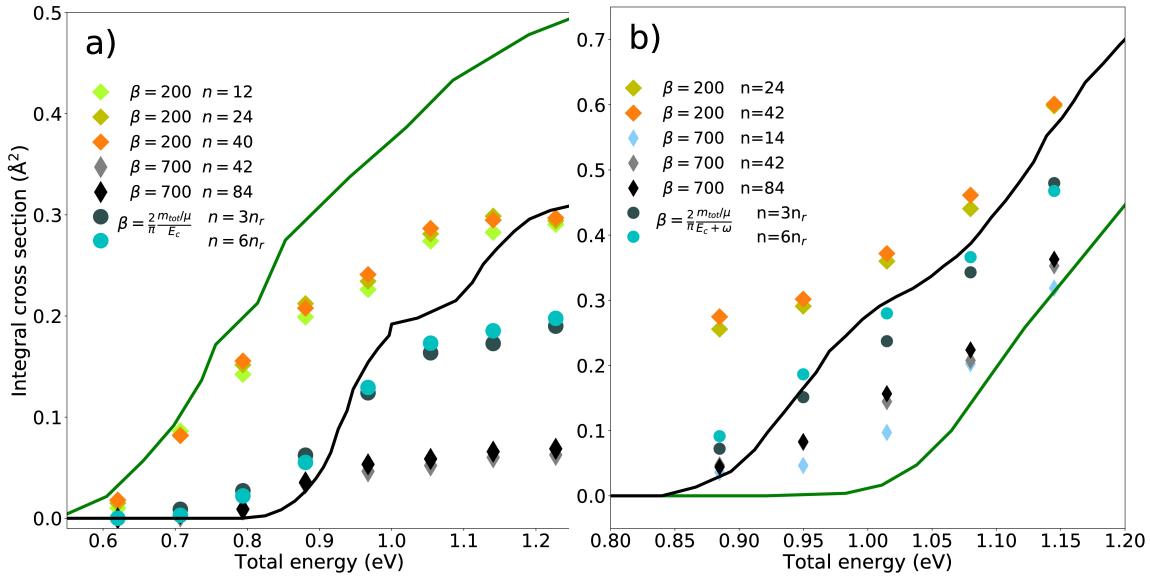

FIGURE 4.4: a) Mu + $H_2(\nu = 0; j = 0)$ and b) Mu + $H_2(\nu = 1; j = 0)$ QCT-RPMD ICSs for several fixed values of β and β chosen according to Eq. (4.26) with $\alpha = \frac{4}{\pi}$ with varying number of beads given in Table 4.1, $n_r = \lceil \beta\omega_{H_2} \rceil$.

E_{tot}(eV)	β	$n = 3\lceil\beta\omega_{H_2}\rceil$	$n = 6\lceil\beta\omega_{H_2}\rceil$	E_{tot}(eV)	β	$n = 3\lceil\beta\omega_{H_2}\rceil$	$n = 6\lceil\beta\omega_{H_2}\rceil$
0.50	1509	90	182	1.05	441	26	54
0.55	1236	74	148	1.10	414	24	50
0.60	1047	64	126	1.15	390	24	48
0.65	908	54	110	1.20	369	22	44
0.70	802	48	96	1.25	350	22	42
0.75	718	44	86	1.30	333	20	40
0.80	650	40	78	1.35	318	20	38
0.85	593	36	72	1.40	304	18	36
0.90	546	32	66	1.45	291	18	36
0.95	506	30	60	1.50	279	16	34
1.0	471	28	56	1.55	268	16	32

TABLE 4.1: The values of β (in Hartree^{-1}) and the number of beads, n, employed in the Mu+H_2(ν=0,1) simulations. β is chosen according to Eq. (4.26) and the number of beads is set relative to β and the vibrational frequency of H_2, ω_{H_2} to allow for systematic convergence tests (see Fig. 4.4 and Sec. 4.4).

4.5.2 D/H/Mu+H_2

These systems were studied in our previous work which dealt with the ICSs for the corresponding systems around their thresholds [149]. Here we recomputed the ICSs with a different β, i.e., with the previous smooth energy dependent cut-off instead of the abrupt $\beta_- = 300$ cut-off, as well as a wider range of collision energies. First we focus on the reactivity of H/D with H_2 in its vibrational ground state. The ICSs for the two reactions are shown in Fig. 4.5. For those systems β reaches its cut-off values $\beta_-(E_{\text{tot}})$ around the thresholds, i.e. for total energies of 0.62 eV (threshold at 0.57 eV) and 0.55 eV (threshold at 0.58 eV) for H and D, respectively. As in our previous paper, the QCT-RPMD ICSs match closely with the quantum ICSs around the threshold and we now observed the same match for high collision energies up to 1.4 eV. The almost classical behavior of the ICSs for all collision energies above the threshold is consistent with β reaching its lower cut-off value close to the threshold. However, we like to point out that the Gaussian binning approach, which typically increases accuracy of QCT simulations (see Mu+H_2 below), decreases the accuracy

here. QCT-RPMD on the other hand does not have a need for specifically designed binning schemes. The good agreement at higher collision energies justifies the proposed cut-off scheme for β at high collision energies.

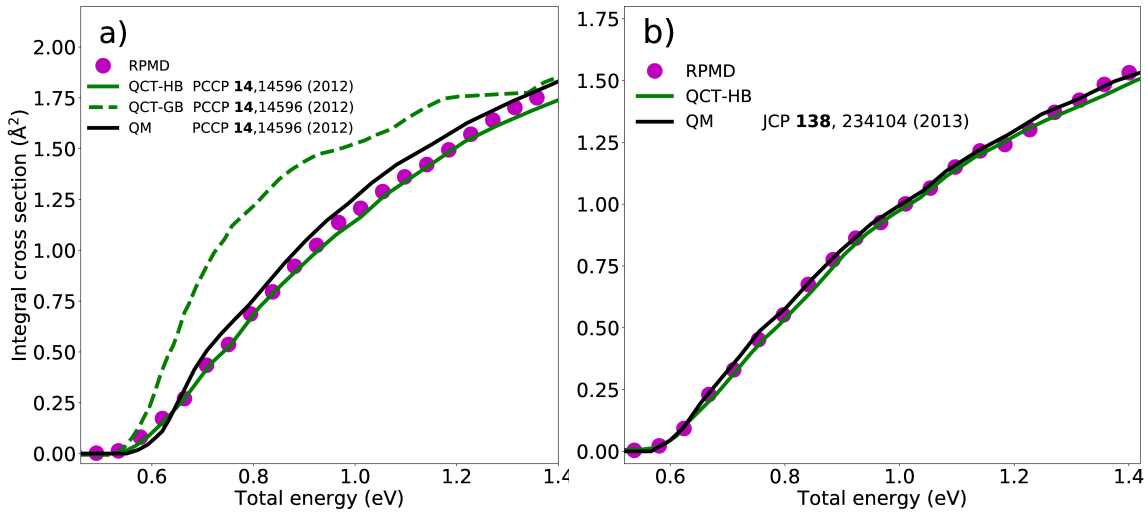

FIGURE 4.5: a) D + $H_2(\nu = 0; j = 0)$ and b) H + $H_2(\nu = 0; j = 0)$ QCT-RPMD ICSs for $n = 6\lceil\beta\omega_{H_2}\rceil$.

For the calculation of ICSs for H/D with H_2 in its vibrational excited state, we have $\beta = \beta_-$ for all collision energies considered, which is consistent with QCT-HB ICSs and QM ICSs being very similar for those energies. The ICSs are shown in Fig. 4.6. In our previous work, we studied this reaction up to a total energy of 1.1 eV and observed good agreements with QM results. We now match for total energies up to 1.4 eV. As in our previous work, we see that RPMD accurately reproduces the threshold energy. Only a slight underestimation for the H+$H_2(\nu = 1)$ reaction is found. The ICSs at higher collision energies are very close to the QM results. This indicates that the proposed ring polymer vibrational excitation scheme for $H_2(\nu = 1)$ works acceptably well from the threshold energies to reasonably high energies.

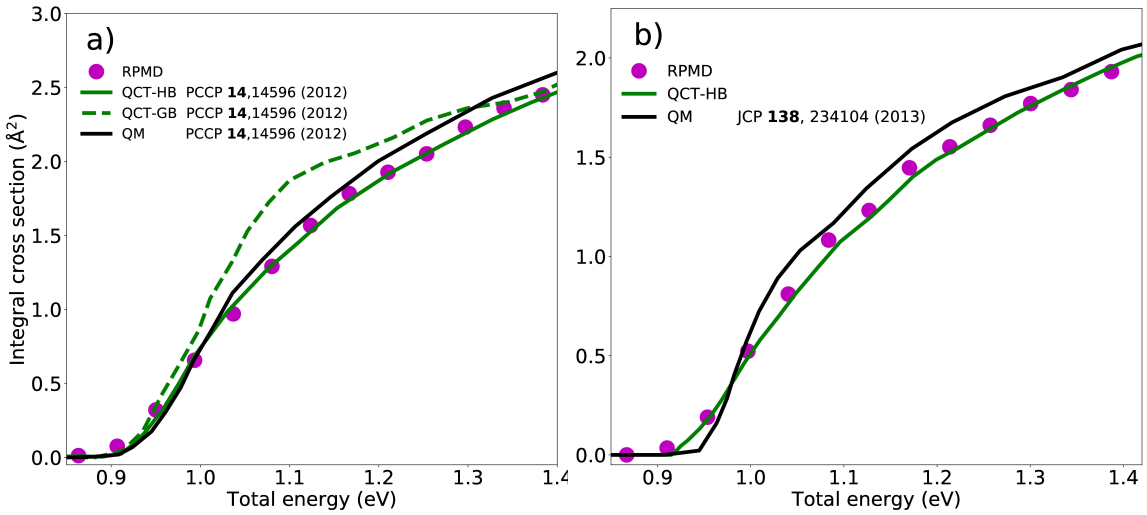

FIGURE 4.6: a) $D + H_2(\nu = 1; j = 0)$ and b) $H + H_2(\nu = 1; j = 0)$ QCT-RPMD ICSs for $n = 6\lceil\beta\omega_{H_2}\rceil$.

We switch our focus on the reactivity of Mu with $H_2(\nu = 0, 1)$. For $\nu = 0$, quantum effects govern the reactivity for the full energy range considered here. For ν=1 quantum and QCT results start coming close at $E_{tot} = 2.2$ eV. We studied these two reactions in our previous paper for total energies close to the threshold. In this study we extend the energy range as to see how RPMD performs at approximating NQE for higher collision energies. The corresponding ICSs are displayed in Fig. 4.7. For the reaction of H_2 in its ground state (Fig. 4.7 a)), we restate that the QCT-RPMD scattering results very well reproduce the exact QM ICSs calculations around the threshold. The QCT calculations using histogram binning (HB), i.e., treating every trajectory equally, show a much lower reactivity threshold compared to the QM calculations due to the absence of ZPE constraints [115, 181, 211]. This problem can be partly avoided making use of Gaussian binning (GB) as it can be seen in Fig. 4.7 [186]. GB lowers the contributions to the reactivity for trajectories which violate the ZPE constraint when considering their products' classical energies, i.e., more precisely, for which the products' energies are far from the quantum vibrational energies. QCT with GB predicts well the threshold energy but underestimates the cross section away from the threshold and for higher energies it starts to overestimate the ICSs. For higher collision energies away from the threshold we note that the RPMD results tend to underestimate the exact ICS. This is mostly noticeable above a total energy of 1.1 eV. In Fig. 4.7 b), we show the RPMD results for the same reaction but with H_2 vibrationally excited, ν=1. Both QCT variants

(HB and GB) cannot reproduce the exact QM results and display a higher threshold for reactivity due to the absence of quantum effects contributing to the reactivity, i.e., tunneling through the vibrationally adiabatic barrier [115]. As mentioned in our previous paper, QCT-RPMD finds a similar threshold for the reaction as the QM results, but slightly overestimates the reactivity for $E_{tot} < 0.95$ eV. Our RPMD vibrational excitation approach slightly underestimates the QM scattering results for higher collision energies but approximates tunneling contributions to some extent and describes the exact quantum ICSs better than the different QCT variants. This shows that our model with RPMD approximates the tunneling contribution through the $\nu = 1$ vibrationally adiabatic barrier well as the finite extension of the ring polymer allows to stretch over the barrier and reduce the effective barrier height. Only a slight increase in computational cost is required and less than 60 beads are needed for convergence.

In order to study how the spatial extension of Mu accounts for the ZPE effects we ran the same simulations using two different values of β for each reactant, i.e, $\beta = 10$ au for Mu (shrinking the gyration radius of Mu to around 0.1 bohr) and $\beta = 200, 400$ au for $H_2(\nu = 0)$ and $H_2(\nu = 1)$, respectively. A comparison of these results with QCT-HB is shown in Fig. 4.8. For $H_2(\nu = 0)$ the QCT-HB results are recovered with only a slight under-estimation of the ICSs past $E_{tot} = 1.1$ eV. This emphasizes the role of the spatial extension of the Mu ring polymer to describe the ZPE effects for the energy range considered. Comparison with the $\beta = 200$ QCT-RPMD ICS curve from Fig. 4.4 shows that the sampling of ring polymer H_2 at high enough β to avoid thermal contributions to the energy is essential at low collision energies. For $H_2(\nu = 1)$ we observe that a "point-like" Mu decreases the reactivity, but the RPMD results still show a lower threshold than the QCT results. The spatial extension of Mu only partly accounts for the NQE important for this reaction.

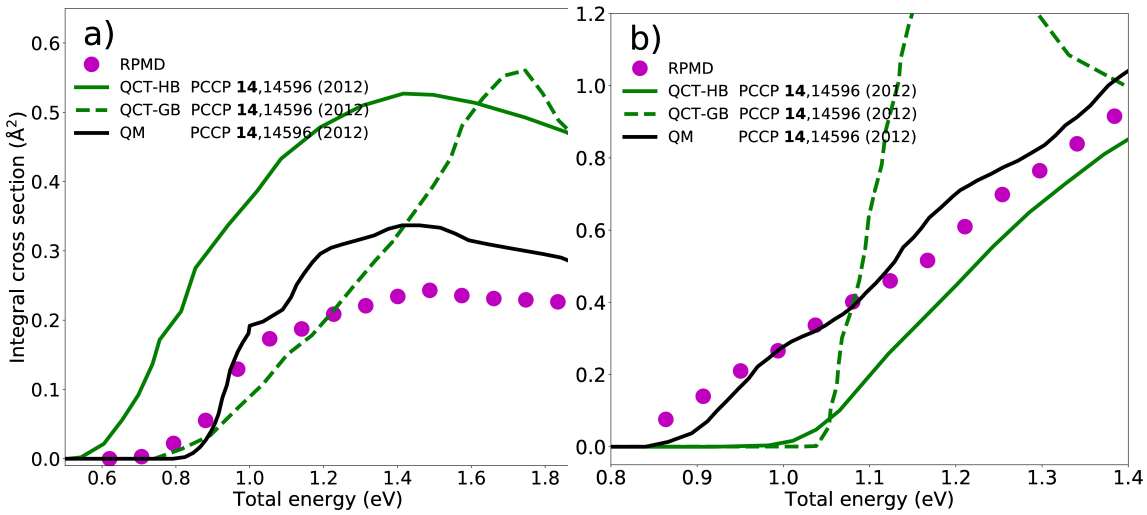

FIGURE 4.7: a) Mu + $H_2(\nu = 0; j = 0)$ and b) Mu + $H_2(\nu = 1; j = 0)$ QCT-RPMD ICSs for $n = 6\lceil\beta\omega_{H_2}\rceil$.

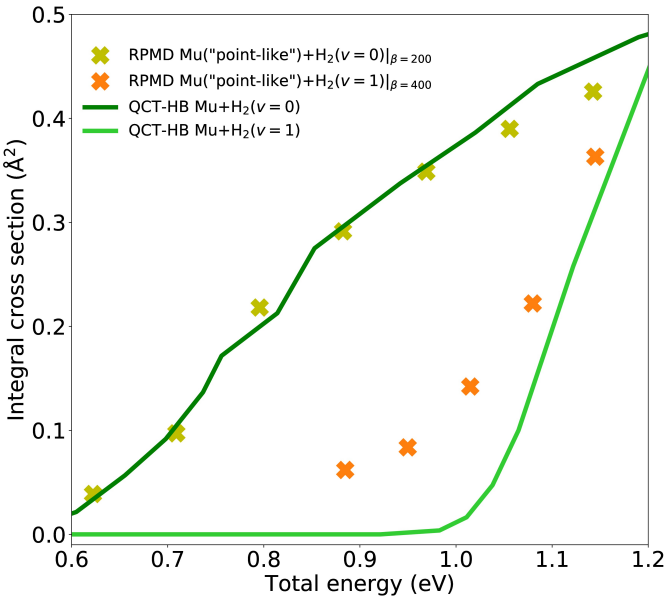

FIGURE 4.8: Mu + $H_2(\nu = 0, 1; j = 0)$ ICSs comparisons for QCT-RPMD with Mu almost point-like (gyration radius ≈ 0.1 bohr) for ($n = 4\lceil\beta\omega_{H_2}\rceil$) vs. QCT-HB.

4.5.3 Cl+H_2

We now apply our method to study the reactivity of Cl with H_2 in its vibrational ground and first excited state. This reaction involves vibrational non-adiabaticity

and the atom A is now much more massive [184]. This is the first time that the vibrational effects for Cl+H_2 are studied using RPMD. This makes it a good benchmark system to further test the applicability and the robustness of our method. Electronically non-adiabatic effects and spin-orbit couplings are not considered. The results for the RPMD ICSs compared with QCT-HB and the quantum dynamics results are displayed in Fig. 4.9. For Cl+$H_2(\nu = 0)$ we observe a good match with the QM results for all collision energies considered which is expected since QCT-HB only slightly underestimates the reactivity. Yet, we find a small improvement over the QCT results for all energies considered.

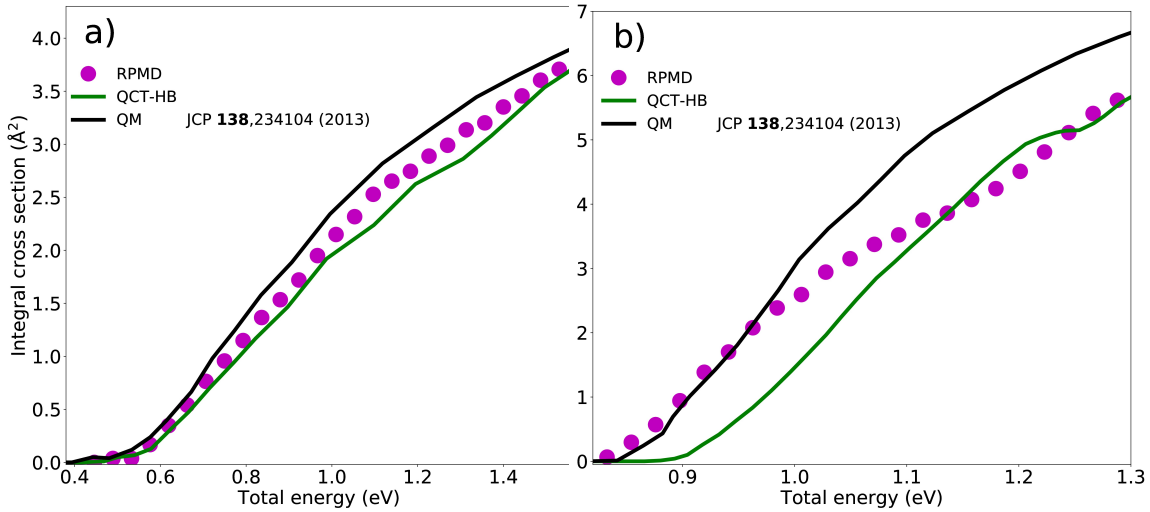

FIGURE 4.9: a) Cl + $H_2(\nu = 0; j = 0)$ and b) Cl + $H_2(\nu = 1; j = 0)$ QCT-RPMD ICSs for $n = 6\lceil\beta\omega_{H_2}\rceil$.

As for Cl+$H_2(\nu = 1)$ which involves vibrational non-adiabaticity effects helping at overcoming the barrier, we observe that RPMD predicts correctly the threshold, contrary to QCT which, just as with Mu+$H_2(\nu = 1)$, overestimates the threshold [184]. RPMD reproduces the threshold correctly and predicts well the exact quantum ICSs for $E_{tot} < 0.95$ eV, while QCT-HB underestimates the ICSs for all energies considered. In this regime, RPMD describes the contribution of vibrational excitation to the reactivity correctly, while QCT seems to be to a certain extent vibrationally adiabatic [184]. This correct prediction of the threshold behavior by our approach has to be partially tempered and put into perspective considering the presence of the direct switching approximation which can potentially lead to a slight spurious shift of the threshold predicted by RPMD. Nevertheless, the RPMD results would remain an improvement over the QCT predictions. Between 0.95 eV

and 1.10 eV for the total energy we observe that RPMD results start to underestimate the QM ICSs and tends towards the QCT-HB results. For higher total energies ($\geq$ 1.1 eV) QCT-RPMD ICSs coincide with QCT ICSs which hints that with the high masses involved here RPMD becomes more classical at higher collision energies contrary to Mu+$H_2(\nu = 0, 1)$ where RPMD approximated the quantum effects very well even at similarly high energies.

4.5.4 F+H_2

We now test our method with the important and notoriously intricate F+$H_2(\nu = 0, 1)$ benchmark reactions. The F+H_2 system has a very low barrier, a bent transition state geometry and is governed by quantum effects at low energies such as tunneling and resonances [212, 213]. The ICSs increase very quickly with collision energy, and the considerable shift in the threshold between F+$H_2(\nu = 0)$ and F+$H_2(\nu = 1)$ indicates vibrational adiabaticity and a low vibrational enhancement. The resulting ICSs are displayed in Fig. 4.10.

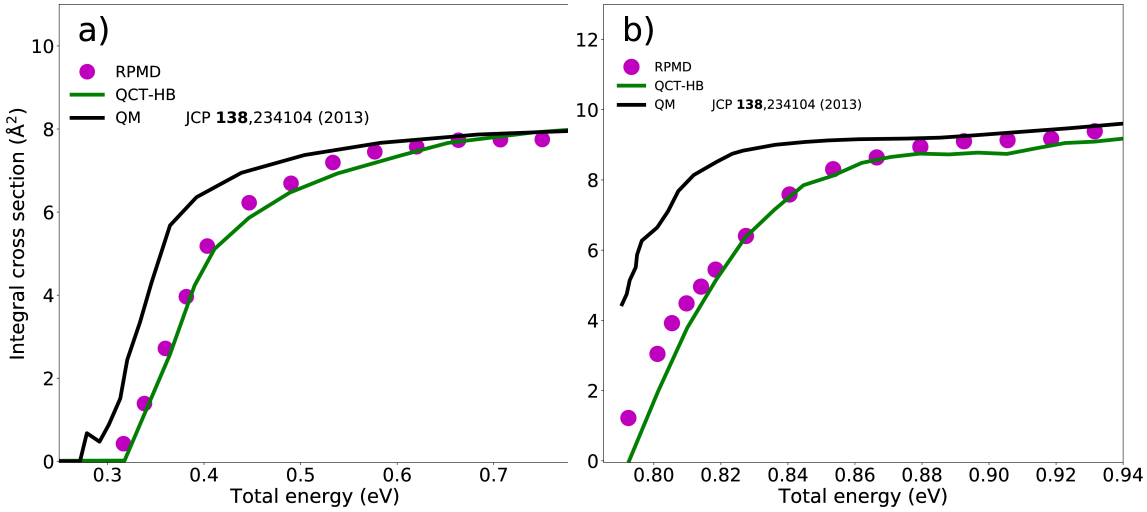

FIGURE 4.10: a) F + $H_2(\nu = 0; j = 0)$ and b) F + $H_2(\nu = 1; j = 0)$ QCT-RPMD ICSs for $n = 6\lceil\beta\omega_{H_2}\rceil$ and $\beta_{max} = 1500$.

Overall agreement between QCT-RPMD and QM simulations is less good for this case. For $\nu = 0$ and for total energies below 0.65 eV QCT-RPMD predicts slightly higher reactivity than QCT but underestimates the reactivity from QM simulations. It was partially expected since RPMD is not suited to describe quantum dynamical resonance effects which are important in this system and known to enhance the

tunneling at very low collision energies for this reaction [210, 212]. For the $\nu = 1$ case, QCT-RPMD also underestimates the reactivity, but does a bit better than QCT-HB around the threshold capturing partially the enhancing quantum effects near the threshold. It was shown, contrary to the $\nu = 0$ case, that no reactive resonance occurs in the F+$H_2(\nu = 1, j = 0)$ reaction with this work instead indicating that the reaction mainly occurs via direct abstraction with a very strong dependence on the nature of the quantum H_2-vibration [27]. Thus, it is a bit surprising that the QCT-RPMD approach underestimates the reactivity considerably. However, as the F+$H_2(\nu = 1)$ reaction is nearly barrierless it proceeds with minimal collision energy (e.g., $E_{\text{col}} \approx 0.003$ eV at the threshold). This low collision energy leads to significantly increased propagation time and, therefore, the ring polymer H_2 vibrational energy undergoes a damping which can lead to a loss of about 5% (0.04 eV) of its energy. This loss is non-negligible for this reaction as the reactivity increases drastically a low collision energies. The presence of the possible spurious shift of total energy due to the direct switching approximation also needs to be acknowledged when considering the threshold predictions of our approach. Those considerations constitute a limit of our current approach for very low collision energies and can contribute to QCT-RPMD underestimating the reactivity in this particular case. Extensions of the present approach to reduce those effects need to be investigated.

4.5.5 Discussion

So far our method describes well the exact quantum ICSs around the threshold and medium collision energies for the reactive systems Cl/D/H/Mu+$H_2(\nu = 0, 1)$. However, RPMD tends to underestimate the reactivity at higher collision energies. We saw above in the previous convergence studies that ICSs around the threshold are well reproduced by RPMD for low values of β and that RPMD ICSs tend to differ more with different β values at higher collision energies. Our ansatz for β is a first attempt at inferring the right physical choice for β but, as we mentioned for the ICSs, seems to overestimate its values at high collision energies. Taking $\alpha = 1$ on the other hand renders better the ICSs at higher collision energies but fails to reproduce the right shape of the threshold. We are currently working on a more systematic choice of β in the framework of our method. To our best knowledge, the only attempt at tuning β as a function of the energy was done with a single ring polymer to compute microcanonical rate for the Eckart barrier with RPMD [148].

Combining QCT and RPMD to describe initial-state selective quantities for triatomic reactive systems was the first natural step. The method presented here can be straightforwardly generalized to polyatomic molecule reactants and can also be directly applied to the study of gas-surface reactions. The initialization of well-defined vibrational initial states using an adiabatic switching procedure adapted for RPMD is currently under investigation. In addition, the initialization of distinct rotational and ro-vibrational initial states on the basis of the previous step and the latest QCT techniques adapted to RPMD will improve the applicability of the approach. In future work, the resolution of final ro-vibrational states needs to be worked out. To this end, one can also employ adapted successful QCT procedures [66, 214]. This will allow for the subsequent computation of the state-to-state differential cross sections.

4.5.6 Conclusion

In this manuscript, we discussed the robustness, convergence and accuracy of a very recently proposed method to approximately calculate quantum initial state-selected reactive cross sections which combines QCT and RPMD. For testing we focused on prototypical triatomic systems X+H_2, X=Mu, H, D, Cl, F, with H_2 in its vibrational ground- or first-excited state and considering collision energies of up to 1.5 eV. We find that the proposed excitation scheme is robust and reasonably accurate and that even for very light reaction partners, such as Muonium, less than 100 ring polymer beads are required for convergence.

Good agreement for the Mu/H/D + H_2(ν=0,1) reactions with exact quantum scattering calculations is found over the whole collision energy range. In particular, the case of Mu+H_2(ν=0) shows that the proposed approach correctly describes the ZPE constraints posed by the MuH product and the case of Mu+H_2(ν=1) shows that the new approach can approximately describe tunneling through a vibrationally non-adiabatic barrier. The latter feature is also confirmed by the good results for the Cl+H_2(ν=1) reaction at lower collision energies. However, larger deviations are found at higher collision energies, where the results coincide with cross sections obtained from QCT.

QCT-RPMD for the F+H_2 reaction slightly improves over QCT simulations, but cannot fully reproduce exact QM simulations. For low energies, this difference can partially be due to reactive resonance effects in this reaction, but overall there are also

some shortcomings in our vibrational excitation scheme at low collision energies, which needs improvement. Ideas to improve the current approach in this regard are under investigation. The method can be generalized to polyatomic systems, is numerically efficient, easily implemented and shows encouraging improvement over QCT simulations. Several extensions to include electronically non-adiabatic effects and the resolution of final states are planned for future work.

Chapter 5

Initial state-selected scattering for the reactions H+CH_4/CHD_3 and F+CHD_3 employing ring polymer molecular dynamics

This chapter is centered on the following publication of which I am the first author, and has been included verbatim:
"Initial state-selected scattering for the reactions H+CH_4/CHD_3 and F+CHD_3 employing ring polymer molecular dynamics", Marjollet, A., Inhester, L., Welsch, R., J. Chem. Phys. **156**, 044101 (2022) [119].
It is reproduced with the permission of AIP Publishing for the purpose of this thesis. My contributions include the investigation and theoretical work, programming the simulation tools, data analysis and writing the article.

In this chapter, the robustness and applicability of the approach is assessed for reactions involving more atoms. In particular, the ground state reactions H+CH_4/CHD_3 are considered as strong ZPE leakage occurs when simulated using QCT. NE-RPMD ICS are computed to assert the capicity of NE-RPMD at preventing the leakage. The reliability of the vibrational excitation scheme is evaluated for the C-H stretch excitation in CHD_3. The vibrational excitation model is further benchmarked by computing the ICS for the reaction F/H+CHD_3 is the presence of the C-H stretch excitation. The method is also applied to compute ICS for the more intricate ground state F+CHD_3 reaction. We analyze the NE-RPMD results and put them into perspective with the current state of the method.

5.1 Introduction

One of the challenges of physical chemistry is to study in detail the dynamics of chemical reactions. The detailed understanding of the underlying mechanisms is important for many domains of research such as atmospheric [3–5] and interstellar chemistry [6–8], combustion [2] and catalysis [9]. A key step in this direction of study is to develop accurate reactive scattering methods in order to qualitatively and quantitatively assess the influence of the reactants' rovibrational state on the reaction dynamics [68, 195]. In this context, nuclear quantum effects (NQEs) can have great impact on the reaction dynamics [25–27, 118, 188, 215].

Unfortunately, initial state-selected full-dimensional quantum scattering simulations that incorporate NQEs are only computationally feasible for systems up to 6 atoms with a vanishing angular momentum, although significant development in this direction has been achieved [47, 48, 60, 163, 169–171, 216, 217]. Consequently, there is a demand to develop computationally efficient simulation methods which take NQEs into account, at least approximately.

One possibility is to employ quantum simulations with constraints on the dynamics [47, 50–52, 54–56, 58–63, 216, 218] to reduce the number of degrees of freedom and make the simulations practical. Those methods are called reduced dimensional quantum dynamics simulations (RDQD). However, dynamical constraints and their potential artifacts have to be elaborated for each system specifically and it is rather challenging to assess their accuracy in describing the dynamics. This renders the RDQD approach non-systematic in contrast to full-dimensional simulations. Moreover, employing effective RDQD models to simulate systems such as the title reactions are nonetheless very expensive and can take many months to be completed [38, 47].

Another very popular alternative is the so-called quasi classical trajectory method (QCT) [64–68]. It circumvents the very high computational cost of quantum simulations by rendering the simulations classical, thus neglecting crucial aspects of NQEs in the dynamics. The atoms are propagated with the classical equations of motion on a potential energy surface (PES) employing initial conditions that mimic quantum rotational-vibrational states. This approach has successfully revealed insights into microscopic details of chemical reaction dynamics [69, 71, 105, 116, 199].

QCT trajectories are often easier to interpret compared to RDQD wave packet calculations. One of the main shortcomings of the QCT approach is the ZPE leakage problem. It originates from the fact that in classical dynamics the zero-point energy (ZPE) contained in the vibrational modes of the molecules typically flows from high to low frequency modes during the simulation. Consequently, parts of the vibrational energy can flow into the reaction coordinates, leading to an artificial enhancement of the reactivity [72, 73, 211]. Moreover, the formation of products having less than their quantum ZPE value can occur, violating the ZPE constraints [77, 114, 115, 118, 181, 211]. In addition, tunneling effects are also absent in classical simulations. The neglect of these NQEs can lead to several inaccuracies when computing energy thresholds, reaction probabilities, and integral cross sections.

A relatively recent approach that combines the advantage of being computationally efficient and at the same time takes NQEs into account is ring polymer molecular dynamics (RPMD) [78, 80, 81, 83–88, 95]. It has been shown that RPMD is able to accurately compute thermal rate constants for many reactions [88, 138, 139, 203, 204]. More recently, RPMD was also successfully applied to the calculations of Kubo-transformed correlation functions for non-equilibrium initial conditions (NE-RPMD) [95]. RPMD and NE-RPMD have been theoretically justified as approximations of Matsubara dynamics [81, 82, 95]. Various results for applications of RPMD beyond the thermal equilibrium ensemble followed [145, 146, 148]. In our earlier works [149, 192], two of us developed a variant of NE-RPMD and applied it to reactive collisions of various atoms with the hydrogen molecule H_2. Here, we extend the application of this method to more complex reactions.

To test newly developed methods, the computation of integral cross section (ICS) constitutes a reliable and precise indicator for the accuracy of the simulations. The ICS can be measured via challenging experiments and its variations with different isotopes and initial rovibrational states reveal important details about the reaction dynamics [69, 219–221].

The elementary reaction $H + CH_4 \rightarrow H_2 + CH_3$ together with its isotopic variants play an important role in combustion chemistry and in interstellar chemistry, and has been the subject of extensive experimental [221–223] and theoretical studies [60, 61, 63, 163, 203, 216, 216–218, 224–230]. This reaction involves a small number of electrons and potential energy surfaces (PES) with quantitative level of accuracy were constructed via extensive high level ab initio calculations [226–229]. QCT

simulations typically overestimate the reactivity for these reactions as classical dynamics ignore ZPE constraints and allow the ZPE to flow to the reaction coordinates [77, 118]. Also, the presence of tunneling effects due to the light H atoms are not described in QCT. Various RDQD methods applied to tackle six-atom systems have been developed to study the reaction [54–56, 216]. In particular, it was shown that restricting the non-reacting CH_3 group under C_{3v} symmetry yields a quantitative level of accuracy for the computation of ICS [51, 52]. Also, the strong reactivity enhancing effects of the vibrational excitation of the C-H stretch in CH_4 and CHD_3 have been studied theoretically [47, 55, 162, 163, 218, 228, 231–235] and experimentally [221, 223]. Therefore, H + CH_4 and its isotopic variants constitute valuable benchmark hexatomic reactions for NE-RPMD.

Another extensively studied reaction is F + CHD_3 $\rightarrow$ FH + CD_3 [58, 71, 188, 199, 236–245]. Czakó and Bowman performed an in-depth QCT investigation of the reaction employing a PES that does not incorporate spin-orbit (SO) coupling effects [241, 244]. Later, they realised that SO effects are relevant at low collision energies and presented an analytical spin-orbit-corrected PES [246]. For this system, the most accurate PES (PWEM-SO) to date has been developed by Palma, Westermann, Eisfeld, and Manthe by considering the spin-orbit coupling in the reactant channel [244]. This intricate reaction has a very low barrier ($\simeq$ 0.8 kcal/mol) and its dynamics involve reactive resonances and are strongly affected by stereodynamics forces at low collision energies [58, 244]. Morever, mode specificity of the reaction dynamics sparked controversies between theoretical models and experimental results regarding the effects of the C-H excited stretch on the reactivity [238, 240, 247]. More precisely, recent experimental studies [240, 247] of the F + CHD_3 reaction found that the excitation of the C-H vibration hinders the overall reactivity while both recent QCT [199, 244] and RDQD [58] simulations predict an overall enhancement of the reactivity. These discrepancies are still unexplained and several speculations exist that ascribe them to shortcomings of the experiments [58, 248] or the theoretical models [58, 59, 244] (QCT, RDQD or the PES). NE-RPMD is capable of approximating NQEs with full-dimensional calculations, thus having the advantages of both QCT and RDQD to some extent. As such, comparing its ICS results with those of QCT and RDQD for this reaction constitutes a good test to explore the capabilities of NE-RPMD. Therefore, this reaction is well suited to benchmark methods capable of approximating NQEs in full-dimensional calculations such as NE-RPMD.

In this paper we compare the accuracy of ICS computed with the NE-RPMD, QCT, and RDQD methods for the aforementioned reactions. We compute initial state-resolved ICS for the reactive collisions $H + CH_4, H + CHD_3$, and $F + CHD_3$. We analyze the impact of NQEs for the reactivity and report to what degree they are incorporated in the respective simulations. We show that the NE-RPMD approach is a promising and computationally efficient method to obtain state-resolved insights for reactive collisions involving complex polyatomic molecules.

The structure of the paper is as follows: In section 5.2, we briefly outline the ideas behind QCT and RPMD and give references for further details. Section 5.3 explains in detail the NE-RPMD approach to obtain the presented results. Section 5.4 consists of an analysis of the obtained ICS results for the title reactions with a discussion on the NQEs described by the approach. Finally, we summarize and give our conclusions in Sec. 5.5.

5.2 Theory

In this section, we discuss the QCT method, RPMD (alongside NE-RPMD) and the NE-RPMD approach we developed, which includes aspects of QCT used in the context of NE-RPMD. Both the QCT and RPMD methods have been widely reviewed [64, 65, 68, 78, 80, 81, 95], so we will only discuss the main aspects related to the NE-RPMD approach. Details of NE-RPMD applied to triatomic systems are given in Ref. [192], thus we only summarize the essential steps here.

5.2.1 QCT

In QCT, the atoms are modelled as classical point-like masses. A standard normal-mode sampling [207] with semiclassical quantization conditions for each vibrational mode is performed to mimic a given initial vibrational state for the reactants. Specifically, positions and momenta are initialized such that the energy in each vibrational mode of the molecule is equal to the corresponding energy in the quantum state employing the harmonic approximation of the potential energy surface. The molecular vibrations are then propagated either by directly (or adiabatically) switching to the full (i.e. non-harmonic) potential. The rotational motion of each reactant is added using an iterative procedure as to limit spurious ro-vibrational

couplings [66, 214]. The relative motion between the reactants is then set according to a fixed collision energy E_{col} in the center-of-mass frame. The atoms are then propagated using Newton's equations of motion. This approach is very efficient, systematic, and enables feasible simulations for systems with many atoms.

There exist various effective techniques to incorporate quantum effects in the dynamics, such as discarding trajectories violating ZPE constraints or partially preventing ZPE leakage. However, these techniques remain intrinsically ad-hoc [75,77, 114, 249].

5.2.2 RPMD

The RPMD approach originally emerged from the isomorphism bridging the equilibrium quantum partition function Z to the classical partition function of fictitious ring polymers Z_n [78]. Each ring polymer consists of n classical replicas (in the following called beads) joined by harmonic springs. The corresponding ring polymer Hamiltonian H_n is derived from the expression of Z_n as

$$\begin{aligned} H_n(\mathbf{p},\mathbf{q}) &= \sum_{i=1}^{N}\sum_{k=1}^{n}\left[\frac{\left(\mathbf{p}_i^{(k)}\right)^2}{2m_i} + \frac{1}{2}m_i\omega_n^2\left(\mathbf{q}_i^{(k)} - \mathbf{q}_i^{(k-1)}\right)^2\right] \\ &\quad + \sum_{k=1}^{n} V\left(\mathbf{q}_1^{(k)}, \mathbf{q}_2^{(k)}, \ldots, \mathbf{q}_N^{(k)}\right) \\ &\doteq H_n^0(\mathbf{p},\mathbf{q}) + V_n(\mathbf{q}), \end{aligned} \tag{5.1}$$

where N is the number of atoms, $\mathbf{q}_i^{(k)}$ and $\mathbf{p}_i^{(k)}$ are the position and momentum vectors of the kth bead of the ith atom (with $\boldsymbol{q}_i^{(1)} \equiv \boldsymbol{q}_i^{(n+1)}$), V is the molecular potential, m_i is the ith atomic mass that is used for each bead of the corresponding atom, and $\omega_n = \frac{n}{\beta}$ is the common frequency of each harmonic springs joining neighboring beads [78]. For equilibrium conditions, the ring polymer phase space is sampled according to the ring polymer Boltzmann distribution associated to H_n at temperature $\frac{n}{\beta}$. This is done either via thermostatted propagation in imaginary time or by employing Monte Carlo techniques [121]. The properly equilibrated ring polymers then allow for computation of exact thermal quantum observables. For example,

the thermal averaged energy can be computed by

$$\begin{aligned} E &= -\lim_{n\to\infty} \frac{\partial \ln\left(Z_n\right)}{\partial\beta} \\ &= \lim_{n\to\infty} \langle \mathcal{E}_n \rangle \\ &= \lim_{n\to\infty} \Big\langle \frac{1}{n} \sum_{i=1}^{N} \sum_{k=1}^{n} \left[\frac{\left(\mathbf{p}_i^{(k)}\right)^2}{2m_i} - \frac{1}{2} m_i \omega_n^2 \left(\mathbf{q}_i^{(k)} - \mathbf{q}_i^{(k-1)}\right)^2 \right] \\ &\quad + \frac{1}{n} \sum_{k=1}^{n} V\left(\mathbf{q}_1^{(k)}, \mathbf{q}_2^{(k)}, \ldots, \mathbf{q}_N^{(k)}\right) \Big\rangle, \end{aligned} \tag{5.2}$$

where $\langle . \rangle$ refers to averaging over the canonical ensemble and $\mathcal{E}_n$ is referred as the primitive energy estimator for a finite number of beads. Note the different sign in front of the harmonic spring terms of the ring polymer in Eq. (5.2) in contrast to the ring polymer Hamiltonian in Eq. (5.1).

ZPE effects and tunneling effects are incorporated through the ring polymer internal structure, which is parametrized by β and n [83, 139]. This incorporation of tunneling effects can be understood from the fact that parts of the ring polymer may enter classically forbidden regions of the potential energy surface. The tunneling effects description in RPMD is further demonstrated in Ref. [135] for a model system.

In 2014, RPMD was derived as an approximation to Matsubara dynamics in the context of time-dependent Kubo-transformed correlation functions [81, 82]. A bit later in 2016, encouraging results for applications of RPMD to non-equilibrium time-dependent correlation functions, for the specific NE cases of a momentum impulse (or "kick") and a sudden mild shift of potential, were successfully carried out. Non-equilibrium initial conditions employed in RPMD (NE-RPMD) can also be derived from Matsubara dynamics for the case of a sudden change of potential or an initial centroid momentum "kick" [95]. The extent and the conditions for which RPMD or NE-RPMD can describe real-time dynamics is not known precisely [81, 82, 95]. Here we employ non-equilibrium initial conditions by "kicking" the reactants centroid momenta to initialize the collision. This approach is also employed for preparing initial conditions with specific vibrational mode excitation, as described in the following section in detail.

5.3 NE-RPMD method

5.3.1 Reactant initialization

The two reactants in the following are labelled as "T" for the target molecule (i.e. CH_4 or CHD_3) and "X" for the colliding attacker atom (H or F). The entire system consists of N atoms, and the target possesses $3(N-1)$ degrees of freedom. Since T is a non-linear molecule, its number of internal vibrational modes is $N_v = 3(N-1)-6$. The PES of the target molecule alone placed far away from X is referred to as V_{T} and is a scalar function of the molecule's N_v internal coordinates. The initial momentum and position of each bead are first sampled according to the harmonic approximation of V_{T}. To that end, the target bead coordinates are transformed into the N_v mass-weighted vibrational mode coordinates of the total potential (including the molecular potential and the ring polymer harmonic springs potential). The resulting Hamiltonian of the ring polymer for the target molecule $H_n^{(\mathrm{T})}$ reads

$$H_n^{(\mathrm{T})} = \sum_{i=1}^{N_v} \sum_{k=0}^{n-1} \left(\frac{1}{2} \left[\widetilde{P}_i^{(k)} \right]^2 + \frac{\omega_{tot}^2(i,k)}{2} \left[\widetilde{Q}_i^{(k)} \right]^2 \right), \tag{5.3}$$

where $\omega_{tot}^2(i,k) = 4\omega_n^2 \sin^2(\frac{k\pi}{n}) + \Omega_i^2$ with vibrational frequencies $\mathbf{\Omega} = (\Omega_1, \ldots, \Omega_{N_v})$ and $\widetilde{Q}_i^{(k)}$, $\widetilde{P}_i^{(k)}$, $i \in [1, N_v]$ are the ring polymer mass-weighted position and momentum vibrational mode coordinates

$$\widetilde{Q}_i^{(k)} = \sum_{j=1}^{3(N-1)} (L^{-1})_{ij} \sqrt{m_j} \sum_{a=1}^{n} C_{ak} \, (q_j^{(a)} - x_{0j}), \tag{5.4}$$

and

$$\widetilde{P}_i^{(k)} = \sum_{j=1}^{3(N-1)} \frac{(L^{-1})_{ij}}{\sqrt{m_j}} \sum_{a=1}^{n} C_{ak} \, p_j^{(a)}, \tag{5.5}$$

where $\mathbf{C}$ and $\mathbf{L^{-1}}$ are the transformation matrices from the bead representation to the ring polymer (internal) normal mode representation and the vibrational mode coordinates, respectively. The coefficients of the matrix $\boldsymbol{C}$ are chosen such that the bead coordinates corresponding to the $k = 0$ index are computed with the coefficient $C_{a\,0} = \frac{1}{\sqrt{n}}$, i.e., the bead coordinates $\tilde{Q}_i^{(0)}$ and momenta $\tilde{P}_i^{(0)}$ are proportional to

the normal mode coordinate averaged over all beads (centroid normal mode coordinate) [121]. The N_v internal vibrational modes are sampled with the ring polymer Boltzmann distribution corresponding to $H_n^{(\mathrm{T})}$. Provided that n is large enough compared to $\beta \max_i(\Omega_i)$ and that β is not too low (this point is discussed in detail later in the manuscript), the ring polymer ensemble is equivalent to the quantum partition function for the vibrational ground state of T. To model the excited state for the ith vibrational mode associated to vibrational quantum number ν_i, we add the right amount of vibrational energy by kicking the ring polymer and shifting the coordinates along a specific vibrational mode coordinate, analogously to the procedure in QCT. To that end, we shift the centroid bead coordinates and momenta by

$$\widetilde{Q}_i^{(k=0)} \leftarrow \widetilde{Q}_i^{(k=0)} + \sqrt{n} K_i^{\overline{Q}} \cos(\phi_i), \tag{5.6}$$

$$\widetilde{P}_i^{(k=0)} \leftarrow \widetilde{P}_i^{(k=0)} + \sqrt{n} K_i^{\overline{P}} \sin(\phi_i), \tag{5.7}$$

where $K_i^{\overline{Q}} = \sqrt{\frac{2\nu_i}{\Omega_i}}$, $K_i^{\overline{P}} = \sqrt{2\nu_i\Omega_i}$ and ϕ_i is a phase randomly chosen in $[0, 2\pi]$.

The resulting thermal averaged energy of T becomes

$$E_{\mathrm{T}} = \sum_{i=1}^{N_v} \left(\Omega_i(\nu_i + \frac{1}{2}) + \delta E_{\mathrm{th}} \right), \tag{5.8}$$

where

$$\delta E_{\mathrm{th}} = \sum_{i=1}^{N_v} \left[\frac{\Omega_i}{2} \coth\left(\frac{\beta\Omega_i}{2} \right) - \frac{\Omega_i}{2} \right] = \sum_{i=1}^{N_v} \frac{\Omega_i}{e^{\beta\Omega_i} - 1}, \tag{5.9}$$

is an extra contribution to the internal energy. The contribution δE_{th} stems from the Boltzmann sampling of the beads with finite values for β. The sampling include effectively the ZPE and the additional Boltzmann-weighted excited energies which have to be distinguished with the excited energy from the shift in Eq. (5.6) and Eq. (5.7). These additional energies can be kept arbitrarily low by setting β high enough. The ring polymer attacker associated with atom X is initially placed far away from T and its internal ring polymer normal modes are sampled according to the free ring polymer Boltzmann distribution.

5.3.2 Collision initialization

The average momentum of the ring polymer atom X is

$$\overline{\boldsymbol{p}}_{\mathrm{X}} = \frac{1}{n}\sum_{k=1}^{n} \boldsymbol{p}_{\mathrm{X}}^{(k)}, \tag{5.10}$$

and the center of mass momentum of the ring polymer molecule T is

$$\overline{\boldsymbol{p}}_{\mathrm{T}} = \sum_{i=1}^{N-1} \frac{1}{n}\sum_{k=1}^{n} \boldsymbol{p}_{i}^{(k)}. \tag{5.11}$$

To prepare the initial conditions for the collision, we shift the bead's momenta of X and T such that

$$\overline{\boldsymbol{p}}_{\mathrm{X}} = -\overline{\boldsymbol{p}}_{\mathrm{T}}, \tag{5.12}$$

and the relative collision momentum is

$$\boldsymbol{P}_{\mathrm{rel}} = \sqrt{2\mu_{\mathrm{X,T}} E_{\mathrm{col}}}, \tag{5.13}$$

where $\mu_{\mathrm{X,T}} = \frac{M_{\mathrm{X}} M_{\mathrm{T}}}{M_{\mathrm{X}}+M_{\mathrm{T}}}$ is the reduced mass of the system and M_{X} and M_{T} are the total mass of X and T, respectively. Moreover, the position of the two reaction partners are shifted orthogonal to the axis connecting X and T by a given impact parameter b. The entire system is then propagated employing a modified velocity Verlet integration scheme [121]. No thermostat is attached to the system during the propagation. The origin of time $t = 0$ coincides in the simulations with the momentum "kick" of the reactants at collision initialization.

5.3.3 Choice of β

The spatial extension and dynamics of the ring polymers strongly depend on the spring constant $\omega_n = \frac{n}{\beta}$. While β is naturally defined as the reciprocal temperature for thermal equilibrium applications of RPMD, the status of β in the present application of NE-RPMD is unclear [95]. Previously, we introduced an ansatz for β in which β was chosen based on the average of the reciprocal kinetic energies of the two reactants [192]. We also tweaked the ansatz so that β would be higher in

the presence of strong ZPE constraints for the products and, furthermore, we introduced the lower limit β_- to keep the thermal energy contributions δE_{th} in Eq. (5.8) low.

Here, we employ a somewhat simpler approach and set β equal to the previously employed lower limit β_-. More specifically, β is given by constraining δE_{th} to be 5% of the total energy of the system, i.e., β solves the equation

$$\sum_{i=1}^{N_v} \frac{\Omega_i}{e^{\beta-\Omega_i}-1} = 0.05 \left[E_{\text{col}} + \sum_{i=1}^{N_v} \left(\frac{1}{2} + \nu_i \right) \Omega_i \right] . \tag{5.14}$$

Consequently, β only depends on the polyatomic reactants' initial vibrational energy and the collision energy E_{col}. The values for β for the different target molecules used here are shown in Fig. 5.1. As can be seen, larger collision energies result in lower values for β. At larger collision energies, the resulting ring polymer becomes therefore spatially more confined. This behavior reflects the expected tendency that in general, for higher collision energies, tunneling effects become relatively less important. We note that other NQEs such as ZPE constraints can still be strongly present in the dynamics for certain reactions also at high collision energies and that these effects are still captured with NE-RPMD also at low β [26, 192].

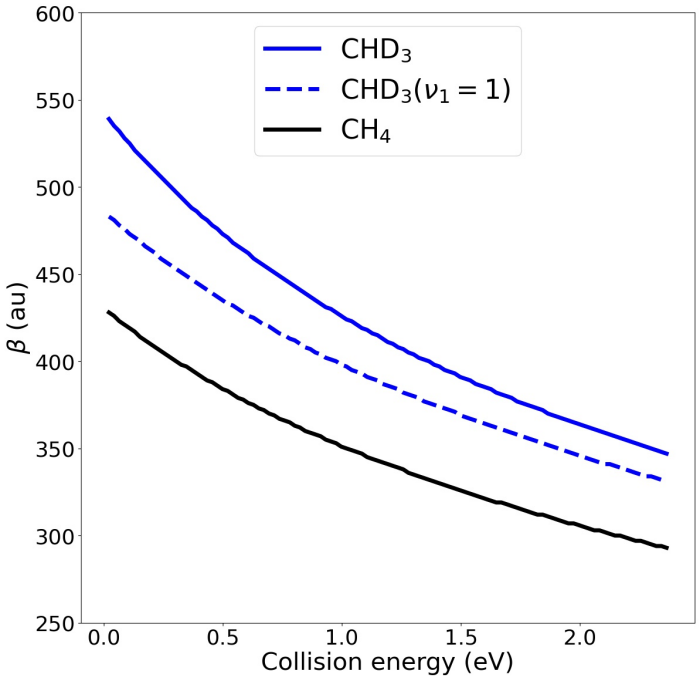

FIGURE 5.1: β values for each reactive system treated.

5.3.4 Calculation of integral cross sections

In our simulations, we propagate the system up to a sufficiently long time after the collision such that the reaction products can be distinguished. $\mathcal{N}$ trajectories are simulated with different impact parameters b that has been sampled such that the squared impact parameter b^2 is uniformly distributed between 0 and b_{max}, where b_{max} is the maximal value beyond which no reaction occurs.

From the set of QCT trajectories, we calculate the integral cross section as

$$\sigma(E_{\text{col}};\boldsymbol{\nu}_T) = \pi b_{\text{max}}^2 \lim_{\mathcal{N}\to\infty} \lim_{\text{“}t\to\infty\text{”}} \frac{1}{\mathcal{N}} \sum_{i=1}^{\mathcal{N}} I_R\left(\boldsymbol{q}^{(i)}(t)\right), \tag{5.15}$$

where the vector $\boldsymbol{\nu}_T$ refers to the initial vibrational quantum numbers of T, and I_R is a function taking as argument the positions $\boldsymbol{q}^{(i)}(t)$ of the atoms of the trajectory i at time t and returns 1 if a reaction occurred or 0 otherwise [64]. It is important to note that QCT trajectories can lead to reaction products with internal energies below their ZPE. Here, the QCT ICS results are computed by considering all product outcomes after collision regardless of any ZPE violations. This approach is the so-called histogram binning (HB) method. The comparison to the QCT (HB) calculations indicates the extent to which NQEs impact the dynamics. This way, we are able to pinpoint how accurate the NQEs are described in NE-RPMD. From now on, QCT with the histogram binning approach will be referred to simply as QCT.

Analogously, for the NE-RPMD simulations, the ICS are computed as follows

$$\sigma_{\text{RPMD}}(E_{\text{col}};\boldsymbol{\nu}_T) = \pi b_{\text{max}}^2 \lim_{\mathcal{N}\to\infty} \lim_{\text{“}t\to\infty\text{”}} \frac{1}{\mathcal{N}} \sum_{i=1}^{\mathcal{N}} I_R\left(\overline{\boldsymbol{q}}^{(i)}(t)\right), \tag{5.16}$$

where $\overline{\boldsymbol{q}}^{(i)}(t)$ are the centroid coordinates for trajectory i at time t. Notably, in QCT all trajectories have a fixed energy as defined by $\boldsymbol{\nu}_T$ and E_{col}, whereas in NE-RPMD, the initial sampling of the ring polymers lead to energy estimator values that follow a distribution with finite width [250]. To compute ICS with NE-RPMD, we proceed by associating the outcome of each trajectory (reaction or not) to the vibrational state associated to the ν_i's in Eq. (5.8), which define the sampling of the ring polymer's internal vibrational modes.

5.4 Results

5.4.1 System details and computational details

The spin-orbit coupled adiabatic PWEM-SO [244] PES and the adiabatic PIP-NN [230] PES are employed for the reactions F + CHD_3 and H + CH_4/CHD_3, respectively. All the simulations are carried out with no initial rotational motion for the target molecule. The vibrational ground state is referred with the notation $\boldsymbol{\nu} = \mathbf{0}$ which indicates that all vibrational quantum numbers are zero. The vibrational mode corresponding to the symmetric C-H excited stretch in CHD_3 has the vibrational quantum number ν_1 and a harmonic frequency of $\Omega_1 = 3147$ cm^{-1}.

NE-RPMD simulation were run with $n = 3\lceil\beta\omega_{\text{max}}\rceil$ where $\lceil\beta\omega_{\text{max}}\rceil$ refers to the smallest integer i such that $i \geq \beta\omega_{\text{max}}$ and ω_{max} is the highest harmonic frequency of the polyatomic reactant. This is the number of beads beyond which we observe little change for the ICS. The time step employed for the QCT and NE-RPMD simulations is 0.02 fs. The initial distances between the reactants' center of mass are 12 a_0 for H + CH_4/CHD_3 and 14 a_0 for F + CHD_3. The maximal impact parameters found for the NE-RPMD simulations are in most cases higher than in QCT. For the H + CH_4/CHD_3 ground state reactions $b_{\text{max}} = 6\ a_0$ is employed, while we have $b_{\text{max}} = 8$ a_0 in the presence of the excited C-H stretch in CHD_3. For the reaction F + CHD_3, b_{max} is set to 10 a_0. For each collision energy and reactant vibrational state, 20,000 trajectories were used to compute the ICS. To benchmark our NE-RPMD approach, we compare the NE-RPMD ICS results with our QCT results and with RDQD results taken from the literature. For the reactions H + CH_4/CHD_3 we compare our results with RDQD ICS taken from Refs. [229, 234, 235] and, for the reaction F + CHD_3 from Ref. [58]. The PIP-NN PES used in our calculations for the H + CH_4/CHD_3 reactions is an improved and optimized neural-network PES over the ZFWCZ PES employed in Refs. [229, 234]. The ZFWCZ and PIP-NN PESs lead to very similar ICS results for the corresponding ground-state and symmetric C-H excited stretch reactions [230, 235]. The employed PWEM-SO PES to compute the QCT and NE-RPMD results for the reaction F + CHD_3 is the same one used as in Ref. [58].

5.4.2 Stability of the centroid vibrational C-H stretch excitation model

ZPE constraints, which in particular forbid the leakage of the zero-point vibrational energy to other degrees of freedom, are described in RPMD intrinsically via the internal ring polymer structure. Conversely, a potential issue when performing initial excitation of a vibrational mode on a ring polymer polyatomic reactant via "kicking" certain coordinates is the possible leakage of the excitation energy to other modes on the time period it takes for the reactants to collide. This leakage occurs because we are not involving the ring polymer spring terms while performing the excitation, rather only the centroids [see Eq. (5.6)]. It is therefore crucial to monitor how the energy in the excited vibrational mode evolves as a function of time which requires a mapping of phase space coordinates to vibrational quantum states. For QCT, the most straightforward assignment of quantum states is the determination of the corresponding harmonic action numbers. This is done by employing a semi-classical quantization of the vibrational modes in the harmonic regime as described in Ref. [249]. Here, we employ an analogous procedure for the ring polymers to assess the stability of the C-H stretch vibrational excitation.

We perform initial sampling corresponding to the C-H stretch excited state as explained in subsection 5.3.1 employing the harmonic approximation of the potential. The ring polymer is then propagated employing the full potential. Computing harmonic action numbers for each vibrational mode along the trajectory requires evaluating the displacements of the molecule in terms of vibrational mode coordinates. For this task, it is desirable to align the molecule at each time step of the simulation via translations and rotations as closely as possible to an equilibrium reference geometry. Following the procedure described in Ref. [251], we shift the molecular coordinates to the center-of-mass frame and employ a rotation defined by the rotation matrix $\boldsymbol{\mathcal{C}}$, such that $\|\sum_i m_i \boldsymbol{\mathcal{C}}\, \bar{\mathbf{q}}_i^{\mathrm{eq}} \times (\bar{\mathbf{q}}_i - \boldsymbol{\mathcal{C}}\, \bar{\mathbf{q}}_i^{\mathrm{eq}})\|$ is minimized, with $\bar{\mathbf{q}}_i$ referring to the ring polymer centroid position of the ith atom and $\mathbf{q}_i^{\mathrm{eq}}$ referring to the position of the ith atom in the equilibrium reference geometry of the molecule [252]. The ring-polymer phase space coordinates are then determined as vibrational mode coordinates and momenta as described in Eq. (5.4) and Eq. (5.5).

The energy for the ith vibrational mode is computed as

$$E_i = \left\langle \lim_{n\to\infty} \frac{1}{n} \sum_{k=0}^{n-1} \left(\frac{1}{2} \left[\widetilde{P}_i^{(k)} \right]^2 + \frac{(\Omega_i^2 - \omega_k^2)}{2} \left[\widetilde{Q}_i^{(k)} \right]^2 \right) \right\rangle, \tag{5.17}$$

and a real harmonic action number for each mode is obtained as

$$\tilde{\nu}_i = \frac{E_i}{\Omega_i} - \frac{1}{2}. \tag{5.18}$$

In order to quantify the extent to which the excitation energy leaks to other modes we have run 100 trajectories for the ring polymer $\mathrm{CHD_3}\,(\nu_1 = 1)$ molecule, and we have computed the harmonic action number for the C-H stretch mode $\tilde{\nu}_1$ at each time step employing the procedure described above. The harmonic action number is shown in Fig. 5.2 as function of time. For this simulation, we used $\beta = 450$ as this value is representative of the β values employed for the collision simulations in this work. We compare these results with the harmonic action numbers obtained from QCT simulations. An initial spike at $t = 0$ can be seen for both, QCT and NE-RPMD. This spike can be attributed to the anharmonicities in the full potential, which are not considered in the preparation of the initial vibrational state. We observe that for times $t \leq 250$ fs after excitation, in which most of the reactions studied here occur, more than 80 percents of the initial energy remains in the initially excited mode and only for longer times the harmonic action number becomes lower than 0.8. For times $t < 400$ fs, the harmonic action numbers obtained from the QCT simulations tend to decay a bit faster than the ones obtained from NE-RPMD. Overall, the harmonic action numbers obtained from the QCT and the NE-RPMD evolve qualitatively similarly. We conclude that the simulations maintain the vibrationally excited state for sufficiently long times. A propagation time of $t \geq 250$ fs becomes potentially problematic for reactions at very low collision energies. As we will discuss later, leakage of excitation energy becomes a problem for the studied F+$\mathrm{CHD_3}(\nu_1 = 1)$ reaction, where very low collision energies are sufficient to trigger a reaction.

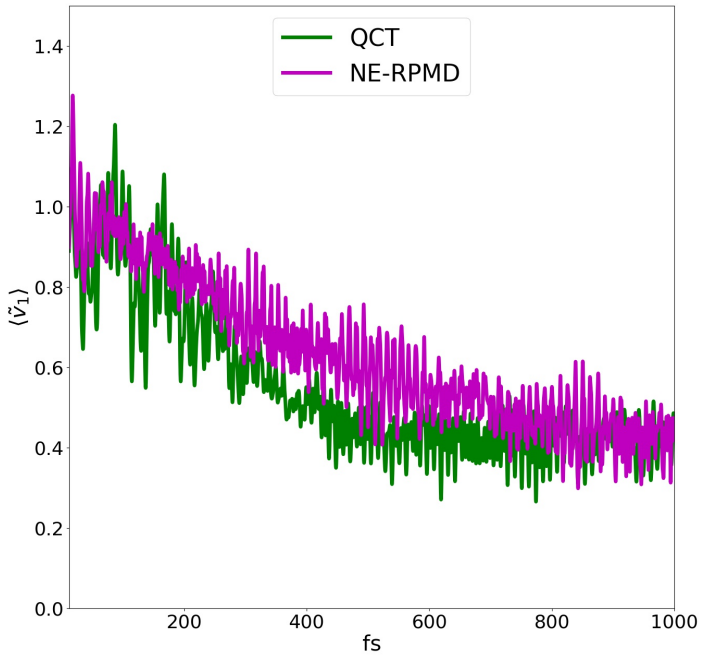

FIGURE 5.2: Average harmonic action numbers for the normal modes of CHD_3 ($\nu_1 = 1$) as a function of integration time for QCT and NE-RPMD. The time $t = 0$ corresponds to the direct switch from the harmonic to the full potential with which the molecule is then propagated. The employed time step is 0.01 fs with $\beta = 450$ and the number of beads is $3\lceil \beta\omega_{\text{max}} \rceil$ where ω_{max} refers to the highest harmonic frequency of CHD_3 (3147 cm^{-1}).

5.4.3 H + CH_4 and H + CHD_3 in their ground state ($\nu = 0$)

In the following we discuss the collisions H + CH_4 and H + CHD_3, where the target molecules are in their ro-vibrational ground states. Figure 5.3 shows the calculated QCT and NE-RPMD ICS as a function of the collision energy for the reactions H + $CH_4 \rightarrow H_2 + CH_3$ [Fig. 5.3 a)] and H + $CHD_3 \rightarrow H_2 + CD_3$ [Fig. 5.3 b)]. We compare this data with ICS calculated via RDQD from Ref. [234]. These results are based on the reduced-dimensional model introduced by Palma and Clary [51] alongside the centrifugal sudden approximation propagated using an established wave packet method to study atom-methane reactions [234]. It has been demonstrated that the frozen coordinates in this reduced-dimensional model act largely as spectators in the reaction dynamics. The model has also been validated by demonstrating that

ICS for the ground state reaction calculated via QCT are unaffected by the dimensional reduction for a wide range of collision energies and different isotopic variants [118]. The ICS results from these RDQD simulations are therefore considered to be quantitatively accurate.

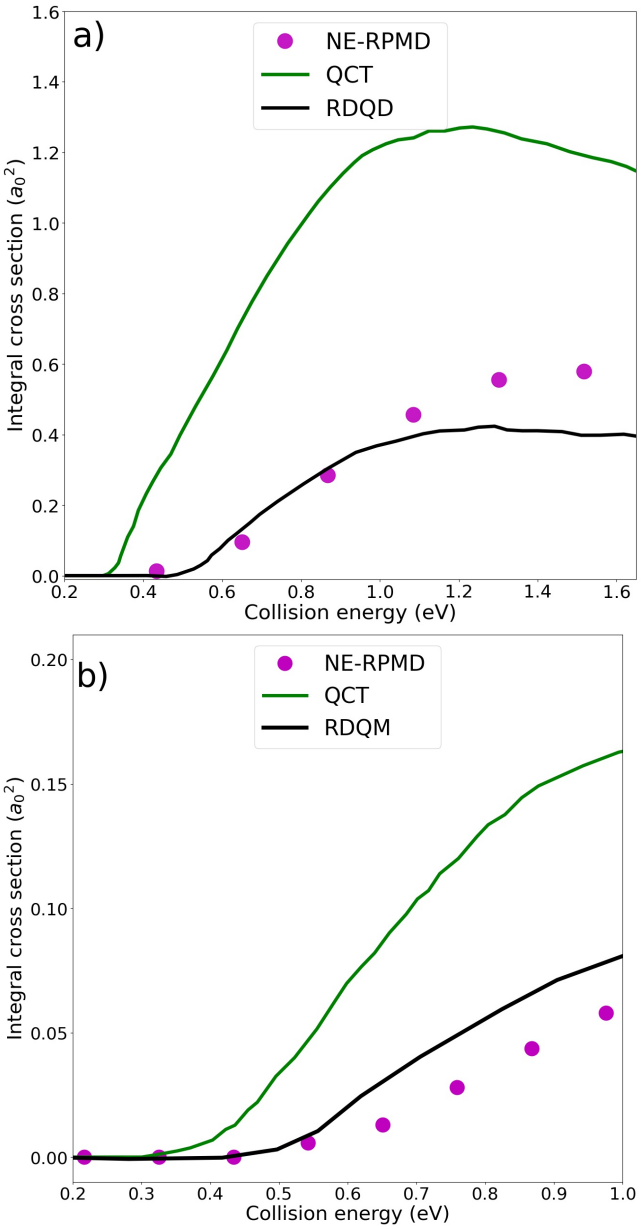

FIGURE 5.3: a) ICS for the reaction $H + CH_4(\nu = 0) \rightarrow H_2 + CH_3$ and b) $H + CHD_3(\nu = 0) \rightarrow H_2 + CD_3$ calculated with NE-RPMD (circles), QCT (green solid line) and RDQD (black solid line). RDQD ICS are taken from Refs. [229, 234].

For both reactions we observe that RDQD predicts almost the same reaction thresholds at around 0.4 eV, below which the reactivity is zero. This is because both reactions have the same ZPE corrected barrier and tunneling effects provide for both reactions the same contributions [234]. The QCT thresholds for both reactions are predicted at around 0.3 eV, which is substantially lower than in RDQD. The lower threshold for QCT is explained by the presence of ZPE leakage that allows vibrational energy to leak into the reaction coordinates and enables the reaction to happen below the barrier height [118]. On a side note, the absence of tunneling contributions in QCT, which increases the threshold, is overcompensated by the ZPE leakage.

Remarkably, NE-RPMD predicts a reaction threshold approximately around 0.4 eV for H + CH_4 and approximately 0.45 eV for H + CHD_3 in good agreement with RDQD. These results indicate that the ZPE leakage is well mitigated with NE-RPMD. As the collision energy increases, the QCT ICS for the H + $CH_4 \rightarrow H_2$ + CH_3 reaction increases more rapidly and also to larger values than the RDQD ICS. A similar observation can be seen for H + $CHD_3 \rightarrow H_2$ + CD_3. Overall, the RDQD cross sections are much smaller compared to QCT, only reaching 0.3 a_0^2 at most compared to 1.3 a_0^2 for QCT for H + CH_4 at 1 eV, while for H + CHD_3 at 1 eV QCT predicts an ICS of 0.16 a_0^2 and 0.075 a_0^2 for RDQD. This suggests that NQEs are relevant for the whole range of collision energies considered above the reaction threshold. More specifically, we attribute this discrepancy to violation of ZPE constraints in QCT that leads to an overestimation of the reactivity. The ICS calculated from NE-RPMD are much closer to those calculated from RDQD. For collision energies above the threshold, NE-RPMD predicts somewhat larger ICS for H + CH_4 and marginally lower ICS for H + CHD_3 compared to RDQD.

We conclude that NE-RPMD covers the major part of the ZPE effects relevant for the two considered reactions. These encouraging results are reminiscent of the previous successes of the method for triatomic systems [149, 192].

5.4.4 H + CHD_3 ($\nu_1 = 1$)

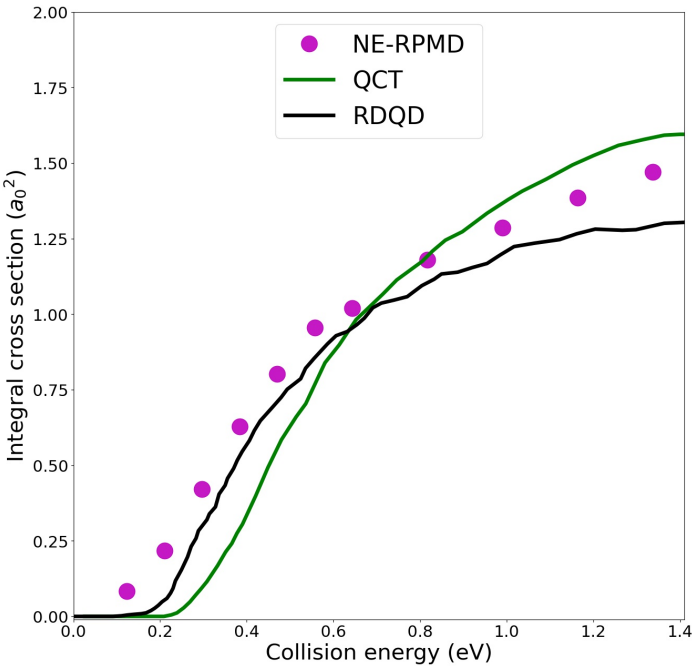

FIGURE 5.4: $H + CHD_3(\nu_1 = 1; j = 0) \rightarrow H_2 + CD_3$ NE-RPMD ICSs for $n = 3\lceil \beta\omega_{\max} \rceil$. RDQD ICS are taken from Ref. [234].

We now turn to the ICS for the reaction $H + CHD_3 \rightarrow H_2 + CD_3$ in the presence of the C-H excited stretch. Figure 5.4 shows a comparison of ICS as a function of collision energy calculated from NE-RPMD, QCT, and RDQD. As for the vibrational ground-state, the RDQD ICS results are taken from Ref. [234]. Accordingly, they involve the same reduced dimensional model as for the ground state reactions.

From the comparison with the ground state ICS (Fig. 5.3 b)), one can see that all simulations consistently indicate that in the presence of the C-H stretch the reactivity is increased substantially which is consistent with earlier simulations [163, 232–234]. The QCT simulations indicate a reaction threshold of $E_{\text{col}} \simeq 0.2$ eV. In contrast to the ground state reactions discussed in Fig. 5.3, where the reaction threshold for QCT was lower than for RDQD, the reaction threshold for QCT is here somewhat larger than the reaction threshold for RDQD of approximately 0.12 eV. This suggests that the excitation energy deposited into the C-H vibrational stretch mode cannot transfer as efficiently to the reaction coordinate in QCT as compared to RDQD. Also, QCT simulations do not account for any tunneling contributions

to the reactivity that may be responsible for the lowered reaction threshold. Interestingly, NE-RPMD predicts a reaction threshold of approximately 0.08 eV which is slightly lower than the one for RDQD. For collision energies up to 0.6 eV we observe that NE-RPMD predicts ICS in good agreement with RDQD while QCT underestimate slightly the reactivity. For collision energies from 0.6 eV to 1.4 eV, both QCT and NE-RPMD ICS remain slightly above the RDQD ICS and NE-RPMD results tend to merge with the QCT predictions at these higher collision energies.

In summary, we find that the NE-RPMD ICS follow the same qualitative trend as RDQD for low collision energies and becomes close to QCT ICS at high collision energies. Compared to the ground state reaction, all simulation methods consistently indicate a considerable reactivity enhancement (around 10 fold) caused by the C-H stretch ($\nu_1 = 1$).

5.4.5 F+CHD$_3$($\nu_1 = 0, 1$)

Here we compare the ICS for the reactions F + CHD$_3$($\nu_1 = 0, 1$) $\rightarrow$ FH + CD$_3$ computed with QCT, RDQD, and NE-RPMD. The RDQD results were taken from Ref. [58] and are based on the aforementioned Palma-Clary reduced-dimensionality model (see Sec. 5.4.3). In addition to the dimensional reductions, a J-shifting approximation [50] was used to compute ICS in Ref. [34]. Because these approximations may impact the resulting ICS, the comparison between RDQD and QCT and between RDQD and NE-RPMD for this reaction should be taken with reservations. We stress that the results for QCT and NE-RPMD have been computed using the same PES as for the RDQD results from Ref. [58].

There have been many discussions about the intriguing discrepancies between experimental results and the QCT and RDQD predictions regarding the influence of the C-H stretch excitation on the dynamics of the F + CHD$_3$ reaction [58,71,238,244]. It is not yet clear what the cause of these discrepancies is and whether the experiments or the simulations are lacking accuracy. One of the possible reasons for disagreement is regarding the QCT simulations the imperfect treatment of quantum effects such as ZPE and tunneling and regarding the RDQD model potential effects of dimensionality reduction. In this context, the presented results may thus provide additional information for investigating this discrepancy, since NE-RPMD describe NQEs to some extent, but on the other hand does not rely on dimensional reduction (as RDQD). Another possible cause of deviation are the limitations of the

potential energy surface. In this work, we focus on assessing the performance of our NE-RPMD approach for computing ICS and describing the quantum effects on the PWEM-SO PES.

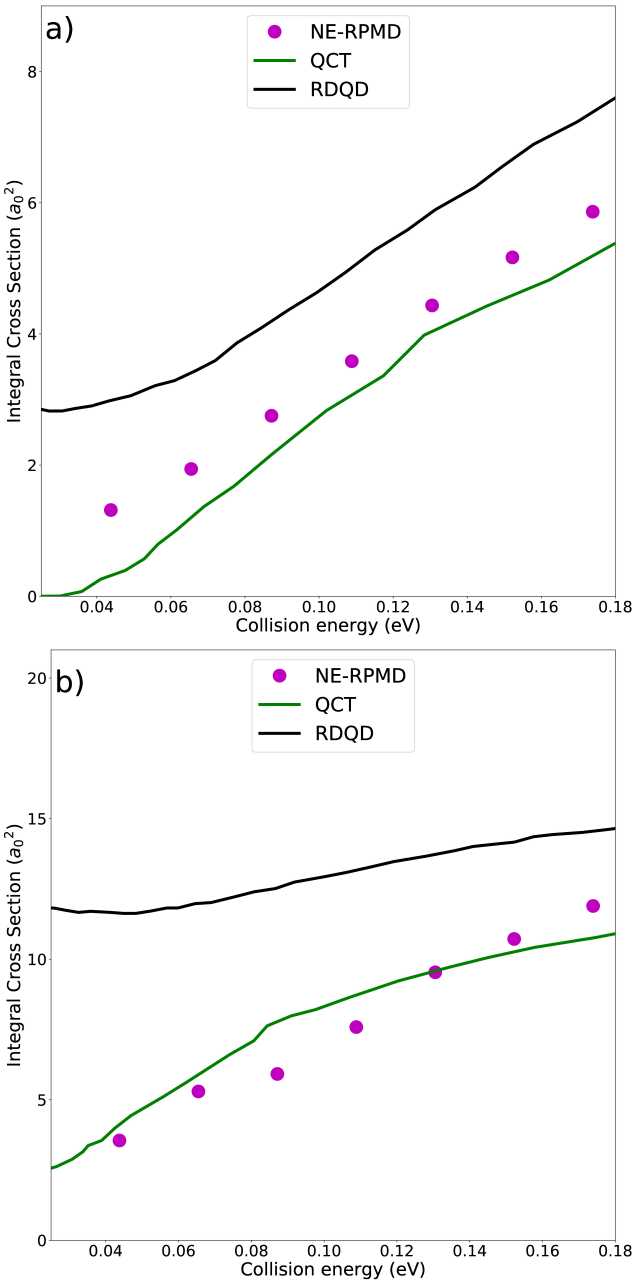

FIGURE 5.5: a) $F + CHD_3(\boldsymbol{\nu} = 0; j = 0) \rightarrow FH + CD_3$ and b) $F + CHD_3(\nu_1 = 1; j = 0) \rightarrow FH + CD_3$ NE-RPMD ICSs for $n = 3\lceil\beta\omega_{\max}\rceil$. RDQD ICS are taken from Ref. [58].

In contrast to the reactions considered in Fig. 5.3 and Fig. 5.4, ZPE constraints are expected to be less relevant, because of the higher mass of the attacker atom. Accordingly, previous works based on QCT trajectories showed that reactivity trends are unaffected by ad-hoc treatments regarding the ZPE of the products [241]. The calculated ICS are shown in Fig. 5.5 as a function of collision energy and compared with the earlier published RDQD results [58]. For the ground state reaction [Fig. 5.5 a)], the QCT reaction threshold is at around $E_{\text{col}} = 0.03$ eV, which corresponds to the classical barrier for the PWEM-SO PES [244]. The RDQD reaction threshold is considerably lower (< 0.010 eV); a complete decline of the ICS is not visible within the range of collision energies considered here. QCT predicts much lower ICS than RDQD for the entire range of collision energies. This has been attributed to the relevance of tunneling contributions that are absent in QCT [58]. NE-RPMD predicts similar ICS results as QCT, nevertheless slightly closer to the values provided by RDQD. We think the fact that RPMD yields ICS results only slightly larger than QCT is related to the fact that certain reaction resonances in combination with tunneling effects are not adequately described [58,212]. Also, the J-shifting approximation employed to compute the RDQD results might lead to an overestimation of the ICS. Thus, the extent to which RPMD describes NQEs is difficult to assess here. The situation is reminiscent of the previously studied F+H_2 reaction, where RPMD tends to underestimate the reactivity [192]. A possible cause is the relatively low employed β coupled with the high mass of F which limits the spatial extension of the ring polymer corresponding to the F atom. This in turn can limit the description of NQEs.

For the C-H stretch-excited case the calculated ICS are compared in Fig. 5.5 b). Similar to what we have seen before for H + CHD_3, vibrational excitation of the C-H bond stretch increases the reactivity considerably. For the collision energies considered here, we observe that the QCT ICS are considerably lower than their RDQD counter-parts. NE-RPMD predicts slightly lower ICS as compared to QCT except at higher collision energies (≥ 0.14 eV) where NE-RPMD ICS are a bit higher than QCT. Compared to RDQD, NE-RPMD underestimates the reactivity considerably. The modeling of the excited state reaction via NE-RPMD faces particular difficulties, mainly due to the fact that the reaction is nearly barrierless. As a result, the collision energies of interest involve a long simulation time and thus substantial vibrational energy leakage (up to 40 % near the threshold) of the C-H stretch

vibrational energy to the other vibrational modes, which are not as efficient at promoting the reaction. In addition to the discussed causes for the discrepancies for the ground and vibrational excited state, we note that the reaction involves resonance effects that are not described in NE-RPMD and that can strongly affect the reaction dynamics [58]. Those considerations constitute a limit of our NE-RPMD simulations for very low collision energies and contribute to NE-RPMD underestimating the reactivity.

5.5 Conclusions

The current work extends the scope of NE-RPMD to the study of state-resolved reactive scattering dynamics for reactions involving more than 3 atoms. We have compared the ICS results for the reactions H + CH_4, H + CHD_3, and F + CHD_3 with and without vibrational C-H stretch excitation in CHD_3. Good agreement for the H+CH_4/CHD_3/CD_4 ground state reactions were found. We show that the NE-RPMD simulations describe the dominant ZPE effects present in the dynamics for a wide range of collision energies. However, we also see that NE-RPMD only performs marginally better than QCT for the reaction F+CHD_3, where relevant tunneling effects cannot be described with NE-RPMD.

For vibrationally excited states, we find that the NE-RPMD method can also give accurate ICS that are similar to those obtained from much more involved RDQD simulations. The centroid stretch excitation scheme employed to excite the C-H stretch vibrational mode in CHD_3 was found to be robust and fairly accurate for the time period of most of the simulations (if $\leq$ 200 fs). When employed to study the C-H excited H + CHD_3 reaction, good agreement with the RDQD ICS is found. In summary, except for the reactive collision F+CHD_3, where tunneling effects are dominant, NE-RPMD simulations show good agreement with RDQD simulations, especially for collision energies around the threshold. In contrast to the ground state calculations, for the vibrational excited states the ICS calculated with the NE-RPMD method show no significant improvement over those calculated with QCT for reactions considered here. For the discrepancies that arise at larger collision energy, one has to keep in mind that the dimensional reduction on which RDQD results rely may not be strictly valid anymore. We can conclude that the NE-RPMD method is able to overcome key limitations of the previously applied QCT methodologies at the cost of extra computational efforts which remain small in comparison

to quantum scattering methodologies. NE-RPMD can be relatively easily built in into existing MD codes and can be applied to considerably larger systems thanks to its scalability. However, the current NE-RPMD method employs an inconsistent and unclear choice for the β parameter. As such, our NE-RPMD approach as it stands and the present choice of β can be seen as a possible starting point for further refinements of the methods toward broader and consistent applications of NE-RPMD for state-selective reactive scattering simulations.

Chapter 6

Conclusions

In this thesis, I have developed and implemented a new method based on ring polymer molecular dynamics using non-equilibrium initial conditions to simulate state-resolved molecular reactive scattering events. The approach allows for the description of specific initial vibrational states in the reactant molecules and the computation of integral cross sections. The method is capable of describing important nuclear quantum effects, such as tunneling and zero-point energy, present in the dynamics of several benchmark reactions. Furthermore, compared to explicit quantum simulations, the method is computationally efficient and scales favorably such that it can be applied to a large number of atoms.

To pave the way for RPMD to tackle state-resolved dynamics, a key step is the initialization of reactants in the ring polymer phase space. By employing at first the harmonic approximation of the potential, I analytically derived and implemented the sampling of the bead coordinates for the initialization of a molecule close to its vibrational ground state. As the presence of the Boltzmann weighted vibrational energies cannot be avoided in this framework, constraints on the internal inverse "temperature" β were derived to achieve an accurate ground state description. The sampling scheme was found to be robust for H_2 and in the case of more complex molecules such as CH_4 and CHD_3, with the resulting ground state energies being close to the exact values. I proceeded by developing a new sampling method to describe excited vibrational states. To that end, I derived and employed non-equilibrium initial conditions applied to specific centroid beads coordinates. Through these coordinates, I added vibrational energy to mimic an excited vibrational state. The employed benchmark molecules were the H_2 molecule in **Chapters 3** and **4**, and the polyatomic CHD_3 molecule in the presence of the C-H excited stretch in **Chapter 5**. The first excited vibrational energy was found to be stable for ring polymer $H_2(v = 1)$ with only a small and very slow energy leakage from the

centroid modes to the internal degrees of freedom. Also for CHD_3 the centroid excitation scheme yields a C-H stretch excitation for most simulation purposes. However, as the excitation energy above the zero-point energy is contained in the centroid coordinates and not the internal ring polymer fluctuations, it undergoes an energy leakage similarly as in QCT.

Another issue for the description of non-equlibrium dynamics using RPMD is the choice of the reciprocal temperature β. I reported an ansatz in **Chapter 3** for β interpreted as the internal inverse temperature of the ring polymers. The ansatz depends on the initial non-equilibrium quantities while assuring good accuracy for the sampling of the internal energies. I defined the initial conditions for the collision and reported a formula for the calculation of integral cross sections (ICS) for NE-RPMD. Despite the formula for the NE-RPMD ICS being in effect the same as in QCT, albeit considering the ring polymers centroid positions instead, investigations of its validity were in order. Test ICS were first computed for the D+$H_2(\nu = 0)$ reaction for which QCT and exact quantum (QM) results are very similar. NE-RPMD ICS were found to match QM ICS. This was followed by other encouraging results for the reaction H+$H_2(\nu = 0)$ which corroborated the intuitive yet non-trivial formula for the NE-RPMD ICS. The comparison with QCT and exact QM ICS results for the systems Mu+$H_2(\nu = 0)$, for which ZPE effects are predominant, showed that the NE-RPMD approach respects ZPE constraints. As for the $\nu = 1$ case, for which the tunneling effect is predominant in the dynamics and enhances greatly the reactivity, NE-RPMD ICS and energy threhsold were found to be in accordance with the exact results. As to interpret the dynamical manifestations of the tunneling effects in the ring polymer phase space, I have plotted the bead density plot at the time the system reaches the transition state for the reaction Mu+$H_2(\nu = 1)$. I found that the tunneling description in RPMD was characterized by a stretch of some of the beads towards the products side which in turn drags the rest of the beads. This can allow certain ring polymer trajectories to "corner-cut" their way through the PES, while reactivity is classically forbidden. The systems Cl/F+$H_2(\nu = 0, 1)$ were considered in **Chapter 4**. Good agreements with exact quantum ICS results and improvements over QCT were found for Cl+$H_2(\nu = 0, 1)$. However, the ICS results for F+H_2 suggest that NE-RPMD is unable to describe the tunneling and resonances effects for this system.

The rest of the thesis is devoted to the application of the approach to more intricate systems involving more atoms. Since strong ZPE leakage can occur in the

presence of multiple vibrational modes in classical simulations, the exemplifying ground state reactions H+CH_4/CHD_3 were employed for benchmarking purposes. I justified the use of a modified and more applicable β ansatz for the reactions H,F+CH_4 in **Chapter 5**. The main drawback with this ansatz is that it can constrain the radius of gyration of the ring polymers. As such, the descriptions of NQEs via the ring polymer structure might be hindered in the simulations. Nevertheless, ring polymer fluctuations are still present and should in turn describe approximately the NQEs. There are other attempts to set β by other groups but none of them included vibrational aspects and are therefore not within our approach [253, 254]. I obtained the NE-RPMD ICS results for these reactions and found a good agreement with their RDQD counterparts. As QCT significantly overestimates the ICS here, I concluded that NE-RPMD can prevent ZPE leakage. To further benchmark the dynamical relevance of the centroid excitation scheme I applied it to compute the NE-RPMD ICS for the H+$CHD_3(\nu_1 = 1)$ reaction. Since RDQD, QCT and NE-RPMD ICS were found to match over a wide range of collision energies, the method was deemed accurate. ICS results were subsequently computed for the system F+$CHD_3(\nu_1 = 0, 1)$ and similar qualitative conclusions were made as with the F+H_2 reaction, that is NE-RPMD does not capture the enhancing NQEs contributing to the reactivity.

So far, including NQEs in the dynamics simulations of chemical reactions was only possible for small systems by conducting expensive quantum simulations. The new techniques developed in this thesis are computationally efficient and allow the state-resolved simulations of reactions consisting of many atoms. Due to its beneficial scalability, the number of degrees of freedom involved in the reaction does not need to be truncated to include quantum effects (as done in RDQD). The method presented in this work thus considerably increases the number of reactions where NQEs can be incorporated for its detailed simulations. In these contexts, the provided method prospectively might constitute an additional tool to extract information on how initial conditions promote or inhibit reactions, the selective breaking or making of chemical bonds, in other words steer chemical reactions into desired product states. It constitutes a step towards developing our understanding of molecular reactive dynamics for which NQEs are present but no quantum treatment, even with a reduced-dimensional model, is possible.

Outlook

The present approach as it stands can be potentially improved in accuracy by the following considerations.

An apparent improvement would be to circumvent the direct switching from the harmonic approximation of the potential to its exact form during the reactant initialization. The current procedure can lead to inaccuracies in the presence of a strongly anharmonic potential and for excited vibrational states where the difference between harmonic energies and exact energies tends to be higher. This problem is already partially addressed in QCT via employing the adiabatic switching (AS) procedure [111]. The direct implementation of the AS procedure within RPMD actually lowers the accuracy of the initialization. Nevertheless, I found that applying a time-dependent thermostat on the centroid momenta alongside the AS leads to a slightly more accurate ground state initialization. However, for the excited state, further investigation is needed.

As a further point, the current way to initialize a given vibrational excited state proceeds by shifting the values of centroid coordinates (see Eqs. (5.6)). The intrinsic description of quantized vibrational motion in RPMD relies mainly on the internal structure of the ring polymers. Thus, an apparent step forward is to perform the excited vibrational state initialization involving both the non-centroid and centroid ring polymer coordinates. This is in theory possible with the adapted use of "non-equilibrium" path integral thermostats [255, 256]. Once this is achieved it would be interesting to see if the adiabatic switching in that case would be applicable and effective.

Furthermore, the initialization of excited ro-vibrational states still needs to be implemented and tested. As the description of quantal rotational motion is not intrinsically described in RPMD, well-established QCT methodologies could be applied in RPMD [111]. However, the task is challenging as the energy differences between different rotational states for a given vibrational state are in general very small. In addition, the choice of β still needs to be made more systematically. Its use and physical meaning for RPMD beyond the canonical ensemble has not yet been clearly understood. β has a strong influence on the internal dynamics in the ring polymers as well as on overall scattering dynamics. Its systematic determination would constitute a great progress towards a complete extension of RPMD to molecular reactive scattering dynamics.

Finally, it would be worthwhile to employ the presented approach to study dynamics involving large or many molecules for which no treatment of NQEs has been possible so far. Potential applications can include the study of the X-ray induced excitation-energy dependence of hydrogen bound configurations in water [257], simulations of equilibration dynamics for proton-transfer in large molecules [258] and direct trajectory simulations of the dissociation dynamics of complex molecules [194, 259, 260].

Appendix A

Properties and applications of the ring polymer normal mode transformation

The ring polymer normal mode coordinates are employed several times throughout the thesis. Their purpose is to diagonalize the free ring polymer Hamiltonian H_n^0

$$H_n^0(\mathbf{p},\mathbf{q}) \doteq \sum_{k=1}^{n} \frac{1}{2m}\left(p^{(k)}\right)^2 + \sum_{k=1}^{n} \frac{1}{2} m\omega_n^2 \left(q^{(k)} - q^{(k+1)}\right)^2, \tag{A.1}$$

into the form of n uncoupled harmonic oscillators. The normal mode coordinates are convenient and insightful for several purposes such a sampling, manipulating intuitively the centroids and simplifying numerous expansions. The case for one particle in one dimension presented here is straightforwardly generalized to any dimension.

Transforming the ring polymer from the bead representation to the normal mode representation,

$$\tilde{p}^{(k)} = \sum_{j=1}^{n} p^{(j)} C_{jk} \quad \text{and} \quad \tilde{q}^{(k)} = \sum_{j=1}^{n} q^{(j)} C_{jk}, \tag{A.2}$$

where in the case of even n the elements of the orthogonal transformation matrix C are

$$C_{jk} = \begin{cases} \sqrt{1/n}, & k = 0 \\ \sqrt{2/n}\cos(2\pi jk/n), & 1 \le k \le n/2 - 1 \\ \sqrt{1/n}(-1)^j, & k = n/2 \\ \sqrt{2/n}\sin(2\pi jk/n), & n/2 + 1 \le k \le n - 1 \end{cases} \tag{A.3}$$

which yields

$$H_n^0(\mathbf{p},\mathbf{q}) = \sum_{k=0}^{n-1}\left(\frac{\left[\tilde{p}^{(k)}\right]^2}{2m} + \frac{1}{2}m\omega_k^2\left[\tilde{q}^{(k)}\right]^2\right), \tag{A.4}$$

with $\omega_k = 2\omega_n \sin(k\pi/n)$.

First property: It follows immediately from Eq. (A.3) and Eq. (A.2) for $k = 0$ that

$$\tilde{p}^{(0)} = \frac{1}{\sqrt{n}} \times n \times \frac{1}{n}\sum_{k=1}^{n} p^{(k)} = \sqrt{n}\, p^c, \tag{A.5}$$

and similarly for the position coordinate

$$\tilde{q}^{(0)} = \frac{1}{\sqrt{n}} \times n \times \frac{1}{n}\sum_{k=1}^{n} q^{(k)} = \sqrt{n}\, q^c. \tag{A.6}$$

Second property: In the absence of external potential ($V = 0$), we have for $k = 1, \ldots, n-1$

$$\left\langle \frac{\left[\tilde{p}^{(k)}\right]^2}{2m} \right\rangle_n = \left\langle \frac{1}{2}m\omega_k^2\left[\tilde{q}^{(k)}\right]^2 \right\rangle_n = \frac{n}{2\beta}. \tag{A.7}$$

It follows that for the momentum centroid

$$\left\langle \frac{\left[\frac{1}{n}\sum_{k=1}^{n} p^{(k)}\right]^2}{2m} \right\rangle_n = \frac{1}{n^2}\left\langle \sum_{k=0}^{n-1} \tilde{p}^{(k)} \right\rangle_n = \frac{1}{2\beta}. \tag{A.8}$$

Third property: If $V(q) = \frac{1}{2}m\omega^2 q^2$, we have

$$\left\langle \frac{1}{2}m(\omega_k^2 + \omega^2)\left[\tilde{q}^{(k)}\right]^2 \right\rangle_n = \frac{n}{2\beta}. \tag{A.9}$$

Also in the harmonic case, we have for all n beads

$$\left\langle \left(q^{(k)}\right)^2 \right\rangle_n = \frac{1}{n}\sum_{k=0}^{n} \left\langle \left(\tilde{q}^{(k)}\right)^2 \right\rangle_n, \tag{A.10}$$

so that for any bead coordinate q (cyclic invariance) we have

$$\left\langle q^2 \right\rangle_n = \sum_{k=0}^{n-1} \frac{1}{m\beta(\omega_k^2 + \omega^2)}. \tag{A.11}$$

Using the formula

$$\sum_{k=0}^{\infty} \frac{1}{\omega_k^2 + \omega^2} = \frac{\hbar\beta}{2\omega} \coth(\beta\omega/2), \tag{A.12}$$

in the limit of infinite beads, the correct quantum position fluctuations are recovered for each bead

$$\lim_{n\to\infty} \left\langle q^2 \right\rangle_n = \frac{\hbar}{2\omega} \coth(\beta\omega/2). \tag{A.13}$$

Thus, the average potential energy estimator yields

$$\lim_{n\to\infty} \left\langle \frac{1}{n} \sum_{k=0}^{n-1} V(q^{(k)}) \right\rangle_n = \frac{\hbar\omega}{4} \coth(\beta\omega/2). \tag{A.14}$$

Fourth property: Combining Eq. (A.9), Eq. (A.10) and Eq. (A.12) yields

$$\lim_{n\to\infty} \left[\left\langle \frac{1}{n} \sum_{k=0}^{n-1} \frac{1}{2} m\omega_k^2 \left[\tilde{q}^{(k)}\right]^2 \right\rangle_n - \frac{n}{2\beta} \right] = -\frac{\hbar\omega}{4} \coth(\beta\omega/2). \tag{A.15}$$

Appendix B

Path integral white noise Langevin thermostat

Applying a white noise Langevin thermostat (WNLT) on an atom in one spatial dimension and undergoing a potential V yields the following equations of motion

$$\frac{\mathrm{d}q(t)}{\mathrm{d}t} = \frac{1}{m}p(t), \tag{B.1}$$

$$\frac{\mathrm{d}p(t)}{\mathrm{d}t} = -\frac{\gamma}{m}p(t) + \xi(t) - \frac{\mathrm{d}V(q)}{\mathrm{d}q}, \tag{B.2}$$

where γ is the friction coefficient and $\xi(t)$ is an uncorrelated, Gaussian distributed random force with unit variance and zero mean such that

$$\langle \xi \rangle = 0, \quad \text{and} \quad \langle \xi(0)\xi(t) \rangle = \delta(t). \tag{B.3}$$

It is known how to combine a WNLT with the velocity velocity Verlet algorithm to sample the canonical distribution in classical statistical mechanics. Ring polymer dynamics is classical dynamics in an extended phase space with a canonical distribution at n times the physical temperature. Thus, it is possible to combine a WNLT with the path integral velocity Verlet algorithm. Bussi and Parrinello have shown [261] that this is amounts to adding the following steps before and after the

Eqs. (2.56-2.60) in Sec. 2.4.3

$$\begin{aligned} \tilde{p}_i^{(k)} &\leftarrow \sum_{j=1}^{n} p_i^{(j)} C_{jk}, \\ \tilde{p}_i^{(k)} &\leftarrow c_1^{(k)} \tilde{p}_i^{(k)} + \sqrt{\frac{m_i}{\beta_n}} c_2^{(k)} \xi_i^{(k)}, \\ p_i^{(j)} &\leftarrow \sum_{k=0}^{n-1} C_{jk} \tilde{p}_i^{(k)} \end{aligned} \tag{B.4}$$

For each mode k and atom i, $\xi_i^{(k)}$ is a different uncorrelated and Gaussian-distributed random force with unit variance and zero mean for each physical degree of freedom and each ring polymer normal mode. The coefficients $c_1^{(k)}$ and $c_2^{(k)}$ are

$$\begin{aligned} c_1^{(k)} &= e^{-(\Delta t/2)\gamma^{(k)}}, \\ c_2^{(k)} &= \sqrt{1 - \left[c_1^{(k)}\right]^2}. \end{aligned} \tag{B.5}$$

The normal mode friction coefficients $\gamma^{(k)}$ are commonly chosen to give an optimal sampling of the canonical distribution for the free ring polymer such that

$$\gamma^{(k)} = \begin{cases} 1/\tau_0, & k = 0 \\ 2\omega_k. & k > 0 \end{cases} \tag{B.6}$$

The parameter τ_0 is left to be tuned to sample the internal modes of the ring polymer as efficiently as possible [121]. The main compromise for this simple thermostat is that the friction coefficients may not be totally optimal for any potential , although it should be very similar for the highest frequency internal modes which are usually decoupled from the physical modes.

Appendix C

Velocity autocorrelation function computed with RPMD

The RPMD approximation of the position autocorrelation function is

$$C_{q\,q}(t) \approx \frac{1}{(2\pi\hbar)^n Z_n} \int d\mathbf{p}_0 \int d\mathbf{q}_0 e^{-\beta_n H_n(\mathbf{p}_0,\,\mathbf{q}_0)} q^c(0)\, q^c(t), \tag{C.1}$$

where $q^c = \frac{1}{n}\sum_{k=1}^{n} q^{(k)}$. Taking the derivative with respect to time twice yields

$$\begin{aligned}
\frac{d^2}{dt^2}\langle q^c(0)\, q^c(t)\rangle_n &= -\frac{d}{dt}\int d\mathbf{p}_0 \int d\mathbf{q}_0 e^{-\beta_n H_n(\mathbf{p}_0,\,\mathbf{q}_0)} q^c(0) v^c(t) \\
&= -\frac{d}{dt}\int d\mathbf{p}_0 \int d\mathbf{q}_0 e^{-\beta_n H_n(\mathbf{p}_0,\,\mathbf{q}_0)} q^c(-t) v^c(0) \\
&= \int d\mathbf{p}_0 \int d\mathbf{q}_0 e^{-\beta_n H_n(\mathbf{p}_0,\,\mathbf{q}_0)} v^c(-t) v^c(0) \\
&= \int d\mathbf{p}_0 \int d\mathbf{q}_0 e^{-\beta_n H_n(\mathbf{p}_0,\,\mathbf{q}_0)} v^c(0) v^c(t).
\end{aligned} \tag{C.2}$$

with $\bar{v} = \frac{d}{dt} q^c = \frac{1}{n}\sum_{k=1}^{n} \frac{p^{(k)}}{m}$ is the centroid velocity. The conservation of the ring polymer Boltzmann factor

$$e^{-\beta_n H_n(\mathbf{p}(t),\,\mathbf{q}(t))} = e^{-\beta_n H_n(\mathbf{p}_0,\,\mathbf{q}_0)},$$

Liouville's theorem

$$d\mathbf{p}_0 d\mathbf{q}_0 = d\mathbf{p}(t)\, d\mathbf{q}(t),$$

and the detailed balance condition have been employed to arrive at the final result in Eq. (C.2). The same arguments apply to correlation functions involving more general momentum dependant operators.

Bibliography

[1] G. Cassone, *Chem. Phys. Lett.* **11**, 8983 (2020).

[2] N. Balucani, F. Leonori, P. Casavecchia, *Energy* **43**, 47 (2012).

[3] T. Rahn, *et al.*, *Nature* **424**, 918 (2003).

[4] D. L. Baulch, *et al.*, *J. Phys. Chem. Ref. Data.* **9**, 295 (1980).

[5] R. C. Chapleski, Y. Zhang, D. Troya, J. R. Morris, *Chem. Soc. Rev.* **45**, 3731 (2016).

[6] T. Lamberts, *et al.*, *Astron. Astrophys.* **570**, A57 (2014).

[7] A. Wagner, M. Graff, *Astrophys. J.* **317**, 423 (1987).

[8] R. I. Kaiser, D. S. Parker, A. M. Mebel, *Ann. Rev. of Phys. Chem.* **66**, 43 (2015).

[9] E. L. Crane, H.-T. Chiu, R. G. Nuzzo, *J. Phys. Chem. B* . **105**, 3549 (2001).

[10] H. Nakai, T. Takemura, J. Ono, Y. Nishimura, *J. Phys. Chem. B* . **125**, 10947 (2021).

[11] A. Franklin, S. Perovic, *The Stanford Encyclopedia of Philosophy* (Metaphysics Research Lab, Stanford University, 2021).

[12] D. Frenkel, B. Smit, eds., *Understanding Molecular Simulation (Second Edition)* (Academic Press, San Diego, 2002).

[13] K. Brezinsky, *Symposium (International) on Combustion* **26**, 1805 (1996).

[14] J. L. Berry, M. S. Ugelow, M. A. Tolbert, E. C. Browne, *Astrophys. J.* **885**, L6 (2019).

[15] J. Stith, *et al.*, *Meteorol. Monogr.* **59** (2018).

[16] D. Truhlar, *et al.*, *Faraday Discussions* **157**, 113 (2012).

[17] C. Xiao, *et al.*, *Science* **333**, 440 (2011).

[18] S. Yan, Y.-T. Wu, B. Zhang, X.-F.-Yue, K. Liu, *PNAS* **105**, 12667 (2008).

[19] W. Zhang, H. Kawamata, K. Liu, *Science* **325**, 303 (2009).

[20] K. Liu, *Annu. Rev. Phys. Chem.* **67**, 91 (2016).

[21] P. Maroni, *et al.*, *Phys. Rev. Lett.* **94**, 246104 (2005).

[22] W. Shiu, J. J. Lin, K. Liu, *Phys. Rev. Lett.* **92**, 103201 (2004).

[23] F. Wang, J.-S. Lin, K. Liu, *Science* **331**, 900 (2011).

[24] B. L. Yoder, R. Bisson, R. D. Beck, *Science* **329**, 553 (2010).

[25] G. C. Schatz, *Annu. Rev. Phys. Chem.* **39**, 317 (1988).

[26] S. L. Mielke, B. C. Garrett, D. G. Fleming, D. G. Truhlar, *Mol. Phys.* **113**, 160 (2015).

[27] T. Yang, *et al.*, *J. Phys. Chem. A* **119**, 12284 (2015).

[28] L. Wang, S. D. Fried, S. G. Boxer, T. E. Markland, *PNAS* **111**, 18454 (2014).

[29] L. Wang, C. Isborn, T. Markland, *Meth. Enzymol.* **577** (2016).

[30] T. E. Markland, M. Ceriotti, *Nat. Rev. Chem.* **2**, 0109 (2018).

[31] M. Born, R. Oppenheimer, *Ann. Phys.* **389**, 457 (1927).

[32] J. C. Tully, *J. Chem. Phys.* **137**, 22A301 (2012).

[33] H. B. Schlegel, *J. Comput. Chem.* **24**, 1514 (2003).

[34] G. Czako, B. Braams, J. Bowman, *J. Phys. Chem. A* **112**, 7466 (2008).

[35] F. Petocchi, V. Christiansson, P. Werner, *Phys. Rev. B* **104**, 195146 (2021).

[36] A. V. Nikitin, M. Rey, V. G. Tyuterev, *J. Chem. Phys.* **145**, 114309 (2016).

[37] J. Kang, T. Sumi, M. Tateno, *Panorama of Contemporary Quantum Mechanics* (IntechOpen, Rijeka, 2019).

[38] R. Welsch, U. Manthe, *J. Chem. Phys.* **138**, 164118 (2013).

[39] B. Jiang, J. Li, H. Guo, *Letters* **11**, 5120 (2020).

[40] J. Chen, X. Xu, S. Liu, D. H. Zhang, *Phys. Chem. Chem. Phys.* **20**, 9090 (2018).

[41] G. C. Schatz, A. Kuppermann, *J. Chem. Phys.* **65**, 4668 (1976).

[42] F. Webster, J. C. Light, *J. Chem. Phys.* **90**, 265 (1989).

[43] S. C. Althorpe, *et al.*, *Nature* **416**, 67 (2002).

[44] S. A. Harich, *et al.*, *Nature* **419**, 281 (2002).

[45] M. Qiu, *et al.*, *Science* **311**, 1440 (2006).

[46] X. Wang, *et al.*, *Science* **322**, 573 (2008).

[47] R. Welsch, U. Manthe, *J. Chem. Phys.* **142**, 064309 (2015).

[48] R. Welsch, U. Manthe, *J. Chem. Phys.* **141**, 051102 (2014).

[49] R. Welsch, U. Manthe, *J. Chem. Phys.* **141**, 174313 (2014).

[50] J. M. Bowman, *J. Phys. Chem.* **95**, 4960 (1991).

[51] J. Palma, D. C. Clary, *J. Chem. Phys.* **112**, 1859 (2000).

[52] J. Palma, D. C. Clary, *J. Chem. Phys.* **115**, 2188 (2001).

[53] R. Liu, H. Xiong, M. Yang, *J. Chem. Phys.* **137**, 174113 (2012).

[54] H.-G. Yu, G. Nyman, *J. Chem. Phys.* **111**, 3508 (1999).

[55] M. Yang, D. H. Zhang, S.-Y. Lee, *J. Chem. Phys.* **117**, 9539 (2002).

[56] M. L. Wang, J. Z. H. Zhang, *J. Chem. Phys.* **117**, 3081 (2002).

[57] S. Liu, J. Chen, Z. Zhang, D. H. Zhang, *J. Chem. Phys.* **138**, 011101 (2013).

[58] J. Qi, *et al.*, *J. Chem. Phys.* **144**, 171101 (2016).

[59] Z. Zhang, Y. Zhou, D. H. Zhang, G. Czakó, J. M. Bowman, *J. Phys. Chem. Lett.* **3**, 3416 (2012).

[60] G. Schiffel, U. Manthe, *J. Chem. Phys.* **132**, 084103 (2010).

[61] F. Huarte-Larrañaga, U. Manthe, *J. Phys. Chem. A* **105**, 2522 (2001).

[62] G. Nyman, H.-G. Yu, R. B. Walker, *J. Chem. Phys.* **109**, 5896 (1998).

[63] D. Wang, J. M. Bowman, *J. Chem. Phys.* **115**, 2055 (2001).

[64] M. Karplus, R. N. Porter, R. Sharma, *J. Chem. Phys.* **43**, 3259 (1965).

[65] R. N. Porter, *Ann. Rev. Phys. Chem.* **25**, 317 (1974).

[66] S. R. V. Aoiz F. J., Herrero V. J., *J. Chem. Phys.* **97**, 7423 (1992).

[67] R. Porter, L. Raff (Plenum Press, New York, 1976).

[68] W. L. Hase, *Encyc. Comp. Chem.* **1** (2002).

[69] W. Zhang, *et al.*, *PNAS* **107**, 12782 (2010).

[70] D. Truhlar, J. Muckerman (Plenum Press, New York, 1979).

[71] G. Czakó, J. M. Bowman, *J. Am. Chem. Soc* **131**, 17534 (2009).

[72] J. F. Castillo, F. J. Aoiz, L. Bañares, *J. Chem. Phys.* **125**, 124316 (2006).

[73] J. Espinosa-Garcia, J. C. Corchado, *Phys. Chem. Chem. Phys.* **19**, 1580 (2017).

[74] M. Mastromatteo, B. Jackson, *J. Chem. Phys.* **139**, 194701 (2013).

[75] L. Bañares, F. J. Aoiz, P. Honvault, B. Bussery-Honvault, J.-M. Launay, *J. Chem. Phys.* **118**, 565 (2003).

[76] G. Czakó, *J. Phys. Chem. A* **116**, 7467 (2012).

[77] G. Czakó, A. L. Kaledin, J. M. Bowman, *J. Chem. Phys.* **132**, 164103 (2010).

[78] M. Parrinello, A. Rahman, *J. Chem. Phys.* **80**, 860 (1984).

[79] B. J. Berne, D. Thirumalai, *Annu. Rev. Phys. Chem.* **37**, 401 (1986).

[80] I. R. Craig, D. E. Manolopoulos, *J. Chem. Phys.* **121**, 3368 (2004).

[81] T. J. H. Hele, M. J. Willatt, A. Muolo, S. C. Althorpe, *J. Chem. Phys.* **142**, 134103 (2015).

[82] T. J. H. Hele, M. J. Willatt, A. Muolo, S. C. Althorpe, *J. Chem. Phys.* **142**, 191101 (2015).

[83] I. R. Craig, D. E. Manolopoulos, *J. Chem. Phys.* **122**, 084106 (2005).

[84] I. R. Craig, D. E. Manolopoulos, *J. Chem. Phys.* **123**, 034102 (2005).

[85] T. F. Miller, D. E. Manolopoulos, *J. Chem. Phys.* **122**, 184503 (2005).

[86] T. F. Miller, D. E. Manolopoulos, *J. Chem. Phys.* **123**, 154504 (2005).

[87] S. Habershon, D. E. Manolopoulos, T. E. Markland, T. F. Miller, *Ann. Rev. Phys. Chem.* **64**, 387 (2013).

[88] Y. V. Suleimanov, F. J. Aoiz, H. Guo, *J. Phys. Chem. A* **120**, 8488 (2016).

[89] T. E. Markland, S. Habershon, D. E. Manolopoulos, *J. Chem. Phys.* **128**, 194506 (2008).

[90] Y. V. Suleimanov, *J. Phys. Chem. C* **116**, 11141 (2012).

[91] M. Shiga, A. Nakayama, *Chem. Phys. Lett.* **451**, 175 (2008).

[92] S. Habershon, G. S. Fanourgakis, D. E. Manolopoulos, *J. Chem. Phys.* **129**, 074501 (2008).

[93] A. Witt, S. D. Ivanov, M. Shiga, H. Forbert, D. Marx, *J. Chem. Phys.* **130**, 194510 (2009).

[94] M. Rossi, H. Liu, F. Paesani, J. Bowman, M. Ceriotti, *J. Chem. Phys.* **141**, 181101 (2014).

[95] R. Welsch, K. Song, Q. Shi, S. C. Althorpe, T. F. Miller III, *J. Chem. Phys.* **145**, 204118 (2016).

[96] D. C. Clary, *Science* **321**, 789 (2008).

[97] C. L. Davis, E. N. Maslen, J. N. Varghese, *Proc. R. Soc. A* **384**, 57 (1982).

[98] C. L. Davis, E. N. Maslen, *Proc. R. Soc. A* **384**, 89 (1982).

[99] S. Bludman, P. B. Daitch, *Phys. Rev.* **95**, 823 (1954).

[100] J. Albert, D. Kaiser, V. Engel, *J. Chem. Phys.* **144**, 171103 (2016).

[101] R. B. Gerber, *Proc. R. Soc. A* **309**, 221 (1969).

[102] P. J. Kuntz, *Interaction Potentials II: Semiempirical Atom-Molecule Potentials for Collision Theory* (Springer US, Boston, MA, 1979).

[103] R. Dawes, E. Quintas-Sánchez, *The construction of ab initio-based potential energy surfaces* (John Wiley Sons, Ltd, 2018).

[104] B. M. Rode, C. F. Schwenk, B. R. Randolf, *Classical Versus Quantum Mechanical Simulations: The Accuracy of Computer Experiments in Solution Chemistry* (Springer Netherlands, Dordrecht, 2004).

[105] Y. Wang, *et al.*, *J. Phys. Chem. Lett.* **7**, 3322 (2016).

[106] H. Pritchard, *Open Chemistry* **9**, 753 (2011).

[107] P. G. Jambrina, *et al.*, *Phys. Chem. Chem. Phys.* **12**, 1102 (2010).

[108] P. N. Argyres, *Physics Physique Fizika* **2**, 131 (1965).

[109] W. H. Miller, *Science* **233**, 171 (1986).

[110] G. Czako, J. Bowman, *J. Phys. Chem.. A* **118** (2014).

[111] T. Nagy, G. Lendvay, *J. Phys. Chem. Lett.* **8**, 4621 (2017).

[112] U. Lourderaj, E. Martínez-Núñez, W. L. Hase, *J. Phys. Chem. A* **111**, 10292 (2007).

[113] W. F. Long, J. S. Kovacs, *Prog. Theor. Exp. Phys* **44**, 952 (1970).

[114] L. Bonnet, J.-C. Rayez, *Chem. Phys. Lett* **397**, 106 (2004).

[115] P. Jambrina, E. García, V. J. Herrero, V. Sáez-Rábanos, F. J. Aoiz, *Phys. Chem. Chem. Phys.* **14**, 14596 (2012).

[116] J. Cao, *et al.*, *PNAS* **106**, 13180 (2009).

[117] C. Qu, J. M. Bowman, *A* **120**, 4988 (2016).

[118] A. Vikár, T. Nagy, G. Lendvay, *J. Phys. Chem. A* **120**, 5083 (2016).

[119] A. Marjollet, L. Inhester, R. Welsch, *J. Chem. Phys.* **156**, 044101 (2022).

[120] T. Ichinose, H. Neidhardt, V. A. Zagrebnov, *J. Funct. Anal.* **207**, 33 (2004).

[121] M. Ceriotti, M. Parrinello, T. E. Markland, D. E. Manolopoulos, *J. Chem. Phys.* **133**, 124104 (2010).

[122] M. Parrinello, A. Rahman, *J. Chem. Phys.* **80**, 860 (1984).

[123] D. Callaway, A. Rahman, *Phys. Rev. Lett.* **49** (1982).

[124] B. De Raedt, M. Sprik, M. L. Klein, *J. Chem. Phys.* **80**, 5719 (1984).

[125] D. J. E. Callaway, A. Rahman, *Phys. Rev. Lett.* **49**, 613 (1982).

[126] R. W. Hall, B. J. Berne, *J. Chem. Phys.* **81**, 3641 (1984).

[127] D. M. Ceperley, *Rev. Mod. Phys.* **67**, 279 (1995).

[128] Y. V. Suleimanov, J. W. Allen, W. H. Green, *Comp. Phys. Commun.* **184**, 833 (2013).

[129] T. M. Yamamoto, *J. Chem. Phys.* **123**, 104101 (2005).

[130] B. J. Berne, G. D. Harp, *On the Calculation of Time Correlation Functions* (John Wiley Sons, Ltd, 1970).

[131] H. Kim, *Chem. Phys. Lett* **436** (2007).

[132] R. Ramırez, T. López-Ciudad, P. Kumar P, D. Marx, *J. Chem. Phys.* **121**, 3973 (2004).

[133] S. C. Althorpe, *Eur. Phys. J. B* **94**, 155 (2021).

[134] J.-M. Sanz-Serna, M.-P. Calvo, *Numerical hamiltonian problems* (Courier Dover Publications, 2018).

[135] J. O. Richardson, S. C. Althorpe, *J. Chem. Phys.* **131**, 214106 (2009).

[136] R. Pérez de Tudela, *et al.*, *Letters* **5**, 4219 (2014).

[137] R. Collepardo-Guevara, Y. V. Suleimanov, D. E. Manolopoulos, *J. Chem. Phys.* **130**, 174713 (2009).

[138] Q. Meng, J. Chen, D. H. Zhang, *J. Chem. Phys.* **143**, 101102 (2015).

[139] R. Perez de Tudela, F. J. Aoiz, Y. V. Suleimanov, D. E. Manolopoulos, *J. Phys. Chem. Lett.* **3**, 493 (2012).

[140] S. Habershon, D. E. Manolopoulos, *J. Chem. Phys.* **131**, 244518 (2009).

[141] X. Li, P. Huo, *Letters* **12**, 6714 (2021).

[142] J. Zuo, C. Xie, H. Guo, D. Xie, *Letters* **8**, 3392 (2017).

[143] Y. V. Suleimanov, J. Espinosa-Garcia, *J. Phys. Chem. B* **120**, 1418 (2016).

[144] Y. V. Suleimanov, F. J. Aoiz, H. Guo, *J. Phys. Chem. A* **120**, 8488 (2016).

[145] Q. Liu, L. Zhang, Y. Li, B. Jiang, *J. Phys. Chem. Lett.* **10**, 7475 (2019).

[146] H. Jiang, *et al.*, *Letters* **12**, 1991 (2021).

[147] J. R. Duke, N. Ananth, *J. Chem. Phys.* **6**, 4219 (2015).

[148] X. Tao, P. Shushkov, T. F. Miller, *J. Chem. Phys.* **152**, 124117 (2020).

[149] A. Marjollet, R. Welsch, *J. Chem. Phys.* **152**, 194113 (2020).

[150] H. Chadwick, R. D. Beck, *Annu. Rev. Phys. Chem.* **68**, 39 (2017).

[151] P. M. Hundt, B. Jiang, M. E. van Reijzen, H. Guo, R. D. Beck, *Science* **344**, 504 (2014).

[152] A. J. Orr-Ewing, *J. Chem. Phys.* **140**, 090901 (2014).

[153] F. Wang, J.-S. Lin, K. Liu, *Science* **331**, 900 (2011).

[154] W. Shiu, J. Lin, K. Liu, *Phys. Rev. Lett.* **92**, 103201 (2004).

[155] W. Zhang, H. Kawamata, K. Liu, *Science* **325**, 303 (2009).

[156] B. L. Yoder, R. Bisson, R. D. Beck, *Science* **329**, 553 (2010).

[157] K. Liu, *Ann. Rev. Phys. Chem.* **67**, 91 (2016).

[158] P. Maroni, *et al.*, *Phys. Rev. Lett.* **94**, 246104 (2005).

[159] D. R. Killelea, V. L. Campbell, N. S. Shuman, A. L. Utz, *Science* **319**, 790 (2008).

[160] G. Schiffel, U. Manthe, *J. Chem. Phys.* **132**, 191101 (2010).

[161] R. Welsch, U. Manthe, *J. Phys. Chem. Lett.* **6**, 338 (2015).

[162] R. Ellerbrock, U. Manthe, *Chem. Phys.* **482**, 106 (2017).

[163] R. Ellerbrock, U. Manthe, *J. Chem. Phys.* **147**, 241104 (2017).

[164] R. Ellerbrock, U. Manthe, *J. Chem. Phys.* **148**, 224303 (2018).

[165] W. H. Miller, S. D. Schwartz, J. W. Tromp, *J. Chem. Phys.* **79**, 4889 (1983).

[166] D. H. Zhang, J. C. Light, *J. Chem. Phys.* **104**, 6184 (1996).

[167] F. Matzkies, U. Manthe, *J. Chem. Phys.* **106**, 2646 (1997).

[168] U. Manthe, *Mol. Phys.* **109**, 1415 (2011).

[169] R. Welsch, F. Huarte-Larranaga, U. Manthe, *J. Chem. Phys.* **136**, 064117 (2012).

[170] R. Welsch, U. Manthe, *Mol. Phys.* **110**, 703 (2012).

[171] U. Manthe, R. Welsch, *J. Chem. Phys.* **140**, 244113 (2014).

[172] H.-D. Meyer, U. Manthe, L. S. Cederbaum, *Chem. Phys. Lett.* **165**, 73 (1990).

[173] U. Manthe, H.-D. Meyer, L. S. Cederbaum, *J. Chem. Phys.* **97**, 3199 (1992).

[174] H. Wang, M. Thoss, *J. Chem. Phys.* **119**, 1289 (2003).

[175] U. Manthe, *J. Chem. Phys.* **128**, 164116 (2008).

[176] U. Manthe, *J. Chem. Phys.* **105**, 6989 (1996).

[177] U. Manthe, *J. Chem. Phys.* **130**, 054109 (2009).

[178] F. Gatti, B. Lasorne, H.-D. Meyer, A. Nauts, *Applications of quantum dynamics in chemistry*, vol. 98 (Springer, 2017).

[179] R. Welsch, U. Manthe, *J. Chem. Phys.* **137**, 244106 (2012).

[180] U. Lourderaj, *et al.*, *Comp. Phys. Commun.* **185**, 1074 (2014).

[181] P. Jambrina, E. García, V. J. Herrero, V. Sáez-Rábanos, F. J. Aoiz, *J. Chem. Phys.* **135**, 034310 (2011).

[182] Y. V. Suleimanov, *et al.*, *Phys. Chem. Chem. Phys.* **15**, 3655 (2013).

[183] A. I. Boothroyd, W. J. Keogh, P. G. Martin, M. R. Peterson, *J. Chem. Phys.* **95**, 4343 (1991).

[184] B. Jiang, H. Guo, *J. Chem. Phys.* **138**, 234104 (2013).

[185] L. Bonnet, J. Rayez, *Chem. Phys. Lett.* **277**, 183 (1997).

[186] L. Bonnet, J.-C. Rayez, *Chem. Phys. Lett.* **397**, 106 (2004).

[187] L. Che, *et al.*, *Science* **317**, 1061 (2007).

[188] J. Palma, U. Manthe, *J. Chem. Phys.* **146**, 214117 (2017).

[189] J. O. Richardson, M. Thoss, *J. Chem. Phys.* **139**, 031102 (2013).

[190] P. Shushkov, R. Li, J. C. Tully, *J. Chem. Phys.* **137**, 22A549 (2012).

[191] X. Tao, P. Shushkov, T. F. Miller, *J. Chem. Phys.* **148**, 102327 (2018).

[192] A. Marjollet, R. Welsch, *Int. J. Quantum Chem* **121**, e26447 (2021).

[193] L. Juurlink, D. Killelea, A. Utz, *Prog. Surf. Sci* **84**, 69 (2009).

[194] X. Ma, W. L. Hase, *Philosophical Transactions of the Royal Society A: Mathematical, Physical and Engineering Sciences* **375**, 20160204 (2017).

[195] D. H. Zhang, H. Guo, *Annu. Rev. Phys. Chem.* **67**, 135 (2016).

[196] J. I. Steinfeld, J. S. Francisco, W. L. Hase, *Chemical Kinetics and Dynamics*, vol. 3 (Prentice Hall Englewood Cliffs (New Jersey), 1989).

[197] U. Manthe, *J. Chem. Phys.* **128**, 064108 (2008).

[198] F. Huarte-Larrañaga, U. Manthe, *Z. Phys. Chem.* **221**, 171 (2007).

[199] R. Ellerbrock, U. Manthe, J. Palma, *J. Phys. Chem. A* **123**, 7237 (2019).

[200] L. Sun, K. Song, W. L. Hase **296**, 875 (2002).

[201] F. J. Aoiz, J. Aldegunde, V. J. Herrero, V. Sáez-Rábanos, *Phys. Chem. Chem. Phys* **16**, 9808 (2014).

[202] B. J. Braams, D. E. Manolopoulos, *J. Chem. Phys.* **125**, 124105 (2006).

[203] Y. V. Suleimanov, R. Collepardo-Guevara, D. E. Manolopoulos, *J. Chem. Phys.* **134**, 044131 (2011).

[204] Y. Li, Y. V. Suleimanov, M. Yang, W. H. Green, H. Guo, *J. Phys. Chem. Lett.* **4**, 48 (2013).

[205] Y. V. Suleimanov, W. J. Kong, H. Guo, W. H. Green, *J. Chem. Phys.* **141**, 244103 (2014).

[206] T. J. Hele, Y. V. Suleimanov, *J. Chem. Phys.* **143**, 074107 (2015).

[207] J. Huang, J. J. Valentini, J. T. Muckerman, *J. Chem. Phys.* **102**, 5695 (1995).

[208] A. I. Boothroyd, W. J. Keogh, P. G. Martin, M. R. Peterson, *J. Chem. Phys.* **104**, 7139 (1996).

[209] G. Capecchi, H.-J. Werner, *Phys. Chem. Chem. Phys.* **6**, 4975 (2004).

[210] J. Chen, Z. Sun, D. Zhang, *J. Chem. Phys.* **142**, 024303 (2015).

[211] A. Varandas, *Chem. Phys. Lett.* **439**, 386 (2007).

[212] D. De Fazio, V. Aquilanti, S. Cavalli, *Front. Chem.* **7**, 328 (2019).

[213] M. Qiu, *et al.*, *Science* **311**, 1440 (2006).

[214] F. J. Aoiz, L. Bañares, V. J. Herrero, *J. Chem. Soc., Faraday Trans.* **94**, 2483 (1998).

[215] Meisner, J., Kamp, I., Thi, W.-F., Kästner, J., *A&A* **627**, A45 (2019).

[216] S. Liu, J. Chen, Z. Zhang, D. H. Zhang, *J. Chem. Phys.* **138**, 011101 (2013).

[217] R. Ellerbrock, U. Manthe, *J. Chem. Phys.* **148**, 224303 (2018).

[218] R. Liu, H. Xiong, M. Yang, *J. Chem. Phys.* **137**, 174113 (2012).

[219] C. Xiao, *et al.*, *Science* **333**, 440 (2011).

[220] M. Brouard, *et al.*, *Phys. Rev. Lett.* **90**, 093201 (2003).

[221] J. P. Camden, H. A. Bechtel, D. J. A. Brown, R. N. Zare, *J. Chem. Phys.* **123**, 134301 (2005).

[222] W. Hu, *et al.*, *J. Phys. Chem. A* **110**, 3017 (2006).

[223] J. P. Camden, H. A. Bechtel, D. J. A. Brown, R. N. Zare, *J. Chem. Phys.* **124**, 034311 (2006).

[224] Y. Kurosaki, T. Takayanagi, *J. Chem. Phys.* **110**, 10830 (1999).

[225] Z. Zhang, D. H. Zhang, *J. Chem. Phys.* **141**, 144309 (2014).

[226] J. Espinosa-Garcia, *J. Chem. Phys.* **116**, 10664 (2002).

[227] J. C. Corchado, J. L. Bravo, J. Espinosa-Garcia, *J. Chem. Phys.* **130**, 184313 (2009).

[228] Z. Xie, J. M. Bowman, X. Zhang, *J. Chem. Phys.* **125**, 133120 (2006).

[229] Y. Zhou, B. Fu, C. Wang, M. A. Collins, D. H. Zhang, *J. Chem. Phys.* **134**, 064323 (2011).

[230] J. Li, *et al.*, *J. Chem. Phys.* **142**, 204302 (2015).

[231] C. Rangel, J. C. Corchado, J. Espinosa-García, *J. Phys. Chem. A* **110**, 10375 (2006).

[232] Z. Xie, J. M. Bowman, *Chem. Phys. Lett* **429**, 355 (2006).

[233] J. Espinosa-García, *J. Phys. Chem. A* **111**, 9654 (2007).

[234] Y. Zhou, C. Wang, D. H. Zhang, *J. Chem. Phys.* **135**, 024313 (2011).

[235] Z. Zhang, J. Chen, S. Liu, D. H. Zhang, *J. Chem. Phys.* **140**, 224304 (2014).

[236] J. Zhou, J. J. Lin, K. Liu, *J. Chem. Phys.* **119**, 8289 (2003).

[237] J. Zhou, J. J. Lin, K. Liu, *J. Chem. Phys.* **121**, 813 (2004).

[238] W. Zhang, H. Kawamata, K. Liu, *Science* **325**, 303 (2009).

[239] G. Czako, Q. Shuai, K. Liu, J. Bowman, *J. Chem. Phys.* **133**, 131101 (2010).

[240] J. Yang, *et al.*, *J. Chem. Phys.* **143**, 044316 (2015).

[241] G. Czakó, J. M. Bowman, *J. Chem. Phys.* **131**, 244302 (2009).

[242] J. Espinosa-García, J. L. Bravo, *J. Phys. Chem. A* **112**, 6059 (2008).

[243] T. Westermann, *et al.*, *Angewandte Angew. Chem* **53**, 1122 (2014).

[244] J. Palma, U. Manthe, *J. Phys. Chem. A* **119**, 12209 (2015).

[245] T. Lenzen, U. Manthe, *J. Chem. Phys.* **150**, 064102 (2019).

[246] G. Czakó, J. M. Bowman, *Phys. Chem. Chem. Phys.* **13**, 8306 (2011).

[247] J. Yang, *et al.*, *J. Phys. Chem. Lett.* **5**, 1790 (2014).

[248] F. Wang, J.-S. Lin, Y. Cheng, K. Liu, *J. Phys. Chem. Lett.* **4**, 323 (2013).

[249] G. Czakó, *J. Phys. Chem. A* **116**, 7467 (2012).

[250] K. R. Glaesemann, L. E. Fried, *J. Chem. Phys.* **116**, 5951 (2002).

[251] C. Eckart, *Phys. Rev.* **47**, 552 (1935).

[252] A. Y. Dymarsky, K. N. Kudin, *J. Chem. Phys.* **122**, 124103 (2005).

[253] X. Tao, P. Shushkov, T. F. Miller, *J. Chem. Phys.* **152**, 124117 (2020).

[254] Q. Liu, L. Zhang, Y. Li, B. Jiang, *Letters* **10**, 7475 (2019).

[255] M. Ceriotti, G. Bussi, M. Parrinello, *J. Chem. Theory Comput.* **6**, 1170 (2010).

[256] M. Ceriotti, D. E. Manolopoulos, M. Parrinello, *J. Chem. Phys.* **134**, 084104 (2011).

[257] M. Odelius, *et al.*, *Phys. Rev. Lett.* **94**, 227401 (2005).

[258] G. Albareda, *et al.*, *Phys. Chem. Chem. Phys.* **22**, 22332 (2020).

[259] L. Sun, W. L. Hase, *J. Chem. Phys.* **121**, 8831 (2004).

[260] T. Uzer, *Dissociation Dynamics of Polyatomic Molecules* (Academic Press, 1989).

[261] G. Bussi, M. Parrinello, *Phys. Rev. E* **75** (2007).

Acknowledgements

I would like to acknowledge my gratitude to Prof. Robin Santra and Dr. Ralph Welsch for giving me the opportunity to dive in an adventurous research direction that has barely been explored at the start of my PhD. I am thankful for the support and supervision provided by Dr. Ralph Welsch and Dr. Ludger Inhester during the first and second half of my thesis, respectively. Ralph gave me the freedom to explore my own ideas while carefully keeping me on the right track with its guidance and valuable insights. I am indebted to Ludger for his dedicated and effective supervision and, his effort to adapt swiftly as my new supervisor as he took this role halfway through my PhD. I also want to thank Dr. Malik Abdullah for his support and lifting my spirit throughout my stay in Hamburg. I am lucky to have been surrounded with friendly and interesting colleagues. In particular, I am happy to have met Benoit, Yashoj, Victor, Micheal, Murali, Konrad, Mickael, Daria, Vladimir and Sophia for making my stay in the group and some weekends very enjoyable. Special thanks to Otfried for his assistance during my PhD, the interesting conversations and his table tennis coaching. I also think about Zoltan who has been very helpful to me and with whom I had uplifting conversations. It was a very special time for me working in this group, and I shall remember all those who were part of my life here.

I close this thesis by thanking my family and my friends from back home.